Advancements in Prosthetics and Joint Mechanisms

by

Robert Lynn Holgate

A Dissertation Presented in Partial Fulfillment
of the Requirements for the Degree
Doctor of Philosophy

Approved July 2017 by the
Graduate Supervisory Committee:

Thomas Sugar, Co-Chair
Panagiotis Artemiades, Co-Chair
Spring Berman
Marc Mignolet
Joseph Davidson

ARIZONA STATE UNIVERSITY

August 2017

ABSTRACT

Robotic joints can be either powered or passive. This work will discuss the creation of a passive and a powered joint system as well as the combination system being both powered and passive along with its benefits. A novel approach of analysis and control of the combination system is presented.

A passive and a powered ankle joint system is developed and fit to the field of prosthetics, specifically ankle joint replacement for able bodied gait. The general 1 DOF robotic joint designs are examined and the results from testing are discussed. Achievements in this area include the able bodied gait like behavior of passive systems for slow walking speeds. For higher walking speeds the powered ankle system is capable of adding the necessary energy to propel the user forward and remain similar to able bodied gait, effectively replacing the calf muscle. While running has not fully been achieved through past powered ankle devices the full power necessary is reached in this work for running and sprinting while achieving 4x's power amplification through the powered ankle mechanism.

A theoretical approach to robotic joints is then analyzed in order to combine the advantages of both passive and powered systems. Energy methods are shown to provide a correct behavioral analysis of any robotic joint system. Manipulation of the energy curves and mechanism coupler curves allows real time joint behavioral adjustment. Such a powered joint can be adjusted to passively achieve desired behavior for different speeds and environmental needs. The effects on joint moment and stiffness from adjusting one type of mechanism is presented.

I dedicate the entirety of my accomplishments as a student, especially while seeking a Ph.D., to my beautiful wife and best friend Kelsey. Thank you for your support and encouragement always. I also dedicate this work to my children, in the hope that they will be inspired to seek knowledge and to accomplish their own dreams.

ACKNOWLEDGMENTS

I would like to acknowledge all those who took part in making this work a reality. My Advisor Dr. Thomas Sugar for allowing me to be a part of his lab. My mentors and examples Dr. Mathew Holgate, Dr. Jeff Ward, Dr. Kevin Hollander, Dr. Kyle Schroeder, and Dr. Martin Grimmer, who encouraged and taught me along the way. The members of SpringActive, Inc. who helped build, test and inspire the chapters of this dissertation. I would like to acknowledge Chase Wheeler, Dustin Vehon, Alex Boehler, Geoff Clark, Luke Dexter, Darren Kinney, Nathan Cahill, Kenneth Greason, Lorri Kinnan, Ray Churchwell and Preston Clouse for the supporting work they each performed. Funding for much of the work with prosthetic ankles came through the National Science Foundation (NSF), National Institute of Health (NIH), Department of Defense Telemedicine and Advanced Technology Research Center (TATRC), and Clinical and Rehabilitative Medicine Research Group (CRM). Most significant to my personal success, was the financial support from SpringActive, Inc. which provided the funding and work environment to inspire research and fuel imagination.

TABLE OF CONTENTS

Page

CHAPTER Page

CHAPTER Page

CHAPTER Page

LIST OF TABLES

Table Page

LIST OF FIGURES

Figure Page

Figure Page

Figure Page

Figure Page

Figure Page

Figure Page

Figure Page

Figure Page

Figure Page

Figure Page

Figure Page

CHAPTER 1

INTRODUCTION

Robotic joints are joints of any degree of freedom (DOF) that are designed to produce a desired behavior. Robotic joints do not have to be controlled and their dynamics and behavior can be a product of their design. Characteristics of joints include parameters such as: joint stiffness, joint speed, joint position, joint power or joint efficiency etc. Robotic joints are usually specific to one task but can be built in a manner to suit multiple situations and needs. Joint configuration and design is also a product of money. The simplicity of the design can decrease the cost.

A robotic joint is considered to be passive if it does not implore the use of a motor to control its motion. The joint is then free to move under the influence of the external forces acting upon it along its degrees of freedom (DOF). Such a mechanical joint can be created to have stiffness along its DOFs which define its ability to resist motion.

A properly tuned passive joint can behave dynamically in a predictable and desired fashion. This can save power by not relying on motors and controls to achieve certain joint behaviors. Passive joints work well for situations where the external forces are repetitive and/or predictable. A passive joint will only react as the mechanical design permits and can only be effective for a certain range of external forces. In other words its effectiveness and efficiency is application dependent. Passive joints do not have the ability to add energy into the motion. They can only convert energy in order to dissipate motion or store and return energy from motion according to its mechanical efficiency.

There are many applications where robotic joints are used for practical reasons. The field of prosthetics is one of these applications, and, with a well-tuned system, a prosthetic ankle can return an amputee's capability and mobility.

There are 1.8 million Americans living with an amputation and the majority of those amputations are of the lower limbs [1]. This is also an important challenge for the military. Over 1600 service members have had a major amputation as a result of Operation Iraqi Freedom, Operation Enduring Freedom, and Operation New Dawn [2] with nearly half having a transtibial amputation [3].

Lower limb amputees typically expend 10-30% additional metabolic cost to walk depending on gait speed and amputation level as compared with able-bodied individuals and a fear of falling is pervasive in this community [4],[5], [6]. Many also experience significant gait asymmetry, lower back pain, slower walking speeds, reduced activity levels, and overuse injuries on their sound limb [7],[8].

A properly functioning ankle joint is necessary to produce a symmetric gait pattern among amputees. Able bodied gait data from biomechanics studies are used to determine the moment and ankle angles during one gait cycle on one foot for different speeds [9]. For slower walking speeds there is a linear relationship between moment and angle at the ankle joint [10]. This means that the ankle joint is not adding energy into the gait cycle during these slower speeds and thus acting similar to a passive joint mechanism. This work will demonstrate the design and functionality of a properly tuned passive mechanism that is able to achieve the required functions of able-bodied gait for slow walking speeds.

As walking speeds increase the required moment also increases and a passive system will not be able to provide additional energy necessary for able-bodied gait. The Ruggedized Odyssey Ankle (ROA), a powered ankle-foot prosthesis, is shown to meet the needs of the higher walking speeds. In addition, the intelligent use of springs amplifies the input of the motor through the mechanism to achieve output moments at the ankle joint to provide full-powered running. ROA utilizes a compliant actuator to store the natural braking energy just after heel strike, while a small lightweight motor adds additional energy to the step[11], [12].

Each mechanism, either powered or passive, has a joint stiffness at specific joint angles that correspond with its motion and behavior [11], [13]–[15]. This stiffness can be controlled or forced in powered systems to reflect able bodied joint behavior [9], [10], [16]–[19]. Stiffness can also be uncontrollable but predetermined from optimally designed passive systems [20]–[22].

While using the application of an ankle joint prosthesis, a method for decoupling the joint stiffness from the joint position in any robotic joint is shown. The advantage of this is to combine the optimization of passive system design and natural mechanism characteristics with a powered system. By using the powered system to adjust the mechanism configuration at specific times a joint can naturally (uncontrolled) achieve desired performance during use. Small adjustments are then made only to optimize the passive behavior.

This work will show how a passive system can compensate for a robot manipulators own weight removing the torque from gravity felt at the joint. The gravity compensating mechanisms can then be intelligently adjusted to handle additional end effector moments induced by the environment. As the design allows, there will be physical requirements of each mechanism limiting the range of external moments the adjustable passive joints will be able to compensate for. Benefits of such a device can include reduced power requirements, broader applications from a single robot and increased safety for human machine interaction [23], [24].

CHAPTER 2

BACKGROUND

2.1 PASSIVE ANKLE JOINTS

2.1.1 SACH Foot

First type of prosthetic feet is the solid ankle cushioned heel. This has a cushioned heel to absorb impact and a firm keel that does not flex much but provides stability to the user. The solid ankle means that there is no rotation about the ankle and limits the agility of the amputee. The benefit of these feet is that they are extremely inexpensive and easy to manufacture.

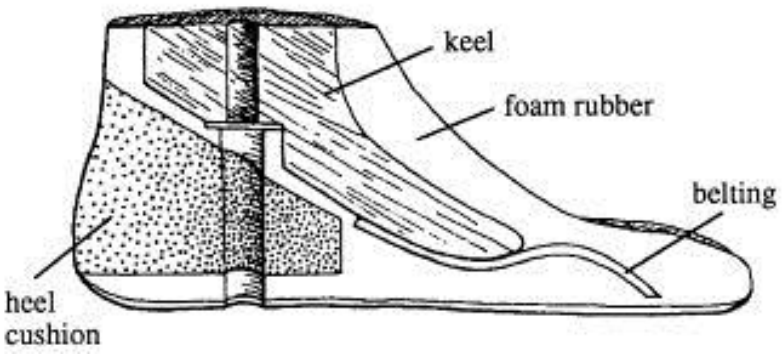

FIGURE 2.1: SOLID ANKLE CUSHIONED HEEL PROSTHETIC FOOT.

2.1.2 ESAR Feet

The next generation of prosthetic feet to come about are the Energy Storage and Return feet. These are based on a simple spring like behavior at the foot. Commonly made from carbon fiber these feet also provide a cushioned, shock absorbing heel strike to the amputee. The added benefit of the ESAR feet is that they also absorb the braking energy of the user during rollover storing it in a spring and return that energy to the user mimicking the push off of an able-bodied gait [14], [18], [25]. Although these feet do not provide the full amount of energy necessary for able-bodied gait they are a step above the non-energy return of the SACH foot [26]–[29]. One example of these types of feet is shown in Fig. 2.2.

FIGURE 2.2: BASIC ENERGY STORAGE AND RETURN PROSTHETIC FEET.

2.1.3 Advanced ESAR Feet

Once the energy storage and return was realized the next objective was to create even more biomechanically sound versions of the ESAR feet and push the limits of energy return in a closed system device. Some first steps include meeting the needs of more active amputees by creating special ESAR feet specifically designed for running [22]. These feet have greater energy storage capabilities as well as increased range of motion to meet the demands of a running gait pattern. Figure 2.3 below shows the Cheetah foot developed by Össur used by amputees for running [30].

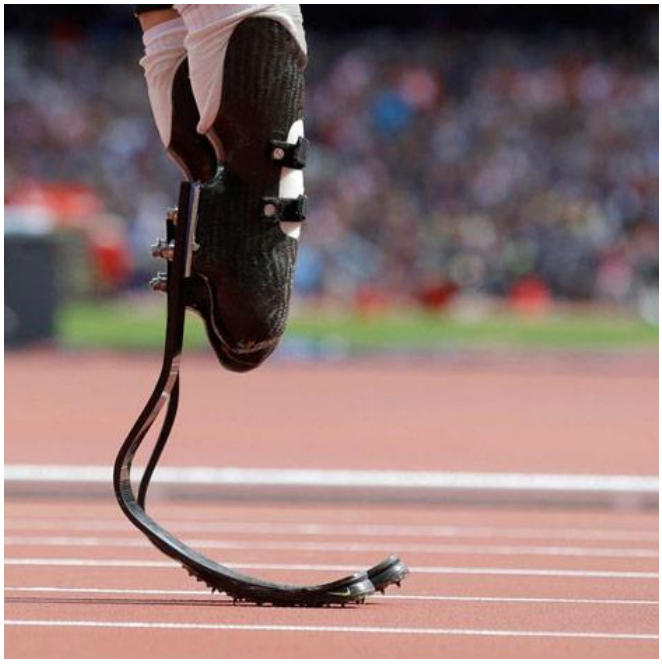

FIGURE 2.3: CHEETAH, AN ESAR RUNNING FOOT.

Other advancements towards able-bodied gait included the use of a 1 DOF joint for proper rotation about the ankle. More types of spring designs began to be used including multiple coil springs in different locations on the foot.

New mechanisms also started to appear that have been shown to create more effective gait patterns at the ankle. In one case a second degree of freedom was introduced in the pylon to absorb the impact of heel strike. Once the pylon was fully compressed the mechanism in the ankle then allowed the braking energy of the amputee to be stored in a coil spring and released back to the user during push off [31].

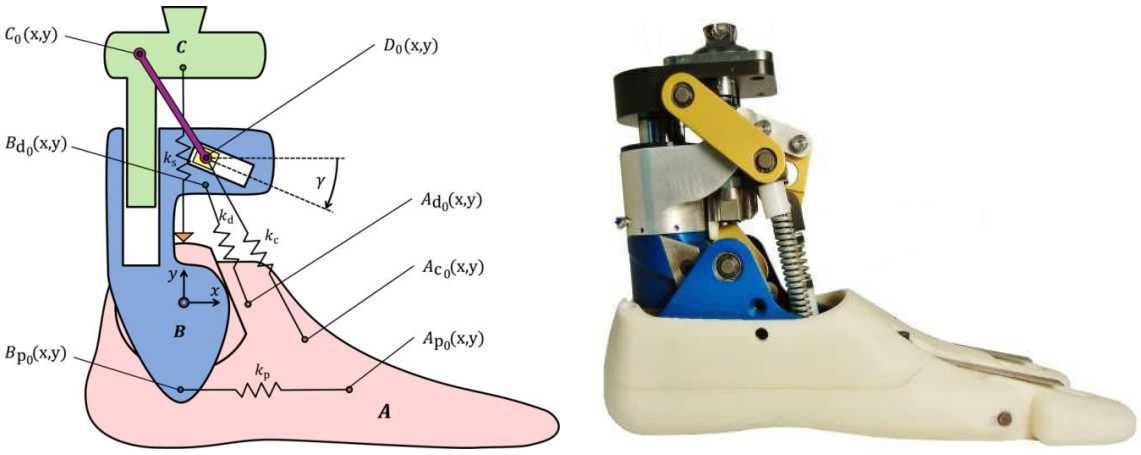

FIGURE 2.4: CAMWALK PASSIVE PROSTHETIC WITH 2 DOF.

Another mechanism more recently used has been a four bar configuration to help remove the reaction torque on the amputee attachment point. The ProFlex by Ossur has 27 degrees of ankle motion and is claimed to have “significantly greater ankle power than conventional carbon fiber feet”. This ankle also “closely mimics regular biomechanics, delivering a proven 11% reduction in load on the contralateral limb” [32].

FIGURE 2.5: PASSIVE PROFLEX BY OSSUR WITH 4-BAR LINKAGE.

There has been other research that demonstrates the importance of the proper timing in energy return among the ESAR feet calling it a Controlled Energy Storage and Return (CESR) [14]. Another form of biomimetic behavior is to match the rollover shape of able-bodied gait [33]–[35]. Most of these passive feet do well on level ground but are not as effective or comfortable on slopes or stairs. Development of a passive prosthetic ankle has been made which adapts to different slopes and still is able to store and return energy to the user [33], [36].

The trend of all these ESAR feet is to be light weight, comfortable and as biomechanically sound as possible in all situations. Although it is impossible to passively achieve greater energy out of the prosthetic system than put in by the users braking energy, it has been shown that for slow to normal walking speeds braking energy from the user is enough [10].

2.2 POWERED ANKLE JOINTS

The overlying theme of current powered ankle-foot prosthesis is that they all use methods of varying the impedance at the ankle joint. Many different mechanisms and control schemes are being tested to recreate the non-linear stiffness of the ankle joint during gait. This section provides an overview of how some of the many powered ankle-foot prosthesis fit into four different categories of how variable impedance is achieved. These categories include: equilibrium controlled stiffness, structural controlled stiffness, mechanically designed stiffness and pure stiffness control. The work here does not attempt to categorize the methods of impedance control by order of effectiveness but is only an overview of a few current methods being used in research.

Compliant actuators are used because of their ability to store energy through elastic deformation and return energy when needed. These mechanisms have equilibrium positions where no output torque is generated. This does not mean there cannot be energy stored internally in the system at these equilibrium positions but that the energy is contained or balanced in its current state. Compliant actuators with the ability to change compliance or stiffness are considered Variable Impedance Actuators (VIA) [24].

2.2.1 Equilibrium Controlled Stiffness

This method is when one end of a spring is controlled by a motor and controller while the other end is attached to the end effector of the joint robot. This actively changes the equilibrium point of the spring and thus changing the effective stiffness felt at the joint at all times, sometimes called virtual stiffness [37]. These types of actuators are called Series Elastic Actuators (SEA) [38]. Some have also used the SEA in combination with an additional parallel spring [39]–[41].

This is the most common method of control for powered ankle joints. The challenge when doing this is the timing and control of the equilibrium point for the desired task such as walking or running. The energy can be large unless mechanical advantages are built into the system. A SEA is not separated from the load but by inserting compliance in between the load and motor the motor speeds can be reduced [42].

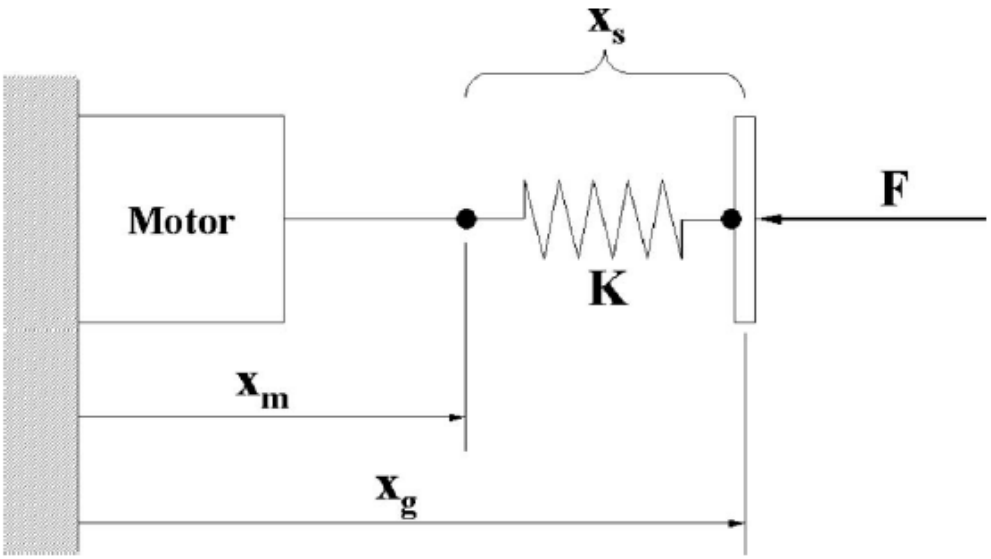

FIGURE 2.6: SERIES ELASTIC ACTUATOR LAYOUT.

Robotic Tendon [43], [44], The proximal side of the spring was positioned and controlled to obtain correct angles and moments and the distal side of the spring is not controlled. This is done using a continuous controller based on the phase angle of the tibia to adjust the proximal side of spring, effectively adjusting the equilibrium point of the spring [45]–[47]. When the actuation timing is controlled properly the negative power can be stored in the series spring then returned to the system reducing the power needed by the motor (Holgate et al., 2017, Power amplification results in Ch. 4).

FIGURE 2.7: HERR DEVELOPED A SERIES OF PROTOTYPE ANKLES THAT USED A SERIES ELASTIC ACTUATOR WITH AN ADDITIONAL SPRING IN PARALLEL TO THE LOAD PATH. THE ANKLE WAS COMMERCIALIZED UNDER THE BIONX BRAND, COURTESY OF WWW.BIONX.COM.

Dr. Hugh Herr at MIT has developed a method of using a SEA in an ankle-foot prosthesis to provide a powered push off for transtibial amputees. These prosthetic devices, shown in Fig. 2.7, are sold under the brand BionX and is said to be the world's first actively powered foot and ankle [48]. Sensors on the prosthesis use measurements from the user's motion and compare it to able-bodied data in order to predict user intention. The SEA is used to control input position to the spring modulating the ankle joint stiffness during gait. In addition to the SEA is a parallel spring which allows a second load path reducing the torque input necessary by the motor [40], [49]. Using a finite-state based control scheme the SEA and parallel spring effectively control output torque providing powered push off and mimicking the nonlinear stiffness in able-bodied gait [50]. The prosthesis has shown improvement in amputee's metabolic cost by up to 20% when using the device for walking when compared with other ESAR feet [40], [49].

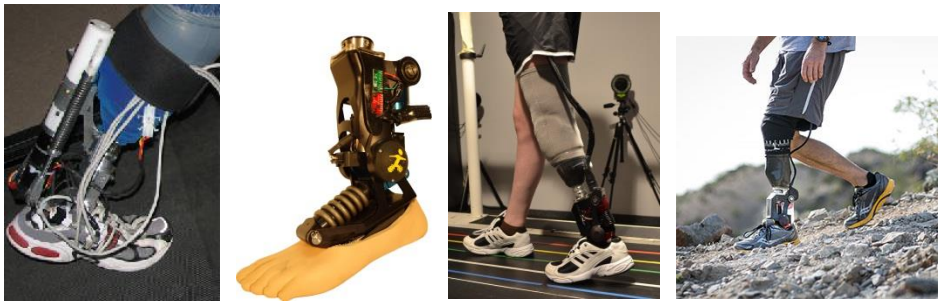

FIGURE 2.8: THE SPARKY ANKLE ALLOWED USERS TO WALK, RUN, JUMP, AND WALK UP AND DOWN MOUNTAINS.

Dr. Tom Sugar at ASU has also developed a method of using a SEA in an ankle-foot prosthesis to provide full powered push off for transtibial amputees [51]–[53]. These prosthetic devices, shown in Fig. 2.8, are sold under the brand SpringActive and is said to provide full powered walking as well as running (Holgate et al., 2017). Sensors on the prosthesis use measurements from the user's tibia motion and compare it to able-bodied data in order to predict user intention [45]–[47]. The SEA is used to control input position to the spring modulating the ankle joint stiffness during gait. The SEA used for SPARKy has been called the robotic tendon and has provided enhanced ankle dynamics achieving 100% push of power while maintaining gait kinematics [43], [53]. The robotic tendon is a SEA that mimics the biological muscle tendon complex and when combined with the continuous control scheme the SEA effectively controls output torque mimicking the nonlinear stiffness in able-bodied gait [43], [44].

FIGURE 2.9: A TRANS-FEMORAL PROSTHESIS WAS DEVELOPED THAT POWERED BOTH THE ANKLE AND KNEE. CURRENT RESEARCH HAS FOCUSED ON AN ANKLE DEVICE AS WELL.

Dr. Goldfarb at Vanderbilt University has been developing trans-femoral prosthetics incorporating an ankle and knee device to help with above the knee amputations [41], [54], [55]. Figure 2.9 shows a few iterations of these devices capable of walking as well as running and allow for up hill and down hill walking [19], [54]. Sensors in the device use joint position and velocity combined with tibia acceleration and absolute angular velocity to properly assist gait. A slider crank mechanism is used at the knee and ankle to regulate each joints torques. The ankle design developed also incorporates the use of a parallel spring to supplement the restoring torque needed after dorsiflexion. They are using an impedance type control scheme to mimic the stiffness of an able bodied joint. The device has shown to transfer significant energy to the user [56], [41].

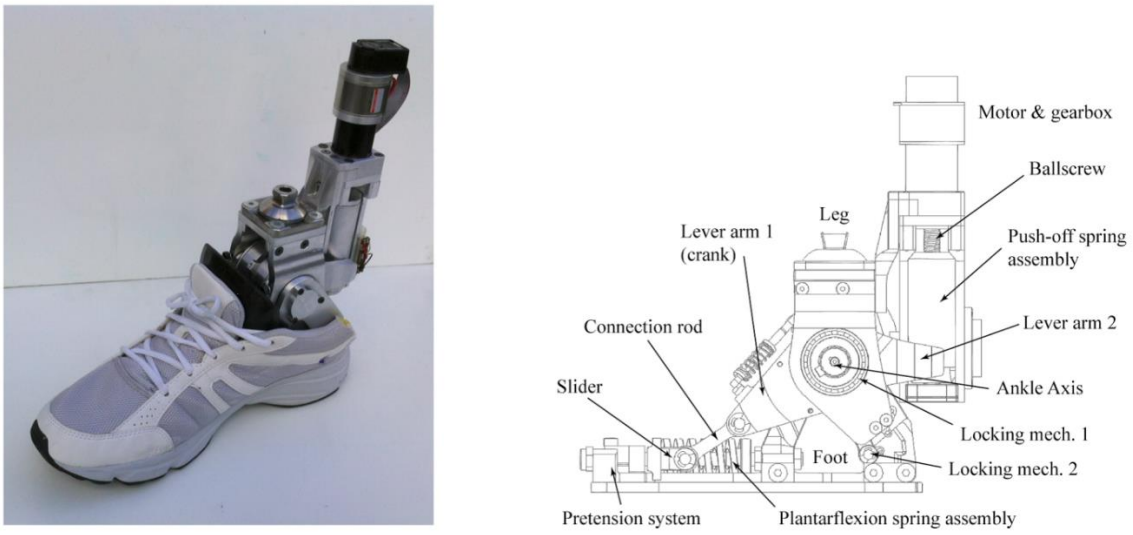

FIGURE 2.10: THE AMP 2 DEVICE USED A LOCKING CLUTCH TO STORE ENERGY IN THE PO (PUSH OFF) SPRING. THE AMP 3 DEVICE USED A RESETTABLE, OVERRUNNING CLUTCH AT THE ANKLE AXIS TO ADJUST THE STARTING ANGLE OF THE DEVICE.

Dr. Lefeber at Vrije Universiteit Brussel has also used SEA in a unique prosthetic system called AMP 2 & AMP 3, see Fig. 2.10 [18], [57]–[60]. These ankle-foot prosthesis use a unique spring and clutch mechanisms to store and release energy. The AMP 2 stores energy in a specific spring to be used later in Push Off. The AMP 3 uses a clutch device to set the "home Position" in the ankle changing the starting angle of the device depending on the terrain [61].

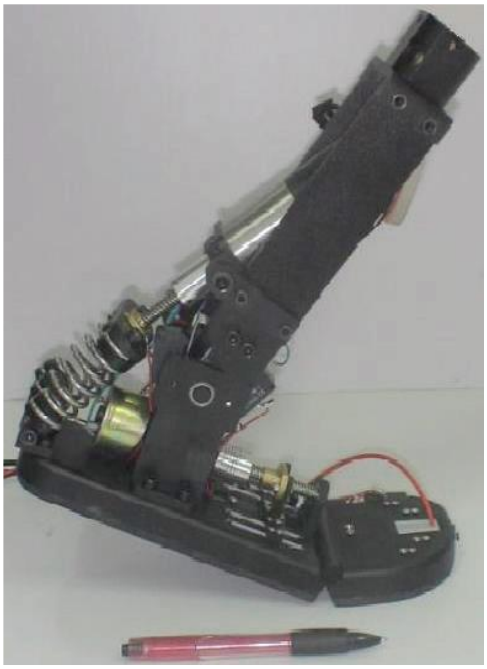

FIGURE 2.11: SERIES, ELASTIC ACTUATORS ARE USED TO CONTROL THE MOMENTS ABOUT THE ANKLE AND TOE.

Dr. Wang at Peking University has used SEA to develop an ankle-foot prosthesis with the ability to apply torque and the toe as well as the ankle [62]. The PANTOE ankle, shown in Fig. 2.11, has two separate SEA each functioning to provide powered push off for the amputee. By using SEA this ankle device can also function as a passive device using the springs and not the motors at the ankle and toe. Testing has shown the PANTOE device improves amputee gait when compared to commercially available passive devices [63], [64].

FIGURE 2.12: A SPRING BASED ANKLE WAS CONTROLLED USING ADAPTIVE OSCILLATORS.

At the Universite Catholique de Louvain researchers have developed a SEA driven ankle-foot prosthesis capable of 2DOF motion, shown in Fig. 2.12 [65]. While only one DOF is controlled the inversion eversion of the prosthesis is passive. The SEA was controlled using an adaptive oscillators to provide ankle joint movement [66].

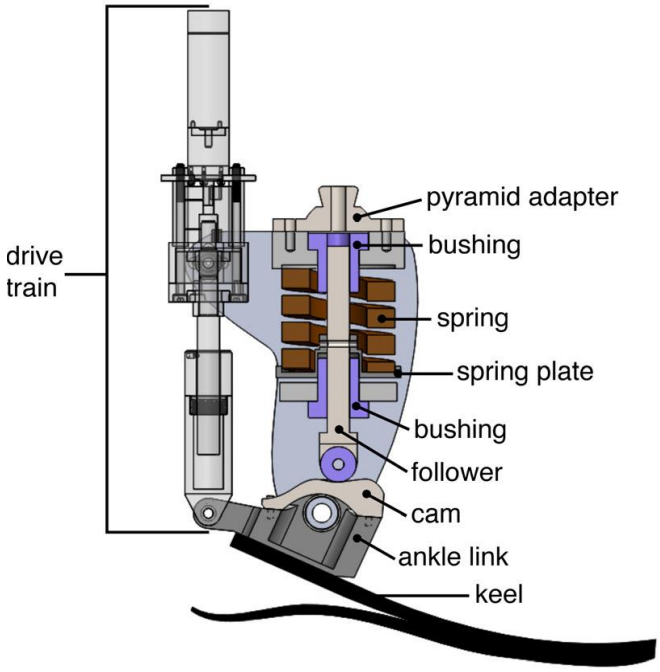

FIGURE 2.13: UNIVERSITY OF WASHINGTON ANKLE CONTROLS TORQUE IN THE SAGITTAL PLANE WITH A PARALLEL SPRING AND CAM MECHANISM CREATING NON-LINEAR STIFFNESS.

Dr. Klute at the University of Washington developed a transtibial ankle-foot prosthesis using a SEA [39]. In addition to the SEA the ankle has an additional spring in parallel to reduce peak torque required by the motor like others have done. Figure 2.13 shows that this parallel spring is also equipped with a cam and roller which creates nonlinearity of the ankle joint passively. Through testing it is shown that by having the cam with the parallel spring the peak motor torque is reduced 74%.

2.2.2 Structural Controlled Stiffness

This method is where you change the actual structure being used for stiffness of the joint. An example of this is found in the Jack Spring where a different number of coils is grabbed on the spring which changes the structure being used for stiffness [67], [68]. Figure 2.14 shows the vsaUT mechanism in which the effective lever arm distance is controllable causing a change in stiffness [69], [70]. Another mechanism that uses a similar concept is the AwAS and AwAS II [71]–[73].

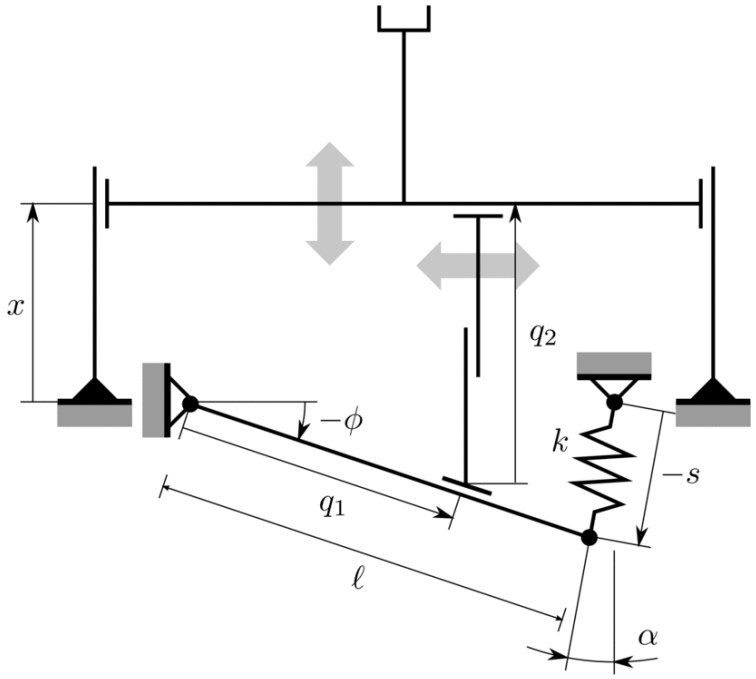

FIGURE 2.14: A VARIABLE STIFFNESS ACTUATOR (VSAUT) BY USING VARIABLE LENGTH LEVER ARM.

The stiffness and the position in these types of mechanisms are changed independently. For the vsaUT and AwAS mechanism the passive stiffness is linear in form but when active that linear stiffness can be adjusted non-linearly. These types of mechanisms make changes to their transmission ratio between the output and the passive spring members that define stiffness. The Maccepa series actuators also do this but the link between the output and spring is passively non-linear [74], [75]. The non-linear stiffness can also be adjusted in these designs but the position and stiffness are coupled by the change in structure.

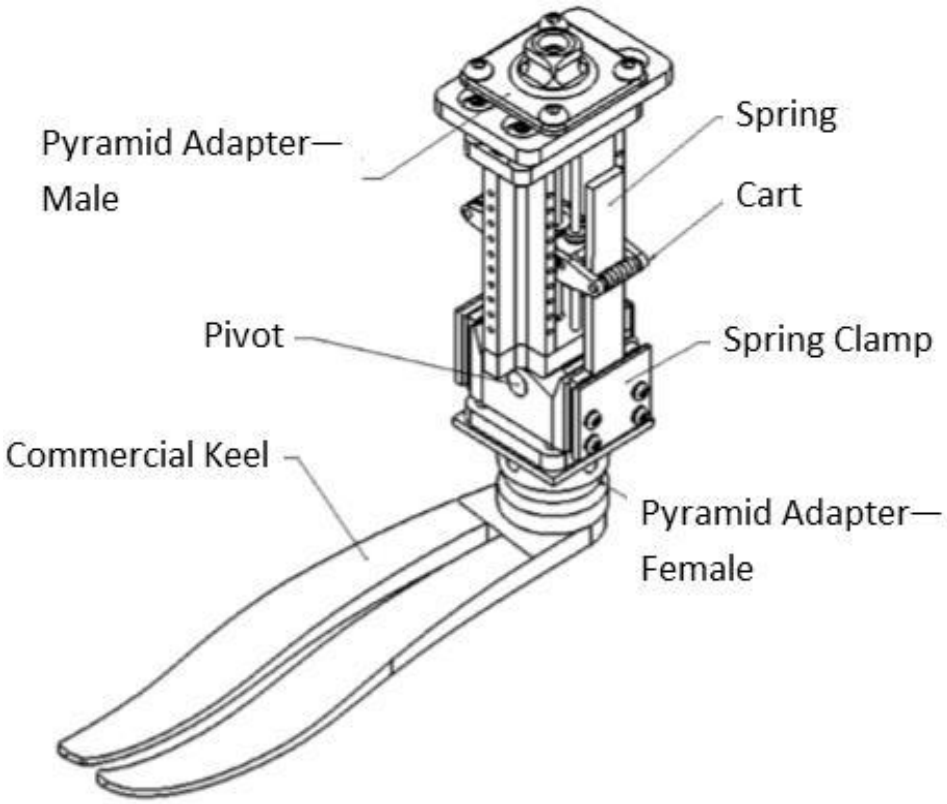

FIGURE 2.15: UNIVERSITY OF WASHINGTON ANKLE CHANGES BENDING POINT ON LEAF SPRING CONTROLLING THE STIFFNESS IN THE CORONAL PLANE.

Dr. Klute at the University of Washington has also developed a transtibial ankle-foot prosthesis using a structural controlled stiffness in the coronal plane, see Fig. 2.15 [76]. The stiffness is changed in the device when the bending point on a leaf spring is controlled through an actuator.

2.2.3 Mechanically Defined Stiffness

Mechanically defined stiffness includes methods of changing the mechanism configuration to incorporate mechanical advantages or non-linearity in speed ratios between links. Mechanical ratio of input movement of lever arm to a distance movement between two points of the mechanism is used in the MACCEPA device [74]. Combining the non-linearity of the mechanism with a cam at the joint the MACCEPA device is able to target specific non-linear stiffness requirements [75], [77]. Figure 2.16 shows an example of the MACCEPA configuration.

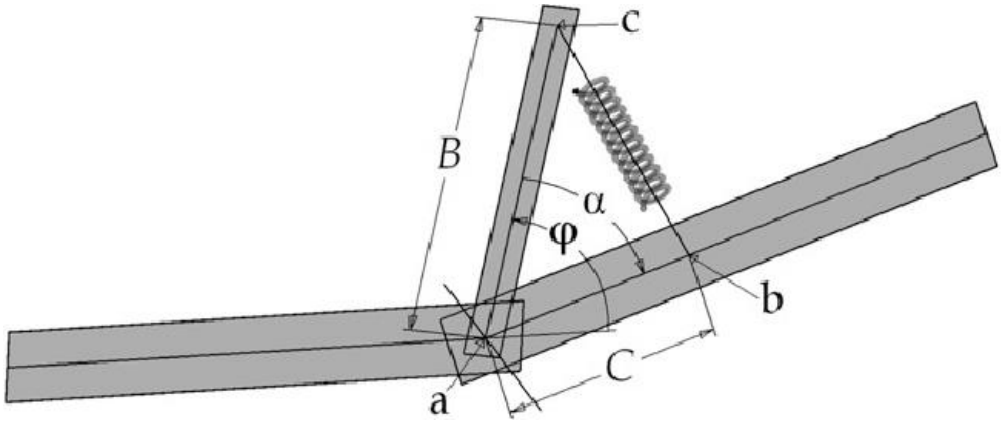

FIGURE 2.16: MACCEPA DEVICE GENERAL CONFIGURATION.

Dr. Lefeber at Vrije Universiteit Brussel has also used the MACCEPA design in a unique transfemoral prosthetic system called CYBERLEGs [78]. The ankle-foot prosthesis portion of the leg uses the MACCEPA device to provide variable ankle joint stiffness. By producing a variable stiffness in this way the ankle joint can have non-

linearity but be adjusted for stride length, walking speed and changes in terrain. The adjustments are made by a small motor on the MACCEPA device and need multiple steps to fully adjust to a new gait pattern.

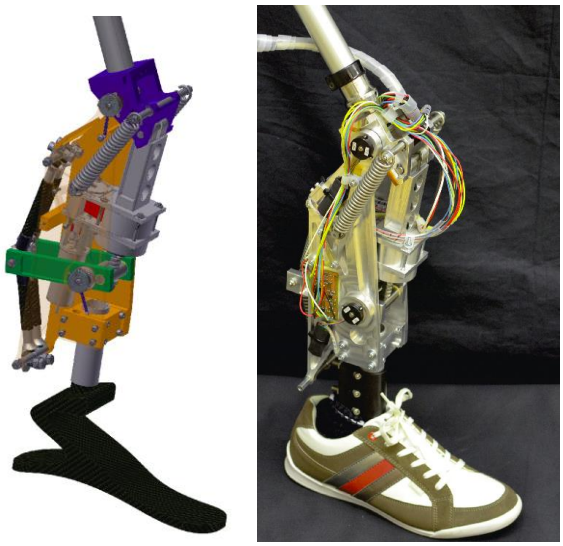

FIGURE 2.17: A SEA IS COMBINED WITH A NONLINEAR MECHANICAL TRANSMISSION IN A TRANSFEMORAL PROSTHESIS.

Reiner and Vallery from ETH Zurich and TU Delft have designed a trans-femoral prosthesis using a SEA attached to a joint mechanism, shown in Fig. 2.17 [79]. The joint mechanism uses mechanically designed ratios to couple actuator stiffness with joint angle. The research shows a method was developed to quantify impedance profiles similar to physiological behavior then the mechanically designed stiffness was modeled after these profiles. The goal was to reduce power necessary for actuation and to better follow able-bodied joint characteristics during gait.

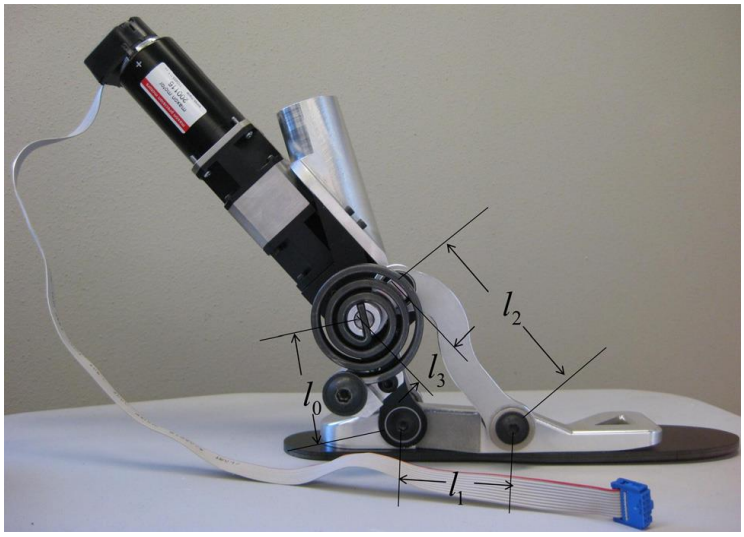

FIGURE 2.18: A TORSIONAL SPRING AND FOUR-BAR LINKAGE IS USED TO CREATE A NON-LINEAR STIFFNESS AT THE ANKLE JOINT.

Dr. Vogelwede at Marquette University has developed a novel four bar linkage with a torsional spring in an ankle-foot prosthesis, shown in Fig. 2.18 [80]. The four bar linkage takes advantage of mechanical ratios of joint rotation to overall shank rotation to produce a non-linear effect. Thus when coupled with a linear torsional spring the ankle achieves powered push-off in a non-linear manner, see Figure 2.18. The current mechanical configuration is tailored to the joint dynamics of a walking gait pattern. The ankle-foot prosthesis testing showed improved moment profile matching to able-bodied data than other passive prosthetics [81].

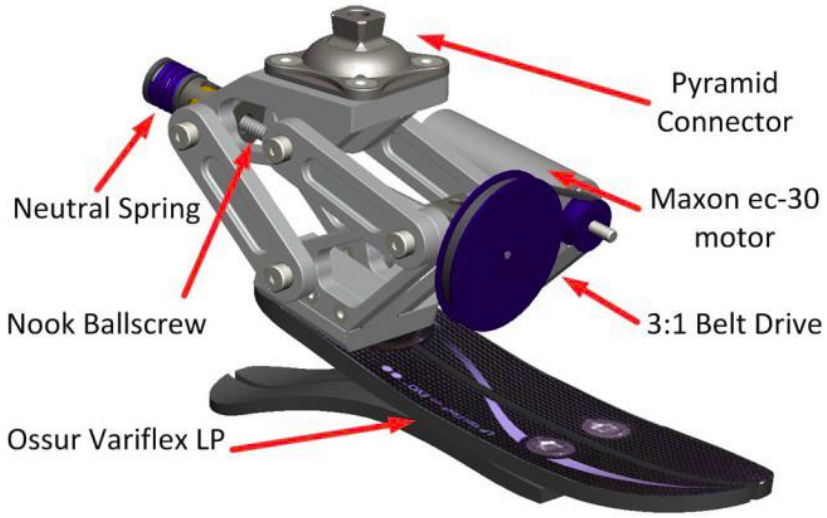

FIGURE 2.19: A NON-ANTHROPOMORPHIC DESIGN TO REDUCE SOCKET FORCES.

Researchers in Dr. Goldfarb's lab at University Massachusetts have used a similar method of using advantages in mechanism design while producing a powered push off [82]. Shown in Fig. 2.19 is the non-anthropomorphic ankle design developed to reduce the socket interface moments while still achieving a proper gait cycle.

These 4 bar systems allow stiffness to be a function of ankle angle in a non-linear relationship. They are also controlled by the motor in series with springs to allow the control scheme to change moment by adjusting the spring tension. This method is the combination of the abilities found in a SEA but with a starting ankle joint stiffness curve more similar to able-bodied data.

2.2.4 Pure Stiffness Control

In most cases when changing physical parameters of a mechanism the output stiffness changes as well. There are some mechanisms that demonstrate a unique way to completely decouple the actuator stiffness from its position. An example of this is the use of antagonistic springs. Figure 2.20 shows a variable stiffness actuator (VSA) where stiffness can be changed without changing the joint position by actuating the motors together [83]. Position is changed separately without changing stiffness by actuating the motors in opposite directions.

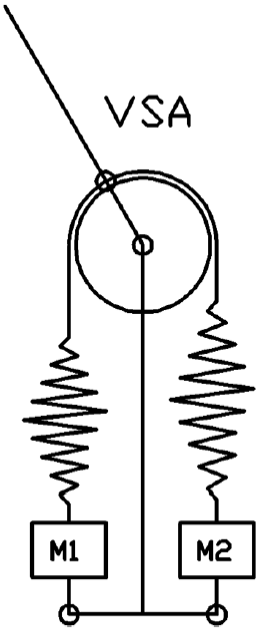

FIGURE 2.20: VSA USING ANTAGONISTIC SEA TO DECOUPLE JOINT STIFFNESS AND POSITION.

Another configuration is the VSJ which only applies a single motor attached to the distal end of both springs that will always adjust the tension in the springs simultaneously [77]. A second motor is then used directly on the joint to adjust position. Other devices use the advantages of antagonistic springs as well as a non-linear transmission ratio. The VSA-HD gets a non-linear transmission ratio by use of a 4-bar linkage with a configuration providing non-linear speed ratios between output and input [84]. These different variable stiffness actuators have been compared in research for different requirements of energy and efficiency [24], [23], [66].

2.3 GRAVITY COMPENSATION METHODS

2.3.1 History of gravity compensation devices

The compliant mechanism to balance the joint moments caused by gravity have sometimes been labeled as an equilibrator. In early designs the methods described a spring which has no free length called a zero free length springs [85]–[87]. Figure 2.21 shows the simple configuration of one of these gravity compensation mechanisms using a zero free length spring.

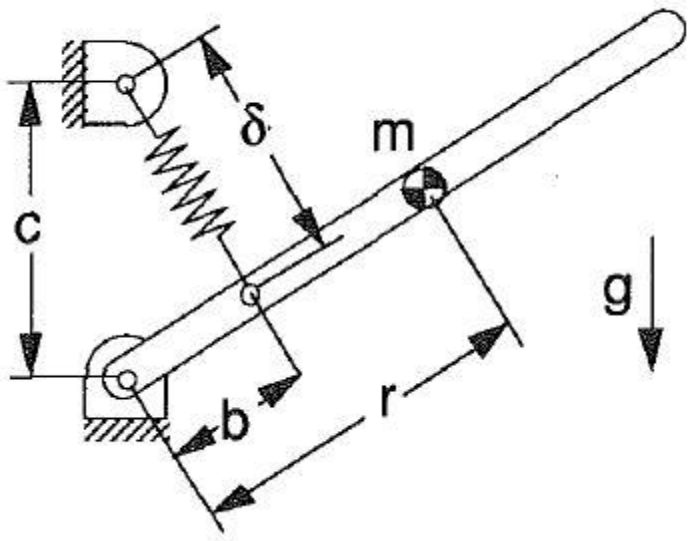

FIGURE 2.21: GRAVITY COMPENSATION ON A SINGLE DEGREE OF FREEDOM ROTATABLE BODY.

This equilibrator has perfect static balancing of the rotatable link for every link orientation using the relationship from Eq. (2.1) where ‘m’ is the mass of the link, ‘g’ is the acceleration due to gravity and ‘k’ is the spring stiffness while dimensions ‘r’, ‘b’ and ‘c’ are shown in Fig. 2.21 [88], [89].

$$\mathrm{m}gr = kbc \qquad (2.1)$$

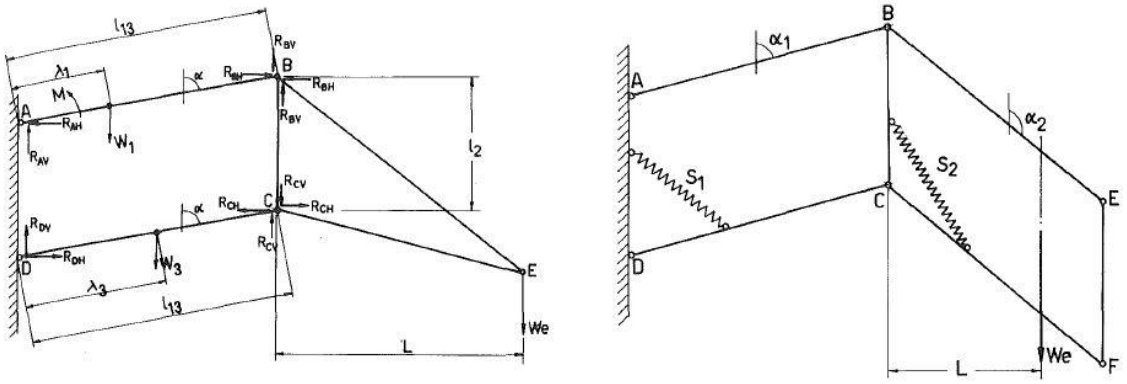

FIGURE 2.22: EQUILIBRATION OF 2-LINK OPEN LOOP REVOLUTE JOINT KINEMATIC CHAIN.

This method has been extended further by adding multiple springs and also moved into three dimensional configurations [88], [90], [91]. Further changes were made to add additional linkages in an n-link open or closed loop revolute joint kinematic chain. Figure 2.22 shows how the weight on the end of the chain does not change the requirements of "equilibrant moment" in ABCD while Fig. 2.23 shows the balancing of a 7-link open loop revolute joint kinematic chain [92].

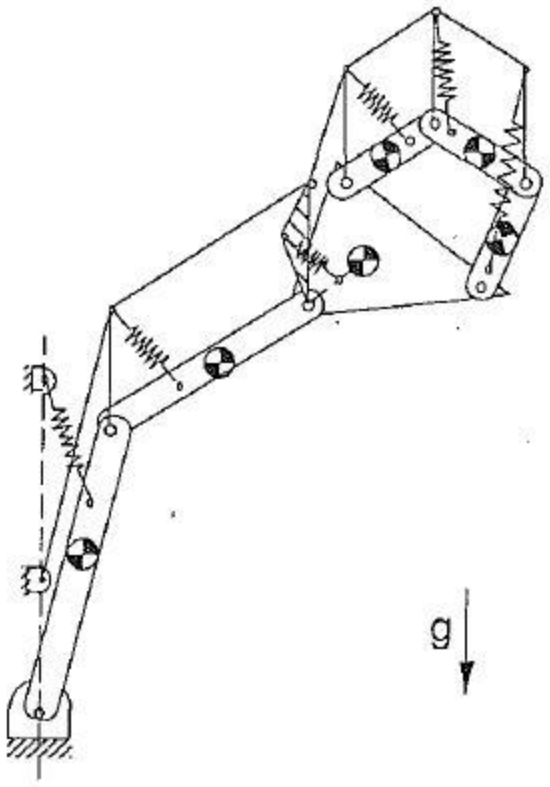

FIGURE 2.23: EQUILIBRATION OF 7-LINK OPEN LOOP REVOLUTE JOINT KINEMATIC CHAIN.

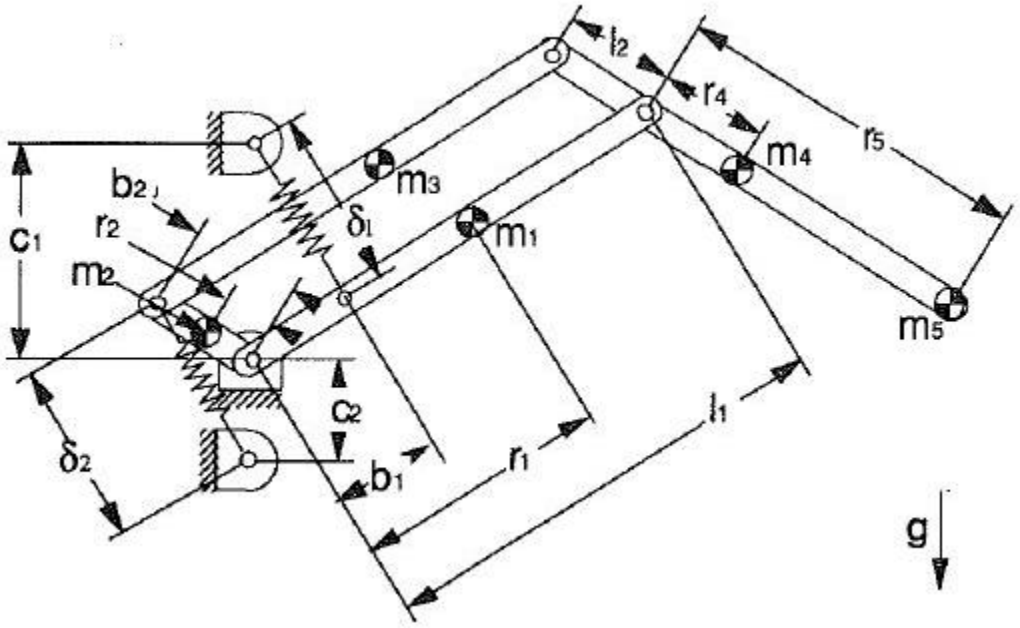

FIGURE 2.24: TWO-DEGREE OF FREEDOM EQUILIBRATING SYSTEM.

More research was done to use pantograph linkages to move all the equilibrating springs to the base of the mechanism. An example is shown in Fig. 2.24 where the equilibration is achieved by satisfying Eq. (2.2) and Eq. (2.3) below [93].

$$[m_1 r_1 + m_3 r_3 + m_4 l_1 + m_5 l_1] g = k_1 b_1 c_1 \tag{2.2}$$

$$[m_2 r_2 + m_3 l_2 - m_4 r_4 - m_5 r_5] = k_2 b_2 c_2 \tag{2.3}$$

2.3.2 Gravity Compensation Examples

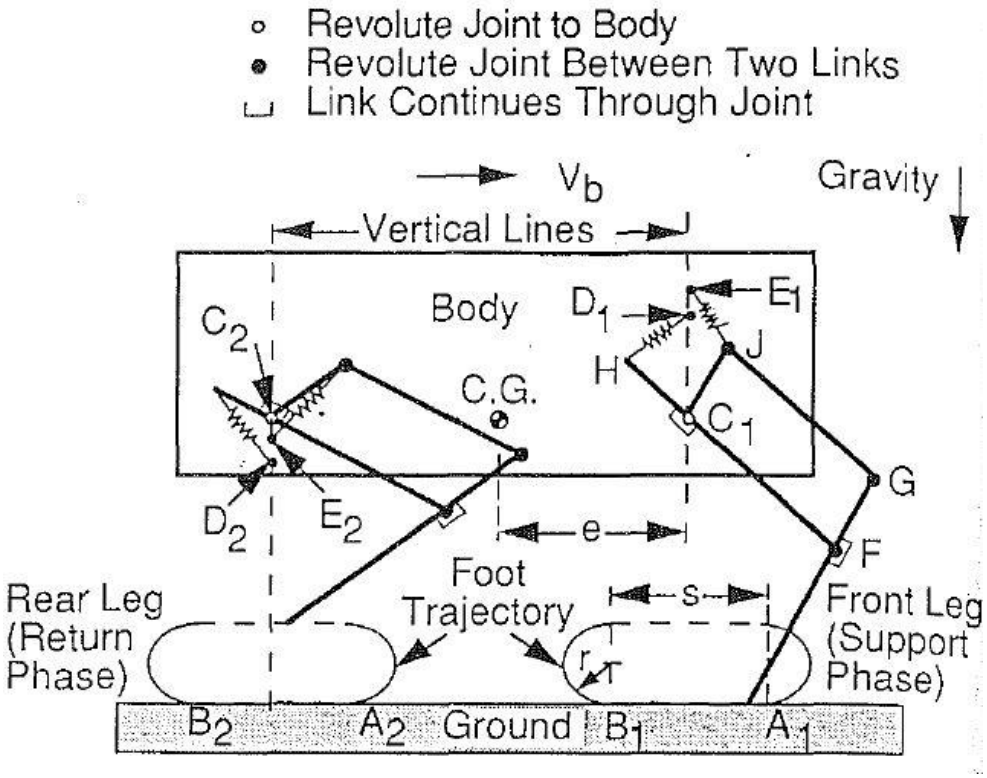

FIGURE 2.25: GRAVITY BALANCED QUADRUPED USING ZERO FREE LENGTH SPRINGS.

Gravity compensation methods have been applied in many different ways and continue to be used. An example is the unique way of balancing a quadruped for walking using zero free length springs in two separate configurations [94]. Figure 2.25 shows the quadruped with the left leg and right leg in two different configurations of gravity compensation. The left leg is configured to balance the mass of the leg itself with the influences of gravity while it swings forward to prepare for the next step. The right leg is configured to balance the mass of the body of the robot while the foot propels the body forward.

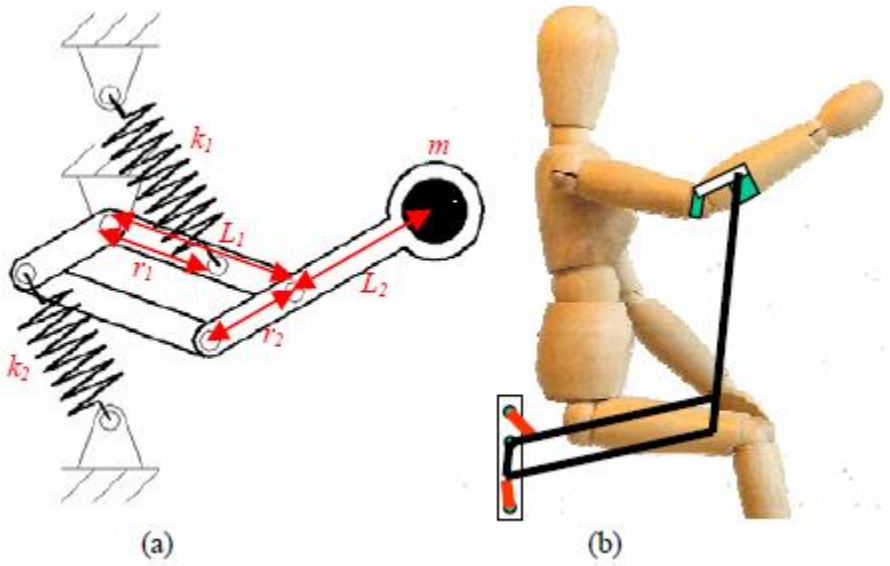

FIGURE 2.26. THE ARMON DEVICE SUPPORTING USERS ARM WEIGHT.

More recent work has been done to develop novel uses for the gravity compensating mechanisms. Dr. Herder has shown the equilibrator methods used to design an anthropomorphic robot arm [95]. This work also recognizes the ability to implement stiffness control in combination with gravity compensation to make safer human machine interaction. A novel application of statically balanced robot arms is seen in the development of ARMON [96]. This device aids people with neuromuscular diseases to assist their muscles in supporting the weight of their own arm [97]. Figure 2.26 shows the ARMON concept and how it uses a parallelogram linkage to keep the balancing springs at the base of the device.

CHAPTER 3

LIGHTWEIGHT ENERGY ASSISTIVE FOOT (LEAF)

There are many applications where passive joints are used for practical reasons. The field of prosthetics is one of these applications and with a well-tuned passive system a prosthetic ankle can return an amputee's capability and mobility. Many different types of passive prosthetic joints have been designed in order to replace ankle and knee joints. This work focuses on the ankle joint. A Lightweight Energy Assistive Foot (LEAF) is a passive joint prosthetic created to replace the ankle joint.

A properly functioning ankle joint is necessary to produce a symmetric gait pattern among amputees. Able bodied gait data from biomechanics studies is used to determine the moment and ankle angles during one gait cycle on one foot for different speeds [9]. A gait cycle is defined as heel strike to the next heel strike on the same foot. As walking speeds change the required moment also changes. Although the moment changes in a nonlinear pattern for increased walking speeds, prior research has proven that for slower walking speeds there is a linear relationship between moment and angle at the ankle joint [10]. This means that the ankle joint is not adding energy into the gait cycle during these slower speeds and thus acting similar to a passive joint mechanism.

The purpose of the LEAF project was to show that a passive joint can be developed to achieve the requirements for able bodied gait at slower walking speeds. It is also important for the passive ankle to achieve proper energy return when walking on a range of inclined surfaces. The energy return will come from an optimized spring which will store the energy during rollover of the gait cycle. The amount of energy available for return to the user will highly depend on the efficiency of energy storage in the spring and effectiveness of converting the stored energy in the spring system to a propelling force similar to able bodied gait.

There are many energy storage and release feet (ESAR) on the market using carbon fiber keel springs. This work differs by adding a revolute joint at the ankle so the LEAF system can adjust to inclines and return energy at the right time.

3.1 THEORETICAL PREDICTIONS AND ANALYSIS

In order for the passive ankle prosthesis to return energy to the amputee there must be energy available to store and release from the gait cycle. The able bodied ankle angle and moment data allow the power to be calculated throughout the gait cycle. This power data is then integrated to find the energy available for storage. The available energy targeted by the LEAF design is found in the rollover portion of the gait particularly from about 10 – 50 percent of the gait cycle. During this period the ankle is using energy to brake the falling motion of the body. The braking motion is ideal for energy harvesting because the mechanism can use the kinetic energy of the falling body by converting it into potential energy in the mechanism. It may be possible to also capture the impact energy from heel strike and release it during push off but this mechanism will only focus on the energy stored from rollover.

The theoretical maximum amount of energy which may be stored by the prosthetic ankle must be considered in order to compare the efficiency of this design with able bodied walking. The power from one step in the gait cycle was calculated shown in Fig. 3.1 using standard biomechanical data [9]. The different portions of the gait cycle power curve were then integrated to find the energy from each of the desired sections. Using this method, heel strike yielded 0.64 J, rollover had 7.43 J, while push off totaled 27.29 J. It was found that the theoretical maximum amount of energy which might be stored during rollover is about 8.07 J. In this set of data during normal/faster walking, a net positive amount of energy is needed to walk. Because we are developing a passive

system, it is not possible to put in additional energy. (We have developed the SPARKy and Odyssey ankles that can supply net positive work [51], [98].)

The 8 Joules of energy theoretically available is only 30% of the positive energy that this able bodied person used during toe off at this speed. Even with a prosthetic design that is perfectly efficient at storing and reusing these 8 Joules it is not enough to achieve a perfectly similar able bodied gait. In order for the mechanism to be maximally effective it will need to aim to store more energy than able bodied ankle shows without compromising how it feels to the amputee.

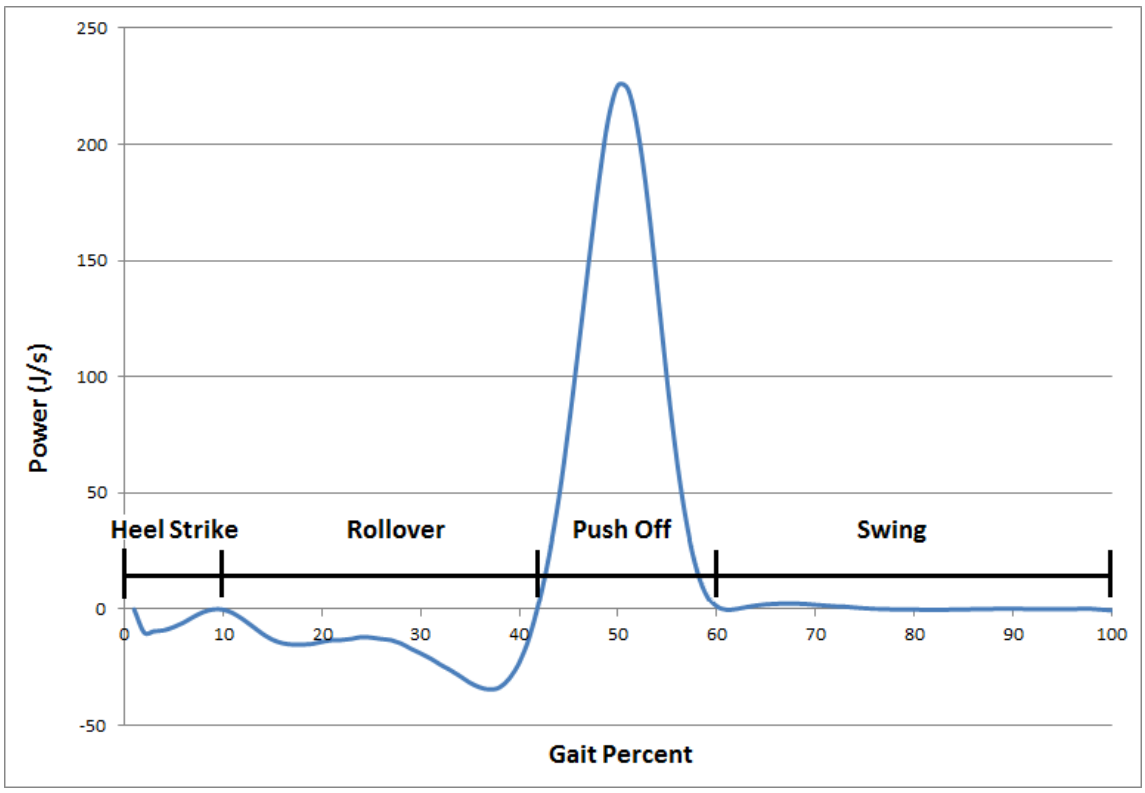

FIGURE 3.1: ANKLE JOINT POWER CURVE THROUGH ONE GAIT CYCLE INTEGRATED TO SHOW WORK DONE FOR SPECIFIC SECTIONS OF THE GAIT CYCLE

Energy contained in an ankle joint is calculated using the torsional stiffness of the joint. Torsional stiffness is defined as a change in moment per change in angle. In order to define the torsional stiffness of the ankle joint during gait and thus find the ankle energy during a specific rotation the ankle moment vs. ankle angle plot is analyzed. Figure 3.2 shows the moment vs. angle plot for able bodied data. In order to visualize energy storage potential during rollover this able bodied data is compared to the predicted behavior of a linear spring of stiffness 325000 N/m with a constant lever arm at 36 mm. (Note, by using the torque angle curve, one can only calculate a quasi-stiffness parameter. The instantaneous derivative at each point will give the exact stiffness value.)

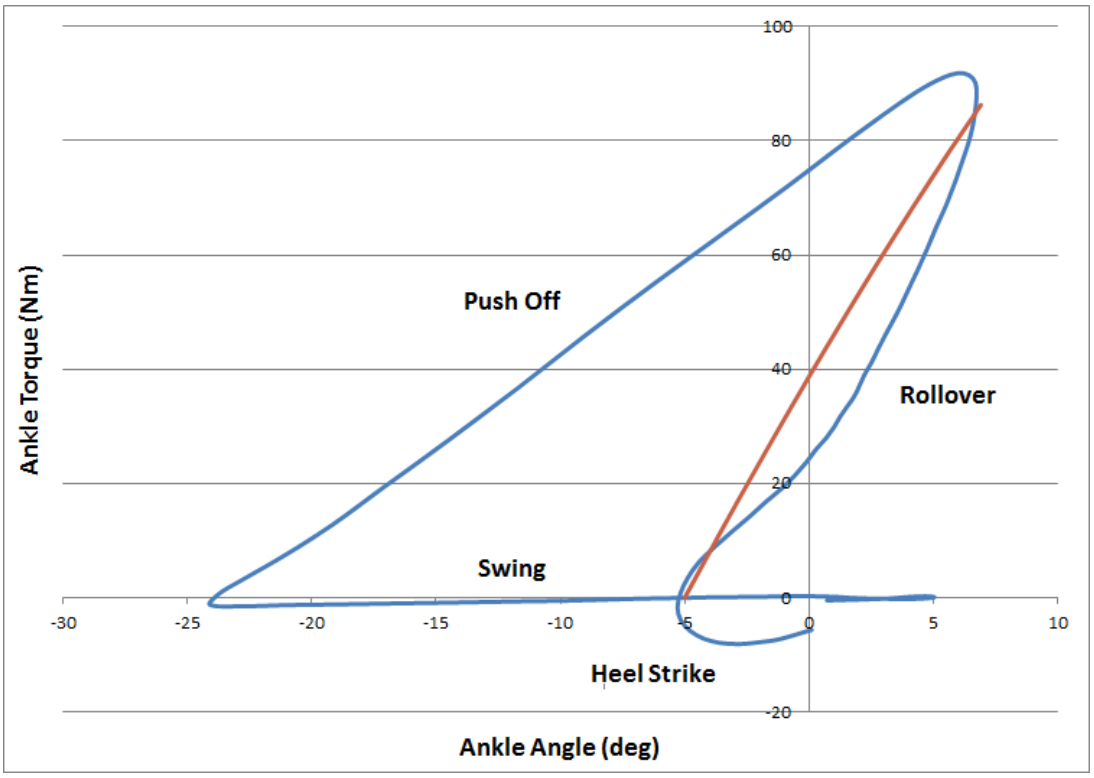

FIGURE 3.2: ANKLE MOMENT VS ANGLE GRAPH FOR ABLE-BODIED GAIT (BLUE) PREDICTED MECHANISM BEHAVIOR BASED ON 325KN/M SPRING WITH A 36MM LEVER ARM (RED)

It is obvious from the comparison in Fig. 3.2 that a linear moment vs. angle behavior comes from a linear torsional stiffness and can be replicated with a simple spring and lever arm mechanism [13], [99], [100]. The rollover portion of the gait cycle can be reproduced passively through a properly tuned mechanism but the release of energy during push off cannot be mimicked by the same device at this walking speed. In order for a simple passive mechanism to mimic the entire gait cycle, the push off portion of the gait cycle can only require as much energy as the rollover portion can provide.

Past research shows that the moment vs angle curve is dependent on walking speed [101]–[103]. More importantly, it has been found that the area inside the moment vs. ankle angle curve approaches zero as subjects reach normal walking speeds [10], [36]. In the same study, it is also evident that the rollover portion of the gait is fairly similar for slow to normal walking speeds. Generally this means that the energy available for storage in a passive system will not be sensitive to speed changes in the range of slow walking.

Based on this theoretical data the ankle can only be effective during certain walking speeds [10], [36]. As walking speeds increase so does the energy necessary to achieve able bodied gait. For slow speeds the passive ankle device should be able to achieve a similar moment vs angle curve. The challenge is to create a device that efficiently stores the most energy possible during heel strike and rollover and then release it smoothly during push off.

3.2 SYSTEM FUNCTIONALITY DESIGN

After careful consideration and analysis of the able bodied data, four specific design criteria were chosen for the LEAF. The ankle foot prosthesis should match the ground slope within a certain range, allow for maximum and efficient energy storage from rollover, smoothly release the stored energy during push off, and properly raise the toe during swing phase resetting the ankle for the next step. These four steps are displayed in Fig. 3.3 in relation with the stages of the gait cycle.

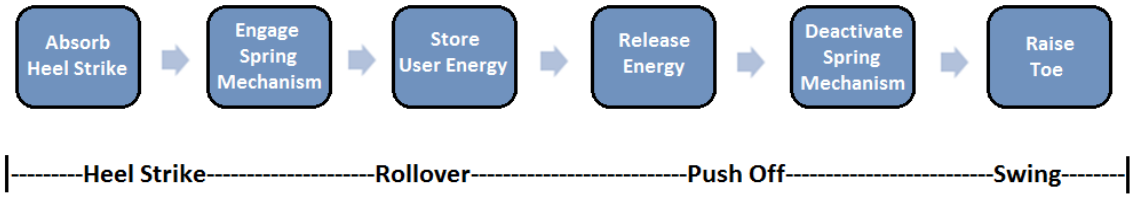

FIGURE 3.3: FUNCTIONAL BLOCK DIAGRAM OF THE CONCEPTUAL DESIGN OVER THE GAIT CYCLE.

A spring system was the optimal choice for energy storage because springs are efficient at storing energy and then quickly returning it while having large ranges of motion [11]. The design requirements are accomplished with two separate subsystems. The first or lower system is responsible for absorbing the heel strike while matching the ground slope as well as raising the toe during swing phase to prepare for the next heel strike. The second or upper system is designed for energy storage during rollover and energy return during push off for the proper ankle angles. Figure 3.4 shows the mechanical device with the two subsystems labeled.

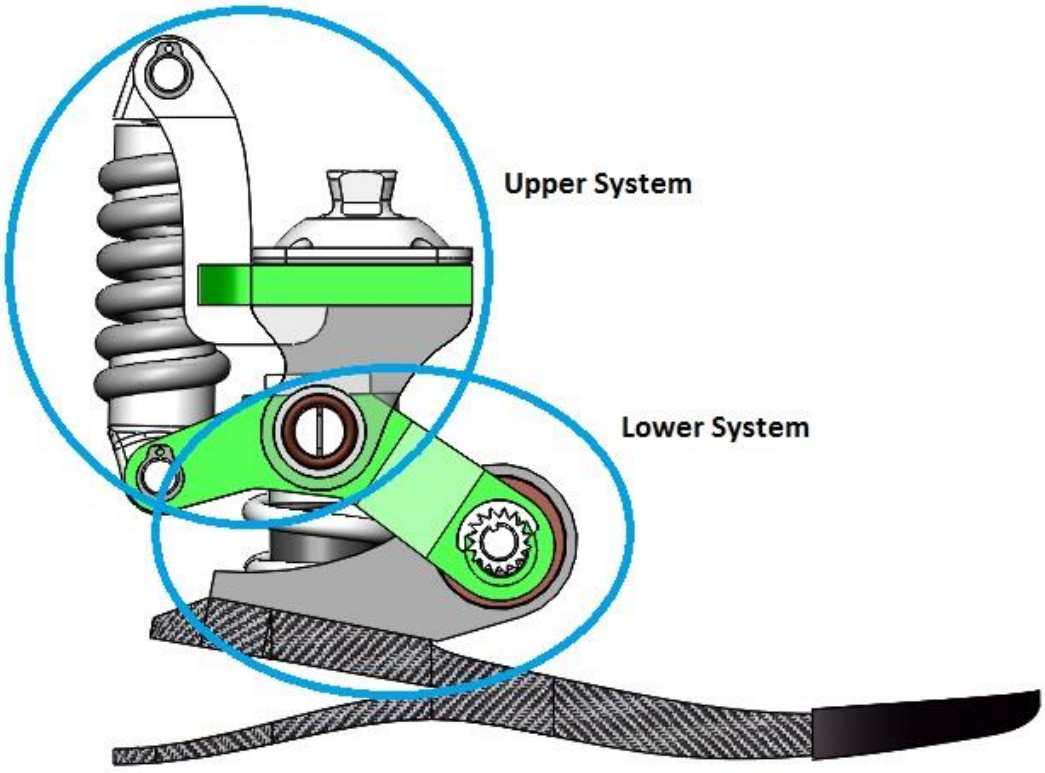

FIGURE 3.4: TWO MAIN SUBSYSTEMS OF THE LEAF.

At heel strike the softer spring in the lower system will compress first shown in Fig. 3.5. The benefit of the heel spring is that it acts as a damper and absorbs the initial shock. Based on the designed location of the ankle joint (the bearing between the top and bottom systems) the weight of the user will also cause the gear teeth on the floating shaft to be locked meshing with the fixed teeth shown in Fig. 3.5.

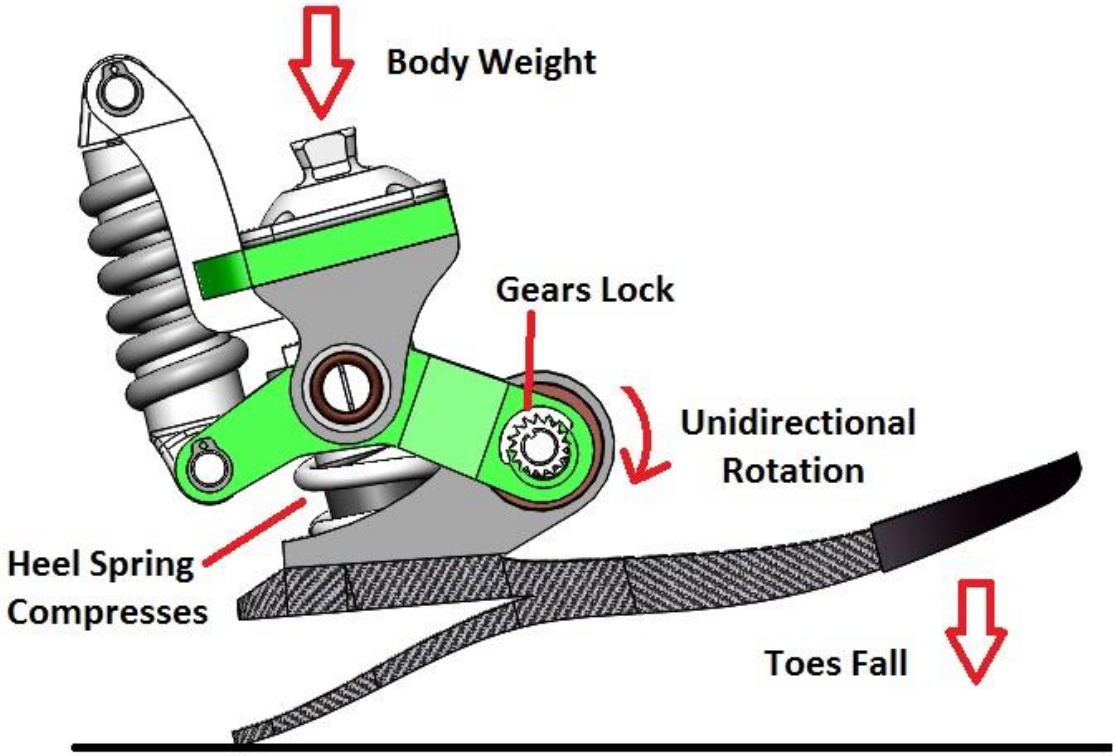

FIGURE 3.5: UNIDIRECTIONAL BEARING PERMITS ONLY THE KEEL TO LOWER MATCHING GROUND SLOPE DURING HEEL STRIKE.

Under load with the gears meshed and the floating shaft constrained the unidirectional bearings will only allow the rotation of the keel towards the ground (Fig. 3.5). This motion along with the softer heel spring in a compressed state will cause the foot to match the slope of the ground (Fig. 3.6). The range of slopes reachable in this way is determined by the compression distance available in the heel spring. This process is demonstrated in Fig. 3.6.

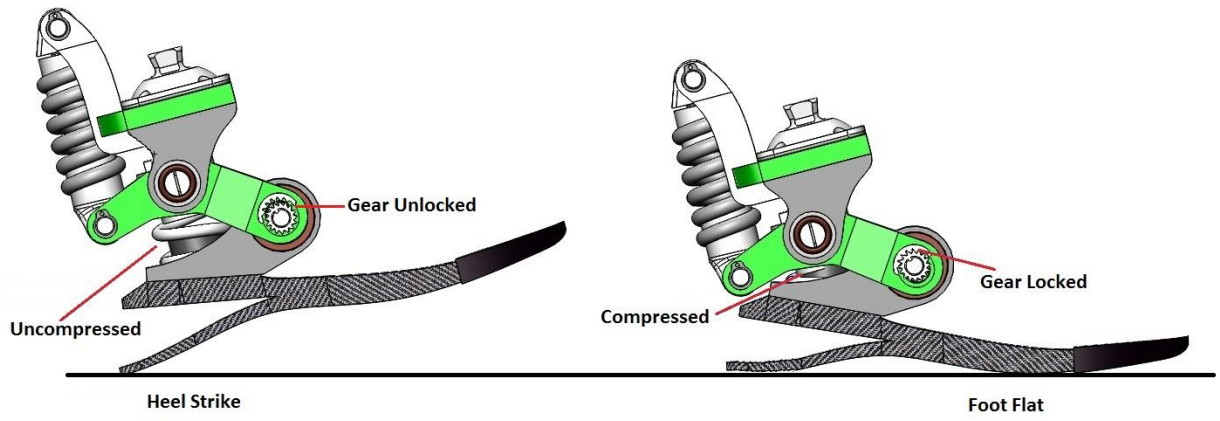

FIGURE 3.6: HEEL SPRING COMPRESSION AND FOOT FLAT DURING HEEL STRIKE.

Once the foot matches the slope and max plantar flexion is reached the rollover portion of gait begins. With the foot on the ground during rollover the body weight of the user will cause the gear teeth to remain locked. With the gears locked the unidirectional bearings do not allow the heel spring to expand thus locking the lower system completely and restricting rollover motion to the upper system. As the user's shank begins to rollover the ankle joint, the upper system spring expands storing energy shown in Fig. 3.7.

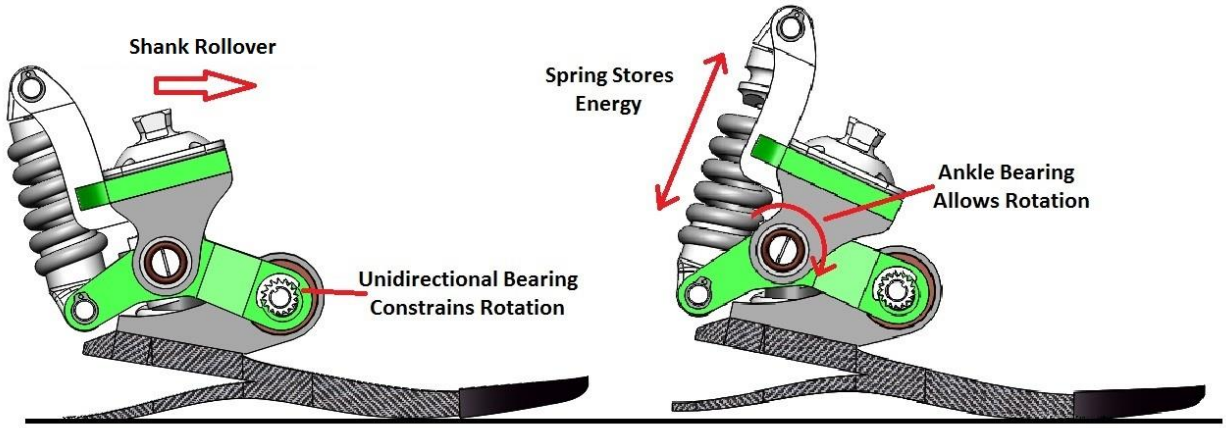

FIGURE 3.7: ENERGY STORAGE IN UPPER SYSTEM DURING ROLLOVER.

The goal is to have the upper spring engage once the foot is flat and disengage after the toe leaves the ground. The top spring will store energy all the way through the rollover and immediately release the energy pushing the keel into the ground and propelling the user forward shown in Fig. 3.8.

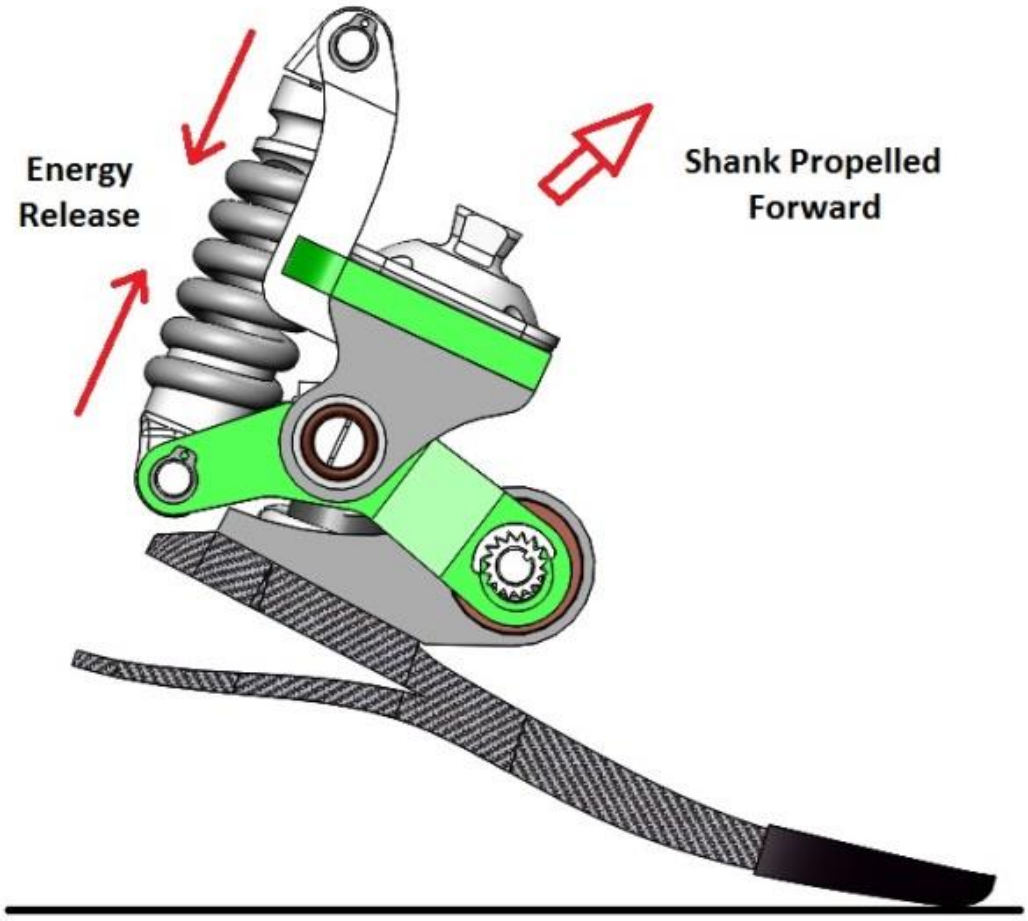

FIGURE 3.8: SPRING ENERGY CAUSES HEEL LIFT AND PROPELS THE SHANK AND LEG FORWARD.

The unidirectional bearing, when engaged during rollover, will only allow the upper spring to store and release energy and will not disengage until the toe has left the ground and the gear teeth are released. The torque from the top spring and the weight of the user constrain the floating shaft. When the user's weight is off the foot, the gear teeth are released shown in Fig. 3.9.

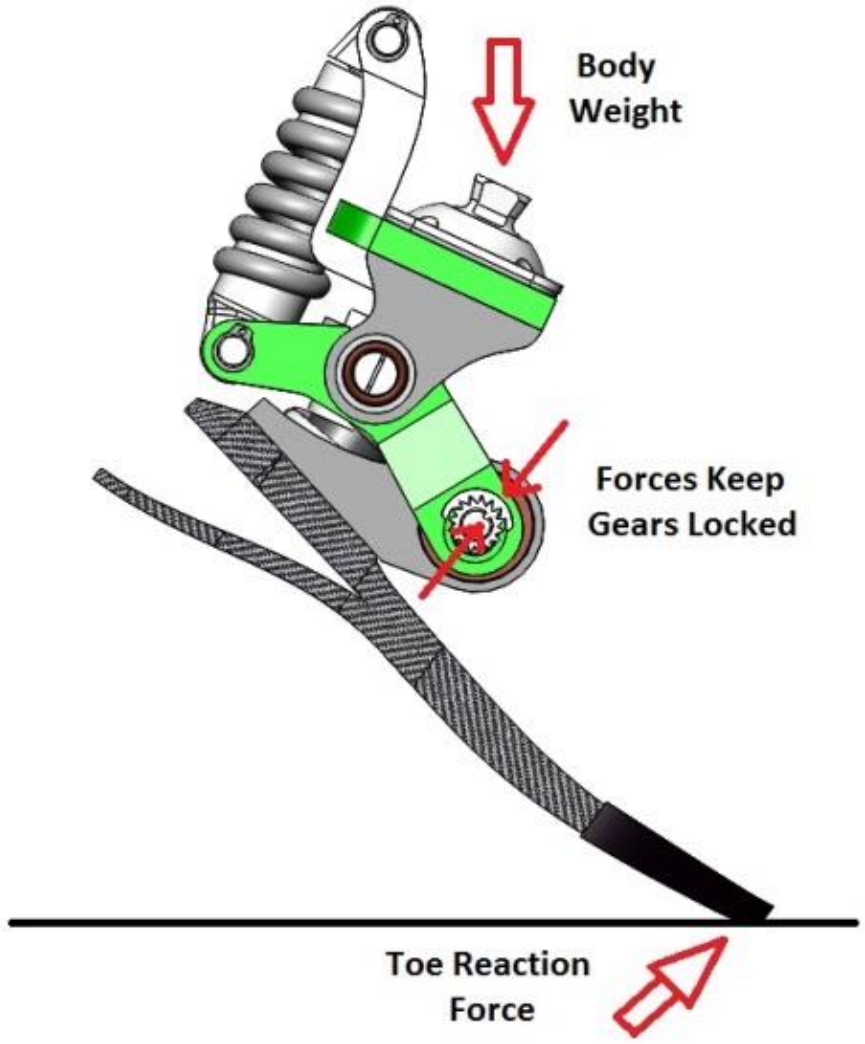

FIGURE 3.9: SPRING FORCES ON FLOATING SHAFT GEAR TEETH.

Once the toe and keel leave the ground, the lower system's own weight will cause the floating shaft to move away from the gear teeth. When this occurs, the softer bottom spring will then expand rotating the floating shaft and raise the toe during swing phase shown in Fig. 3.10. This last action of raising the toe at the start of swing phase resets the lower system for the next heel strike. The ankle prosthesis will then be ready for a new gait cycle.

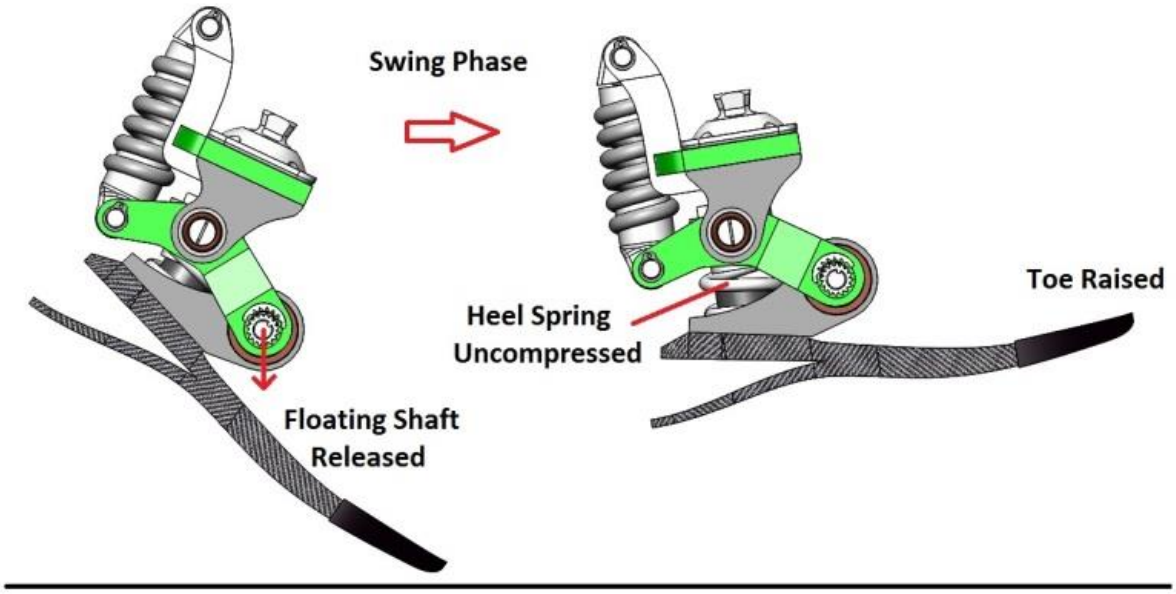

FIGURE 3.10: UNLOCKING FLOATING SHAFT AND TOE RAISED DURING SWING PHASE.

Since prosthetic feet are designed for a specific weight of a person, the LEAF was designed to be easily adaptable for various users. The only changes that would need to be made are different springs accommodating for the stiffness required for a different weight. The spring mounts make it easy to switch springs without affecting the rest of the design.

3.3 DESIGN DETAILS

The initial design was based on a body weight of 73 kg. The ankle design is designed for slower walking speeds. Forces for high impulse running were not modeled in the initial prototype. The initial mechanical design for able bodied comparison is optimized for level ground walking with maximum energy storage and release. Although the ankle has the ability to match different inclines, testing was just started on level ground walking.

3.3.1 Spring Sizing

The springs used in the design of the ankle prosthesis need to match the weight of the amputee. There are two springs in the LEAF design that must be optimized. The heel spring in the lower system needs the ability to absorb the person's body weight at heel strike without excessive impact forces. The upper system spring needs to be stiff enough to absorb the maximum amount of energy during rollover but soft enough as to not restrict the rollover motion.

In order to absorb the impact of a 73 kg user stepping on the heel of the device, the amount of resistance from the heel spring needs to be larger than the downward force from the body weight. From walking data, a 6 degree ankle rotation was determined as appropriate for this design. According to the mechanical design a 6 degree rotation of the foot will amount to a 5.24 mm deflection at the heel spring. Equation (1) equates the force from the user mass (M) with the force from the spring (H_S) with acceleration (a)

while Eq. (2) shows the stiffness (K_H) necessary to satisfy Eq. (1) at the predicted deflection (d_H) according to Hooke's Law.

$$H_S = M \times a \tag{3.1}$$

$$H_S = K_H \times d_H \tag{3.2}$$

Using Eq. (3.1)-(3.2) with a user mass of 73 kg, the heel spring stiffness (K_H) is determined to be $136{,}666\,\frac{\mathrm{N}}{\mathrm{m}}$. For added allowance of dynamic forces due to gait speed a slightly stiffer spring was used in the actual LEAF design of $146\mathrm{k}\,\frac{\mathrm{N}}{\mathrm{m}}$. Once the stiffness was determined, a spring was found with the correct dimensions to fit the design space as well as the stiffness requirements.

While the heel spring will absorb the impact of heel strike, the upper spring will store energy during the rollover portion of gait. To determine the optimal spring stiffness of the upper system, the maximum possible energy storage was used. Equation (3) shows the relationship between a torsional spring stiffness (K_τ) and the energy stored (U) through a set rotation (θ) determined from gait data. Equation (4) is the relationship between torsional stiffness (K_τ) and linear stiffness (K_U).

$$U = \frac{1}{2} K_\tau \theta^2 \tag{3.3}$$

$$K_U = \frac{K_\tau}{l^2} \tag{3.4}$$

By assuming a maximum energy available for storage in the upper spring of 8 Joules and a rotation angle of 12 degrees during rollover, it was determined that the upper spring has a spring stiffness of $281446 \frac{N}{m}$. In order to account for changes in weight or rotation a spring stiffness of $325k \frac{N}{m}$ was used in the actual design.

3.3.2 Safety

Once the spring designs were finalized the next step was to perform stress analyses on all of the parts within the LEAF. This was done first using hand calculations and confirmed further using SolidWorks Finite Element Analysis (FEA) to determine maximum stress, deflection, and factor of safety of each part. It is also useful to know the weakest points in the structural design for safety inspections during use. Figure 3.11 shows an example of the FEA used while Table 3.1 shows each part and their factor of safety for design.

TABLE 3.1: FOS FOR LEAF PARTS.

Part Name	FOS
Spring Top Support	2.6
Ankle Arm	29.9
Mount Plate	32.2
Spring Lever	1.6
Foot Support	3.0

The prosthetic design is only meant for walking but the structure was designed in order to withstand the force from a person running for safety purposes. (find citation) found that running forces can peak at around 2.2 times body weight at the ankle. The design analysis assumes the device will be used by a 73kg person while walking but for safety the maximum force applied during structural analysis was assumed to be 2.2 times body weight.

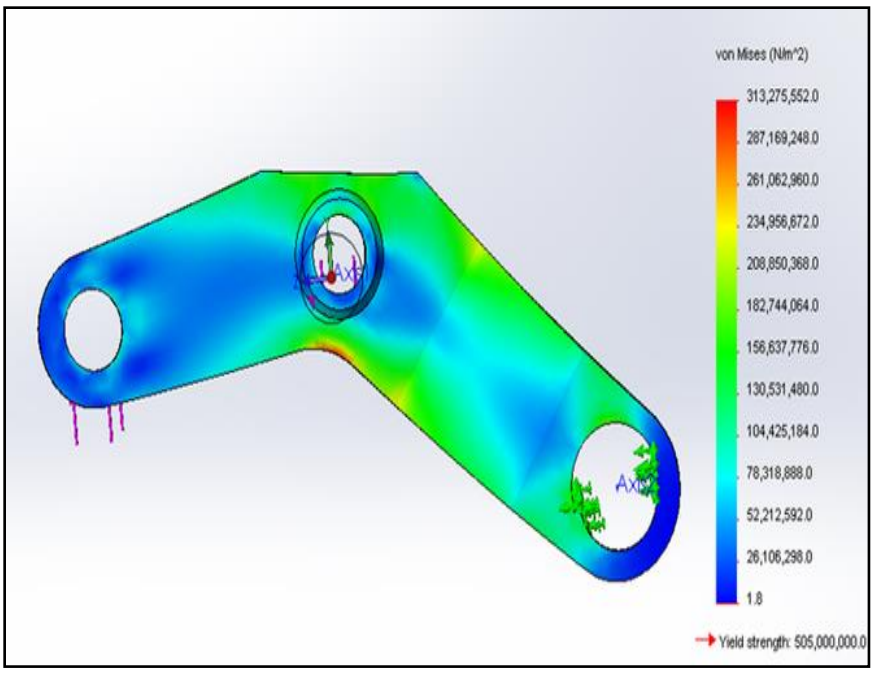

FIGURE 3.11: SPRING LEVER FACTOR OF SAFETY OF 1.6.

From these analyses it was seen that the factor of saftey for the different components was heavily based on the thickness of material chosen. While ideally a 0.16 inch thickness would have been sufficient for most parts, to cut costs of the prototype it was determined that the 0.25 inch thick aluminum would be used for all the parts. The spring lever has the lowest factor of safety and is the critical part for the LEAF. This is the part that is subjected to the most loading and movement. However, at a factor of safety of 1.6 it is still within safety ranges for this prosthetic ankle design.

In conclusion it was determined the LEAF has a minimum factor of safety of 1.6 and will require a heel spring of stiffness $146{,}000\,\frac{N}{m}$ with a linear tension spring stiffness of $325000\,\frac{N}{m}$. The final LEAF product must withstand repeated steps all day by a user

for years with changing loads and ground or climate conditions. To meet these needs the future designs will be optimized for weight and strength becoming more structurally efficient.

3.4 RESULTS

3.4.1 Structural Design and Stiffness Testing

The design requirements were tested to verify device functionality before any human subject testing was performed. Functionality tests include range of motion (ROM), spring deflection and stiffness, unidirectional bearing performance under load, and energy return.

The first ROM test performed measured the angle before and after the bottom spring was compressed representing heel strike during a step. This measurement showed that the keel lowered 5.32 degrees which was slightly less than the desired 6 degrees but was proved to be sufficient. Next the ankle was clamped down to the table and the top plate was pulled through at least 16 degrees in order to verify complete mobility.

To test the unidirectional bearings under load, the floating shaft was locked and the mechanism was pulled through rollover verifying that the heel spring remains compressed. The heel spring did not expand showing that the unidirectional bearings restricted the lower system rotation during the proper motion of the foot. Once these requirements were verified the energy return of the mechanism was also tested.

While analyzing the performance results stated previously, it was confirmed that the one-way bearings also held through the entire push off stage of gait so that the energy can be returned to the user at the proper point in the gait cycle. The mechanism designed was also tested for the amount of torque it can provide at the ankle joint during the gait cycle. In order to test the mechanism, a moment vs. ankle angle curve was developed and compared to that of an able bodied person. Figure 3.12 shows how the prototype mechanism (red) compares to the able-bodied person (blue) for the rollover portion of a gait cycle.

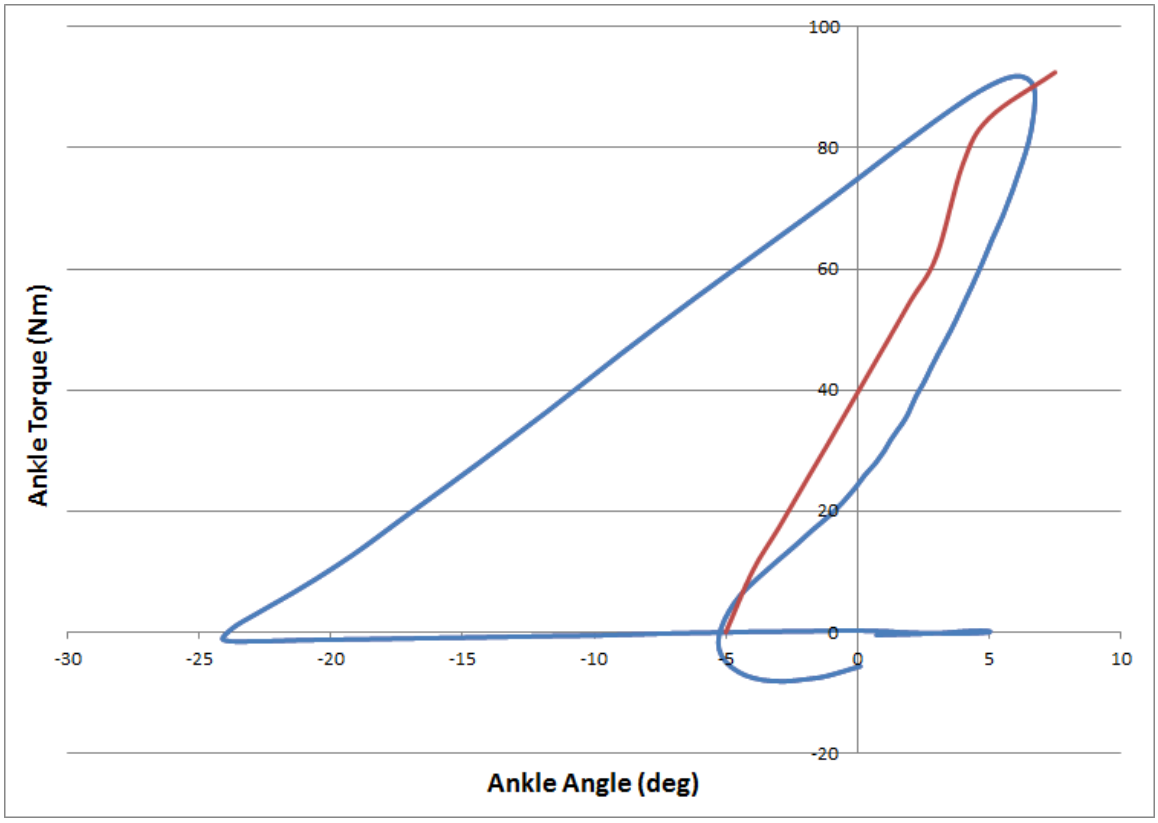

FIGURE 3.12: LEAF MECHANISM TORQUE TEST (RED) COMPARED TO ANKLE MOMENT WITH ANKLE ANGLE FOR 73KG PERSON (BLUE).

The data for this test was taken from prior research (M. Whittle) for an able-bodied person and from a torque test done on the mechanism for the LEAF data. The torque test was performed by mounting the prosthetic foot to the table, and then incrementing a load at a specific lever arm while measuring the change in ankle angle. Figure 3.13 is a picture of the test setup to perform the torque test. The position data was recorded using a camera.

FIGURE 3.13: LEAF MECHANISM TORQUE TEST SETUP.

The data values for this test proved to be very successful and the LEAF prototype performed well. During the able bodied gait the ankle traveled just under 12 degrees during rollover. For this ankle rotation, the LEAF mechanism provided almost 89 Nm of torque around the ankle. This value is 103% of the predicted 86Nm the mechanism was thought to be capable of through 12 degrees of rotation. Not only was the torque produced by the device greater than expected but the energy return was as well. With the 89Nm of torque for a 12 degree rotation, the LEAF was able to return approximately 11 J of energy to the user. The original amount predicted by the design was only 9 Joules.

This discrepancy in predicted vs actual values is due to a non-linear section in the moment vs angle plot shown in Fig. 3.12. The spring starts off with a linear stiffness but

then increases suddenly due to interference in the mechanism. At almost 4 degrees dorsiflexion the spring bumps into the mounting plate and causes the spring to have more resistance. Although this may seem like a favorable attribute the spring stiffness is ideal for mimicking the able bodied data for an amputee's specific weight. The stiffer spring near the end of rollover in this case is desired so that the amputee feels strength and stability from the LEAF foot.

3.4.2 Bypass Trials

Once the device was shown to be functional and rigid, a pilot test was performed. Some of the final desired testing included testing the comfort of the prosthetic foot for a 73 kg person and how it felt during energy return. Although an actual amputee was not able to try the LEAF prototype at this time two 73 kg people were able to wear the prototype using the ankle bypass mount shown in Fig. 3.14.

The next important factor that was discovered during bypass testing was the effects that the carbon fiber foot had on the LEAF performance. A softer carbon fiber foot was used with the ankle bypass at beginning stages of testing and seemed to be a detriment to the design. This foot was replaced with stiffer carbon fiber foot and the LEAF mechanism started to perform much better. The compliance of the carbon fiber foot absorbs some of the energy during rollover which caused the upper system spring design to be suboptimal. In conclusion it was decided that the analysis of the carbon fiber foot as a spring in series with the LEAF design is necessary for future iterations. For this prototype, the stiff carbon fiber foot allowed for sufficient results of the initial concept testing.

FIGURE 3.14: ANKLE BYPASS SYSTEM TESTING WITH 73KG USER.

Both users of the LEAF prototype felt a smooth heel strike and compression and good resistance and stability during rollover/energy absorption. These results are important and help build confidence in the LEAF design in order to trust that it is safe and comfortable enough to have a human subject testing with transtibial amputees.

3.4.3 Leaf Specifications

Over all the design was light weight and cost effective. Figure 3.15 below shows the final model with the different parts labeled. Table 3.2 shows the resulting specifications of the finished LEAF prototype model. The hardware used in the LEAF design totaled approximately $650.00 while the cost of machining was $1495.00. These prices do not include any labor cost of design work or product assembly. Most of these prototyping costs, like machining, will decrease with the large quantity builds of a marketed product. The finished model is shown nicely fitting in a running shoe in Figure 3.16.

TABLE 3.2: KEY PERFORMANCE RESULTS OF DESIGN.

Parameter	Value
Total Weight	4.0 lbs.
Optimum User Weight	161 lbs.
Length	4.3 in
Width	2.82 in
Mount Height	5.5 in
Spring Stiffness – Heel	146000 N/m
Spring Stiffness – Upper	325000 N/m
Factor of Safety	1.6

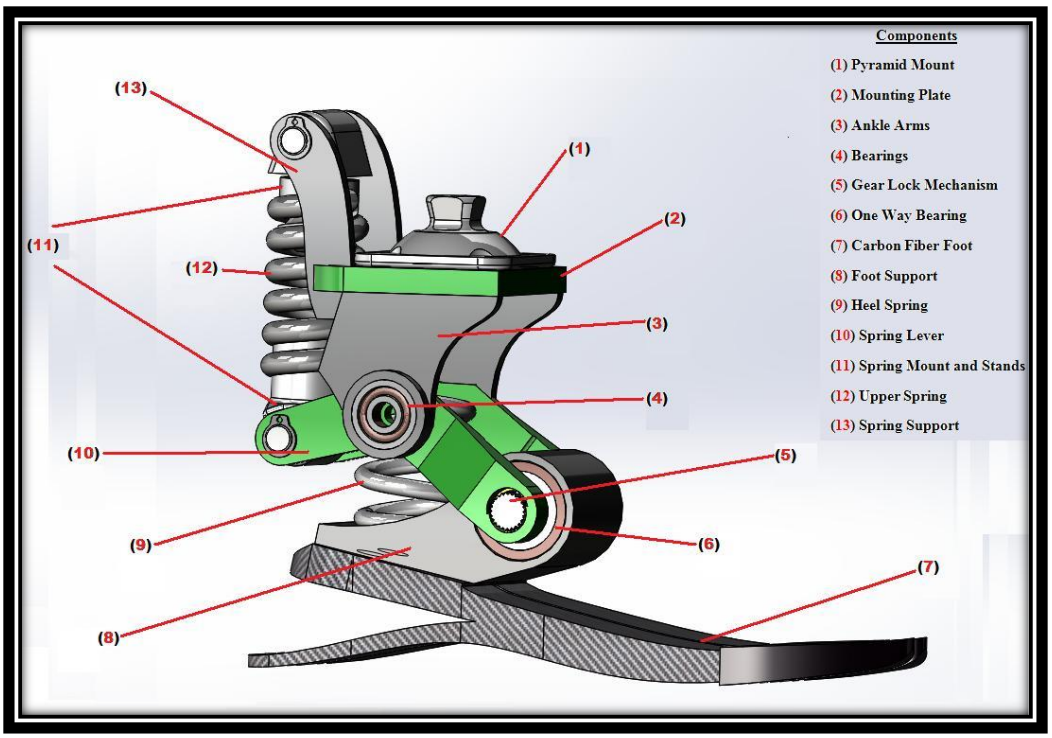

FIGURE 3.15: SOLID WORKS MODEL OF DESIGN WITH LABELED COMPONENTS.

FIGURE 3.16: FINAL LEAF PROTOTYPE RUNNING SHOE FIT.

3.5 CONCLUSION

The LEAF ankle design shown in Fig. 17 met the overall design requirements. The LEAF was able to absorb the impact of heel strike while adjusting for ground slope, efficiently absorb energy during rollover, release the stored energy smoothly and quickly during push off and then lift the toe during swing phase effectively resetting the mechanism for the next step. Also important to future development is that this first proof of concept LEAF design is light weight and low cost and any structural optimization will only improve both of these categories.

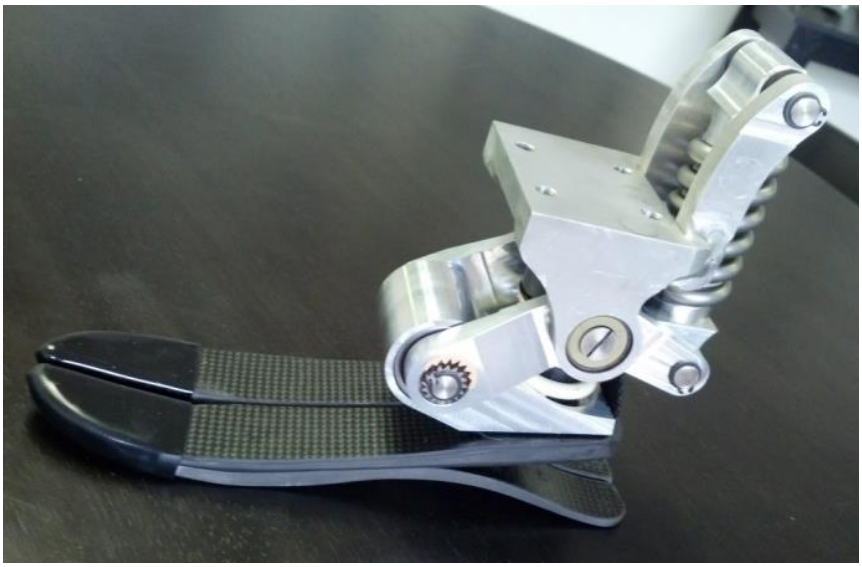

FIGURE 3.17: FINISHED LEAF PROTOTYPE.

Some important rework should be applied to the design before it is completely capable of human subject testing. This includes the accuracy of the locking mechanism. The teeth used in the front part of the foot need to have better resolution when locking and unlocking during heel strike.

The torque vs ankle angle was tested in the lab. Results show that the torque vs angle curve match up similarly to able bodied data but more important will be how the amputee feels when the device is worn. No matter how much assistance is predicted that a person will get from an energy assistive device, each amputee will like and dislike certain characteristics of the mechanism performance during gait. Human amputee testing is critical before any future iterations of the design of the LEAF ankle.

CHAPTER 4

POWERED PROSTHETIC ANKLE

There are 1.8 million Americans living with an amputation and the majority of those amputations are of the lower limbs [1]. This is also an important challenge for the military. Over 1600 service members have had a major amputation as a result of Operation Iraqi Freedom, Operation Enduring Freedom, and Operation New Dawn [2] with nearly half having a transtibial amputation [3].

Lower limb amputees typically expend 10-30% additional metabolic cost to walk depending on gait speed and amputation level as compared with able-bodied individuals and a fear of falling is pervasive in this community [4], [5], [6]. Many also experience significant gait asymmetry, lower back pain, slower walking speeds, reduced activity levels, and overuse injuries on their unaffected limb [7], [8].

The ankle is a critically important joint for gait stability and propulsion. Passive, energy storage and return (ESAR) prosthetic feet store the braking energy of the gait cycle in a spring like structure. However, these types of feet are not dynamically adjustable for gait speed or terrain changes. These feet also are not able to add additional propulsive energy to the gait cycle assisting powered push-off.

SpringActive, Inc. has developed an intelligent, powered ankle prosthesis, Odyssey, that provides the user with a full powered and properly timed push-off, picks the toe up in the swing phase, and provides a more natural and energy efficient gait to below the knee amputees. Odyssey utilizes a compliant actuator to store the natural braking energy just after heel strike, while a small lightweight motor adds additional energy to the step [11], [12].

Similar to Odyssey, our system stores energy in a spring as the shank rolls over the ankle. A motor also pulls on the spring in a controlled timing to add additional energy into the system. The combined elastic energy in the spring from the motor and regenerative braking of the shank is released causing a controlled powerful push-off.

The use of a properly tuned spring allows for this powerful burst of energy at push-off. We use a spring to store energy because it can release the energy quickly and its peak power can be substantially greater than the peak motor power on its own. In our results we compare the peak power of the motor to the peak power supplied by the spring during the gait cycle. We see power amplification of the motor of greater than 2 in walking and greater than 4 in running. Others have also shown the importance of compliant actuators for powered ankle prostheses [104], [105].

SpringActive has been working with the Department of Defense Telemedicine and Advanced Technology Research Center (TATRC) and Clinical and Rehabilitative Medicine Research Group (CRM) in order to design and build a powered prosthetic ankle that is capable of sustaining the human forces induced by walking and running (Walk/Run Ankle) while providing the necessary power to propel the amputee forward in the same manner as an able-bodied person [65]. The next iteration was to build a 'Ruggedized' version of the Odyssey Ankle (ROA) that is water and impact resistant and capable of short duration full powered running.

4.1 CONTROLLER SPECIFICATIONS

The purpose of this particular prosthetic device is to allow the user to walk and run in an able-bodied manner. The task to provide an amputee with complete comfort and mobility as if they were not an amputee is ongoing. Currently the prosthetic device created by SpringActive, Inc. provides more than 80% of the energy required for able-bodied gait while walking. The device stores energy in a spring and releases it during certain times in the gait cycle. The amount of energy released and the timing of release is critical in returning the gait to able-bodied conditions. The speed and position of the wearer's leg is found using rate gyroscopes and accelerometers attached to the front of their leg. The difficulty that arises in trying to adapt the current system to handle both walking and running is not just from the increased energy needed for running but comes from the transition period between a walk and a run. This transition period needs to be smooth and feel natural in order for the user to feel comfortable.

To study the transition period between running and walking, accelerometers and rate gyroscopes were attached to an able-bodied person's leg while they performed this transition. 3-axis IMU sensors equipped with both an accelerometer and a rate gyro for 3 axis of measurement were used for these tests. A Matlab program was created to process the data from the sensors. The mounting position of the 3-axis IMU sensor is critical in collecting the proper data and knowing which data is relevant for these tests. The able-bodied subject was asked to walk at varying speeds then transition to a run for a moment then return to a natural walk. Figure 4.1 shows an example of the data collected. The

area of particular interest is again where the subject transitions between the running and walking speeds.

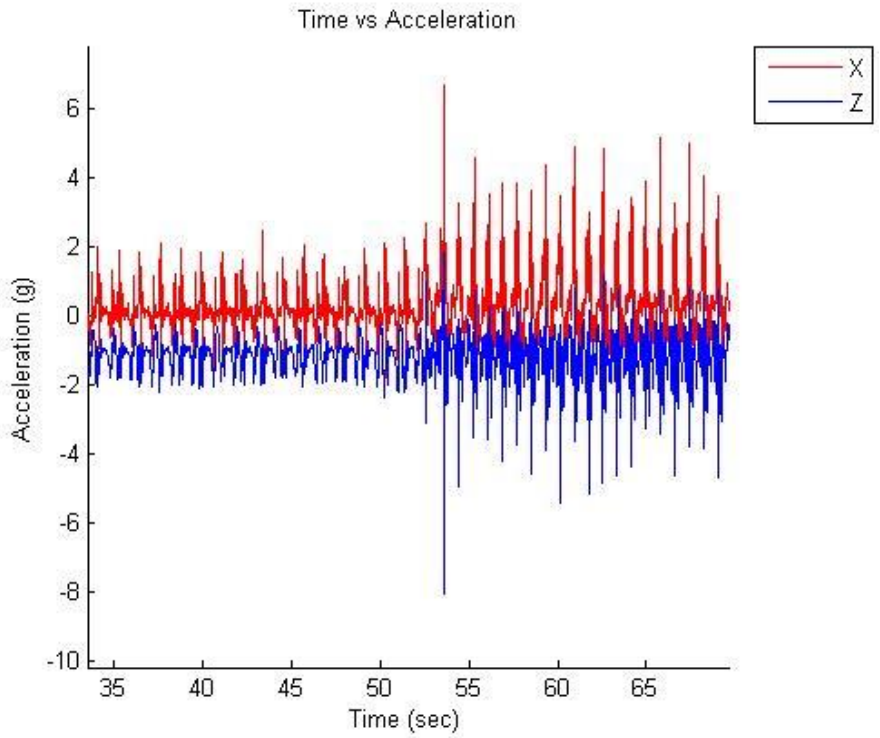

FIGURE 4.1: WALK TO RUN TRANSITION DATA.

The task of turning this data into usable signals and inputs for the robotic ankle system to react properly and smoothly during walk to run transitions is extremely important. The optimal torsional stiffness at the ankle is based on a person's weight and the spring is sized accordingly. Figure 4.2 shows the normal ankle angle data versus the percent the person has gone through one step with one leg. 100 percent of a gait cycle is from heel strike to heel strike of the same foot.

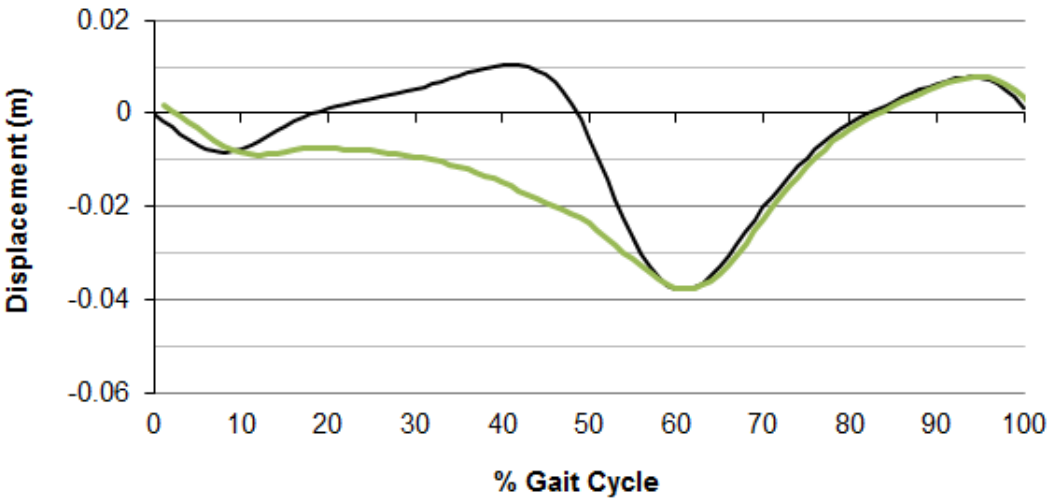

FIGURE 4.2: ANKLE (BLACK) AND MOTOR (GREEN) DISPLACEMENT VS PERCENT GAIT CYCLE.

The blue curve in Fig. 4.2 shows the desired position of the motor during the gait cycle. The idea behind the desired motor position curve is that during the loading phase, when the shank is rolling over the top of the foot just before energy is used to push off the ground, the motor drives the end of the actuated spring in the opposite direction of the foot so as to put more potential energy into the spring. The additional energy forced into the spring with the motor helps propel the user forward in the same way an able-bodied person would use their calf muscle to add energy into their ankle joint propelling them forward. Then during the swing phase the foot is in the air and the motor follows the normal pattern for ankle angle again.

Our control scheme examines the phase plane of the tibia's angular velocity and elevation angle to determine a proper actuator position. A rate gyro measures the angular velocity of the tibia and is integrated to determine the angle. An actuator position surface was developed in terms of walking gait percent and stride length [106]. This surface and controls approach was adapted to include running gait. Able-bodied input data (ankle torque and position) required for defining the running actuator position surface was provided by the Lauflabor Locomotion Lab [105] (TU Darmstadt, Germany, www.lauflabor.de). Figure 4.3 describes the phase-plane relationship to gait percent and stride length. The phase angle is measured continuously during operation and is used to calculate gait percent. The polar radius (r) is a measure of the stride length. Figure 4.4 illustrates the derived actuator surface in terms of gait percent and stride length for walking, a walk/run transition region, and running. The actuator surface plot allows the system to calculate a smooth pattern for the input side or proximal side of the spring.

The phase angle and stride length are continuously calculated at 500 Hz. The values are used to determine the desired motor position from the surface plot in Fig. 4.4. The motor then moves adjusting the input position of the spring.

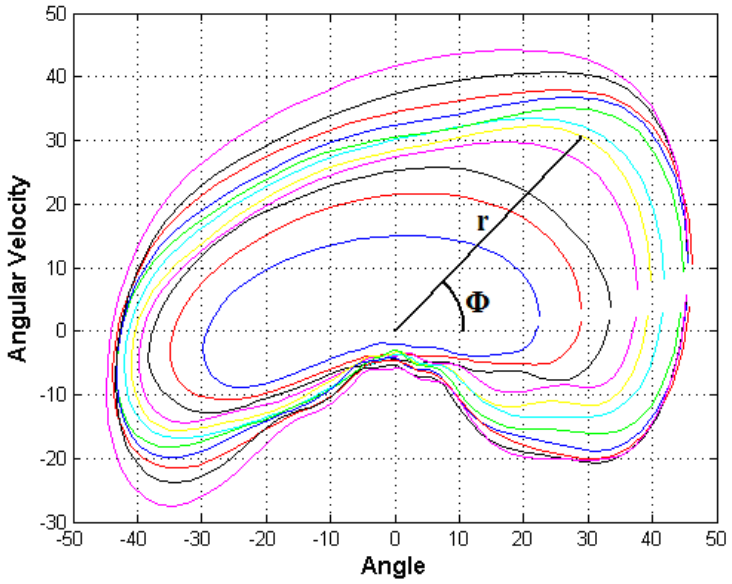

FIGURE 4.3: SHANK ANGULAR VELOCITY VERSUS SHANK ANGLE. POLAR ANGLE Φ REPRESENTS THE PROGRESSION AROUND THE CURVE (GAIT PERCENT). VARIABLE, R, IS THE POLAR RADIUS AND IS RELATED TO THE STRIDE LENGTH. EACH COLORED CURVE IN THE GRAPH IS ABLE-BODIED WALKING DATA COLLECTED AT DIFFERENT GAIT SPEEDS [107].

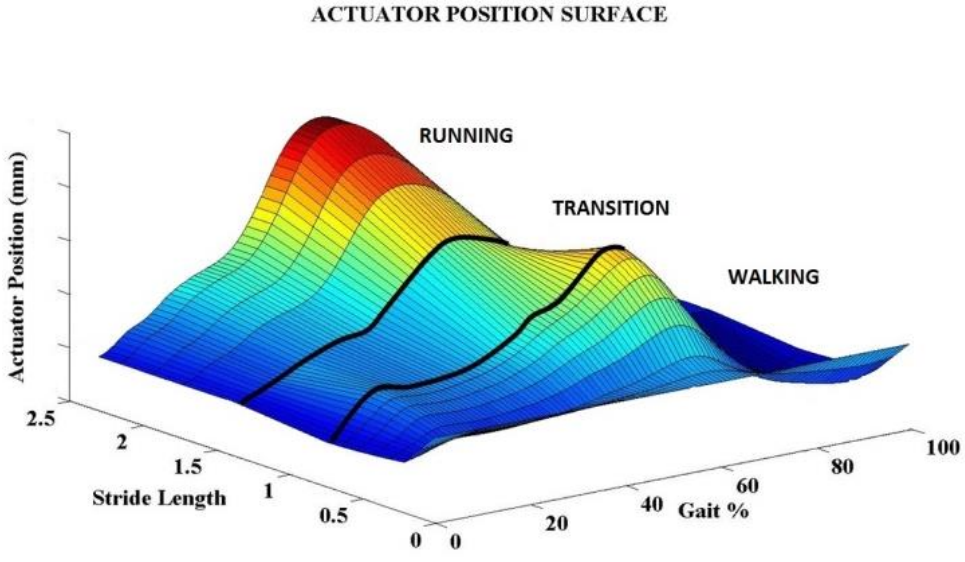

FIGURE 4.4: ACTUATOR POSITION SURFACE; ILLUSTRATES THE WALKING, TRANSITION, AND RUNNING REGIONS. THE ACTUATOR POSITION DETERMINES THE INPUT SIDE OR PROXIMAL SIDE OF THE SPRING.

4.2 SYSTEM FUNCTIONAL DESIGN

Before the mechanical system can be designed the initial requirements set by max user weight, running speed and duration of battery life, etc. Included in these requirements are the use of 30mm EC-4pole motor, a roller screw and nut, titanium spring, a microprocessor board, and a motor controller board. The roller screw and titanium spring are chosen because of their long life during cyclical loading such as walking. Each spring design is also a specific stiffness for certain amputee weight ranges.

After many different sketches and configurations, the layout of the required components was chosen. Figure 4.5 below shows this initial concept for where the components will be in relation to each other. The motor is in the middle of the body housing next to the roller screw and nut. Placing the spring into the foot portion of the ankle will allow more room inside the main body of the robot for electronics.

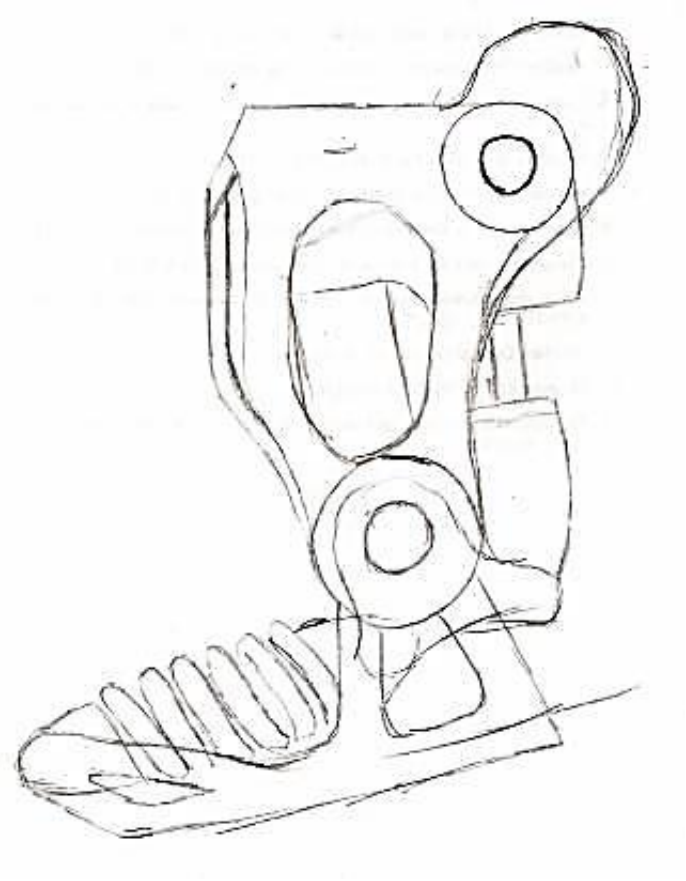

FIGURE 4.5: FINAL COMPONENT LAYOUT.

Once the main transmission design was accomplished the details of housing the transmission were addressed. Main issues involved with the proper transmission housing deal with ranges of motion, friction, efficiency, and load carrying capacity. First the screw was housed in a bearing package such that it can handle thrust loads in both directions along its long axis at the same time radial loads are applied by the motor. The loads transferred during motor actuation need to be properly distributed through a rigid environment.

FIGURE 4.6: ASSEMBLY OF ROBOTIC FOOT ACTUATOR SYSTEM

Once all the parts were created through sketches, the designs were considered and the most promising parts were modeled using Solidworks allowing for increased detail of design and three dimensional images to be analyzed. Figure 4.6 shows the model from Solidworks including all the bearings and screws in the entire assembly.

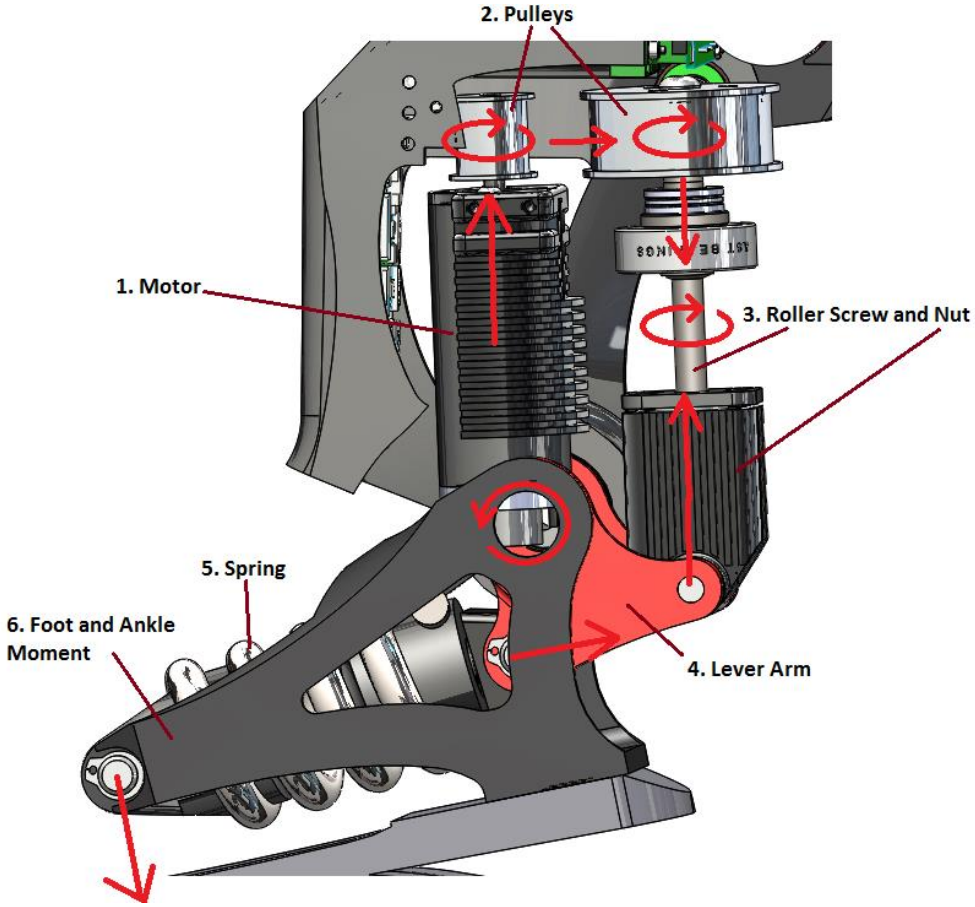

FIGURE 4.7: SIMPLE POWER TRAIN MODEL FOR PROSTHETIC FOOT DEVICE.

The ability to walk and run on a prosthetic device is obtained by adding energy into a person's gait to make up for the energy the person is unable to add due to the loss of a limb. This is done with electrical energy converted into mechanical energy designed to propel the person forward as needed. Starting with an electric motor the power train is used to control the end conditions of this mechanical energy and deliver the results needed for able-bodied gait. The power train is shown in Fig. 4.7 and shows a simple model for how the ankle system works. Individual parts and functions are explained in detail.

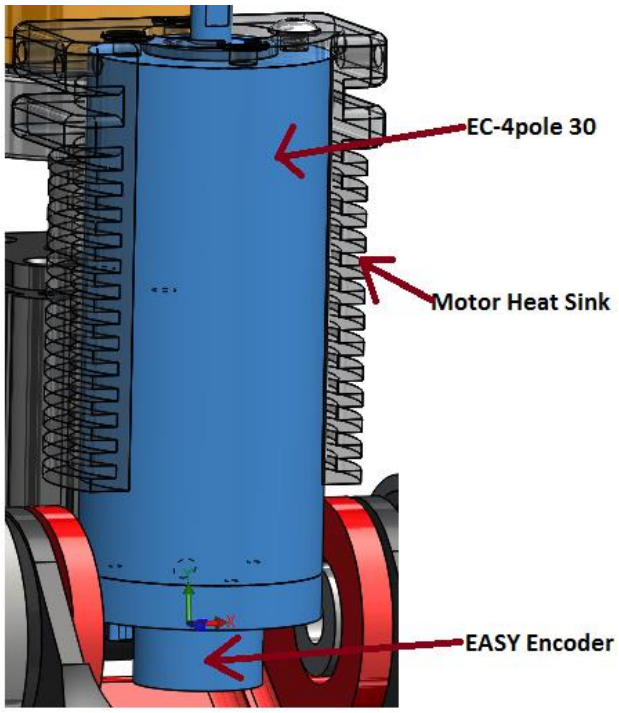

FIGURE 4.8: MOTOR MOUNT AND ENCODER.

The motor selected for the powered ankle system to handle both walking and running speeds is the 200W Maxon EC-4pole 30. Figure 4.8 shows the motor mounted inside the ankle. At the bottom of the motor is mounted an absolute encoder (16mm EASY) used to communicate motor position to the microprocessor and motor controller.

For the motor to efficiently handle the faster dynamics of running it needs to run at higher speeds. One problem that we predicted for the motor capabilities is the amount of heat the motor will generate while trying to keep up with the requirements of the user. This problem was handled by turning the motor mount plate into a heat sink. Figure 4.8 shows how the aluminum is extended over a large surface area of the motor and cooling fins are added to help dissipate the heat into the surrounding air.

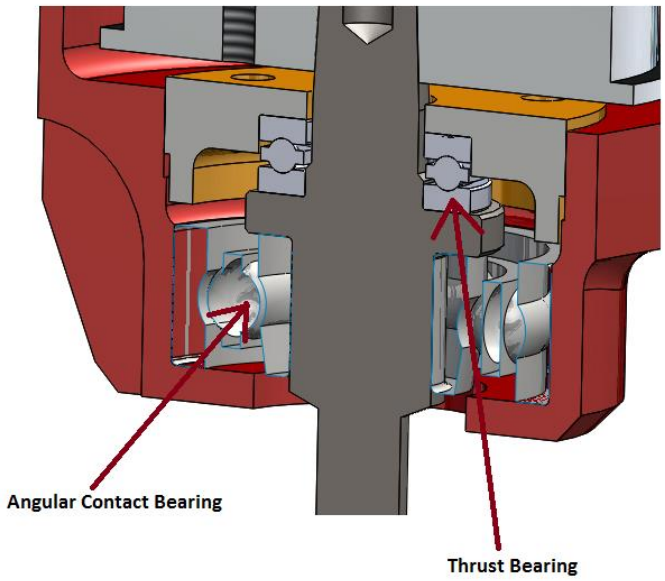

FIGURE 4.9: THRUST BEARINGS CAPTURE ROLLER SCREW.

Pulleys are used to transfer power from the motor shaft to the screw through a preselected gear ratio that optimizes motor efficiency. The high reduction ratio allows the motor to be run at a higher RPM where this motor is more efficient.

The roller screw is held in place by an angular contact bearing. This bearing handles both radial loads and one direction of thrust loads. To handle thrust in the opposite direction a different thrust bearing was used in combination with the angular contact bearing. Figure 4.9 shows the two bearings on the roller screw with the smaller bearing on top just to handle the lighter upwards thrust from the mechanism weight during swing phase.

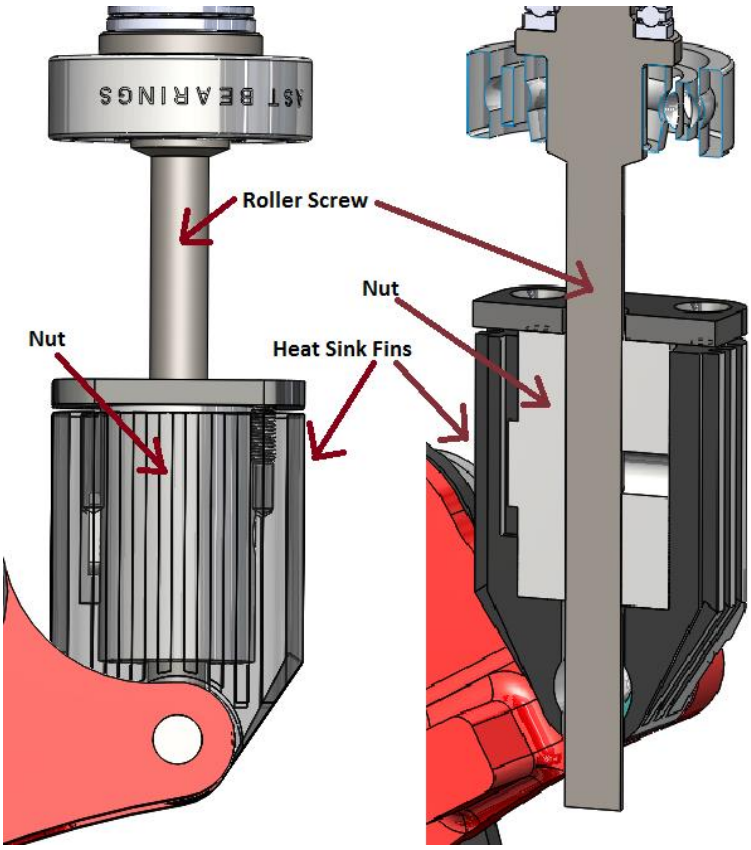

FIGURE 4.10: ROLLER SCREW AND NUT INCLUDING NUT HOUSING.

The roller screw nut converts the rotational motion from the screw into a linear motion to pull and push on the linear spring located in the foot. The nut is incased in aluminum housing with tolerances that inhibit any side loading on the screw. Rubber seals are used to reduce any noise from the screw travel and heat sink fins surround the nut casing to dissipate the heat generated from the high loads and fast movements involved with running. Figure 4.10 shows the heat sink fins and the inside of the nut housing demonstrating how the nut is captured by the design.

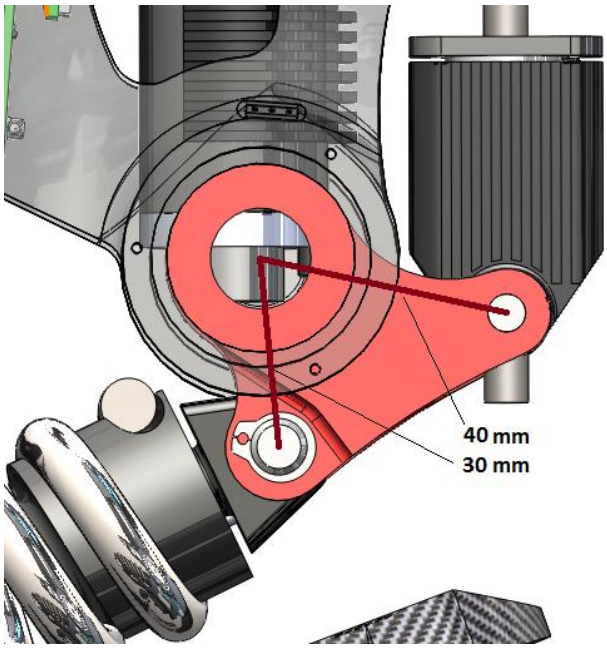

FIGURE 4.11: SCREW TO SPRING LEVER ARM RATIO.

The robotic ankle needs to be as compact as possible to fit the profile of a human foot and ankle. To help decrease size the spring was placed inside the shoe area of the foot and a lever arm rotating about the ankle joint is used to transfer the vertical pull of the roller screw nut into a horizontal pull deflecting the spring. Figure 4.11 shows this lever arm and the gear ratio involved which produces the correct torque around the ankle as a function of motor revolutions.

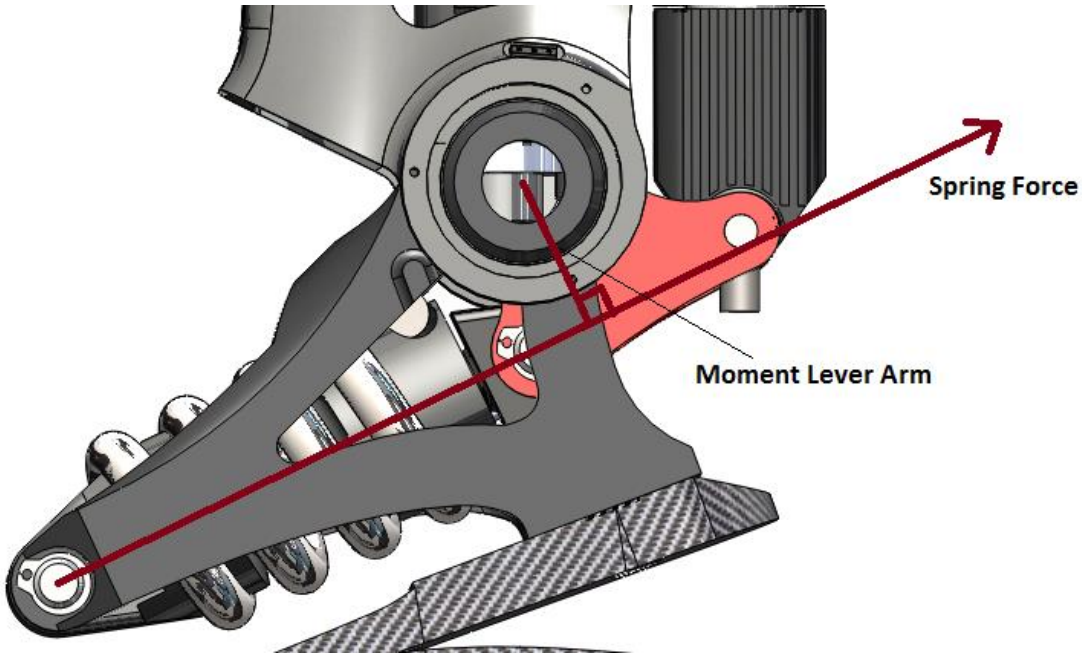

FIGURE 4.12: SPRING FORCE TO ANKLE MOMENT.

When the motor turns the roller screw it will pull on the lever arm which pulls on the end of the spring using it in tension during powered push off. When the person's foot is on the ground, pulling on the spring will generate a torque about the ankle helping propel them forward. The foot piece at the bottom of the design (see Figure 4.12) is used to transfer the spring tension load into the ankle torque. This torque is defined as the force from the spring multiplied by the perpendicular distance between the force vector and the ankle joint. Figure 4.12 calls this distance the moment lever arm. This compact design allows the spring to be located inside the shoe and invisible to onlookers.

4.3 DESIGN SPECIFICATIONS

To make this design a reality the mechanisms needed to be analyzed according to the specifications of the components. The mechanism makes use of a linear spring in combination with a lever arm to create a torsional stiffness around the ankle. Using previously developed analysis tools from SpringActive, Inc. the optimal torsional stiffness (K_T) at the ankle was determined. Equation (1) then converts the desired torsional stiffness into a linear spring stiffness (K) using a lever arm (L). Equation (1) allows the freedom to change the lever arm until the spring stiffness is a value commercially available.

$$K = \frac{K_T}{L^2} \tag{1}$$

$$\frac{\omega_m}{\omega_A} = \frac{2\pi L}{pg} \tag{2}$$

The motor also has specific requirements in order for it to reach the desired torsional stiffness at the ankle with desired motor position. The optimal value for the required motor is a motor velocity to ankle velocity ratio of 700. The transmission uses a pulley system from the motor shaft to the screw shaft combined with the screw pitch and the nut attached to a lever arm on the ankle joint. Equation (2) shows the derived ratio of motor velocity (ω_m) to ankle velocity (ω_A) where 'g' is the pulley ratio from the motor to

the screw, '*p*' is the pitch of the screw and '*L*' is the lever arm from the nut to the ankle. Using Eq. (2), the best combination of lever arm and gear ratio was found while minimizing the size of the overall mechanism.

Hidden inside the design are the electronics which control the motor and gather data during walking. Figure 4.13 is an overview of the electronics layout.

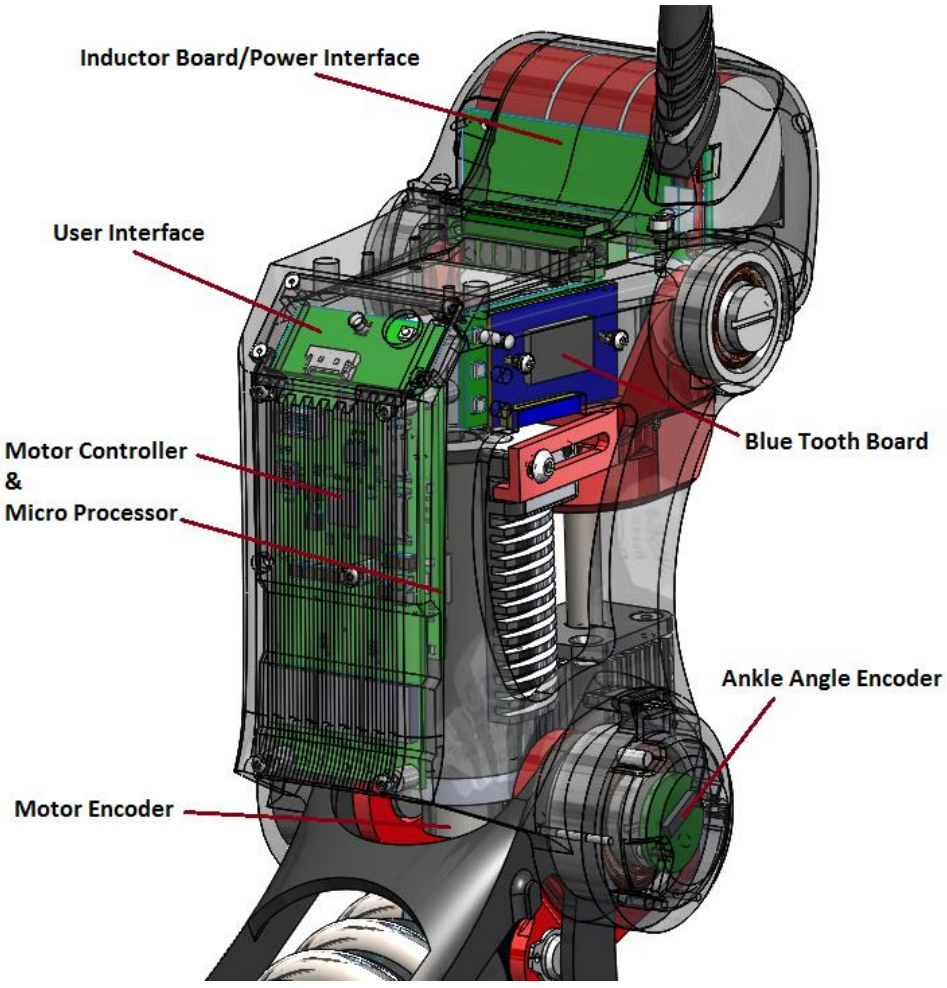

FIGURE 4.13: ELECTRONICS LAYOUT.

Heat developed during long term use of the ankle device was a major concern for this design. To solve this issue the main body of the ankle device is used as a heat sink for the motor controller to help draw the heat away from the electronics. The high heat constant from the aluminum body proved to be very successful as a heat sink. Fins were added to the front of the design to increase the surface area and effectively dissipate the heat into the environment. Figure 4.14 shows the heat sink fins in the front below the user interface cover. The interface cover is incorporated into the design to make the ankle device more user friendly and easily programmable during testing and data collection.

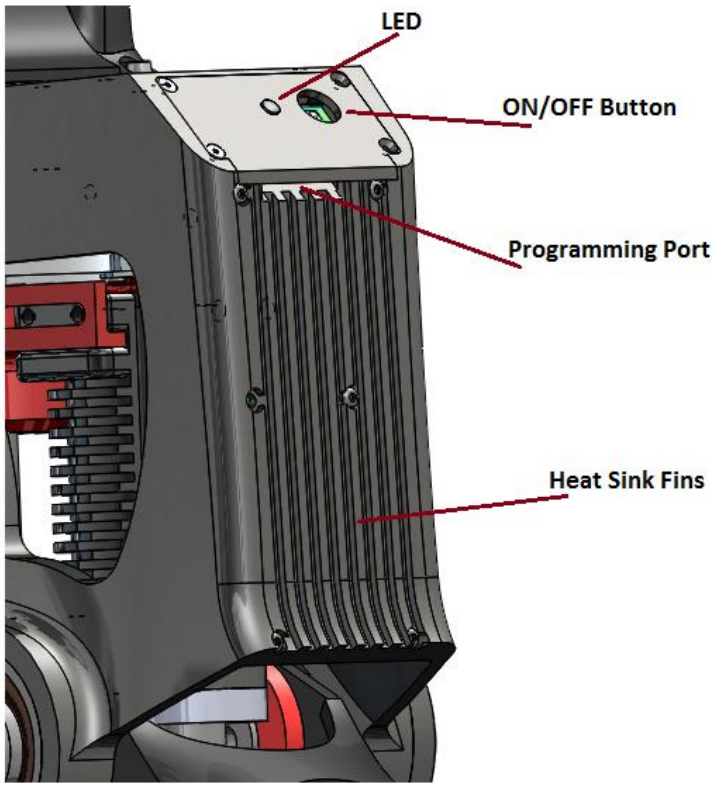

FIGURE 4.14: HEAT SINK AND USER INTERFACE DESIGN.

SpringActive has developed a compact motor controller to fit inside the ROA device. This motor controller handles brushed or brushless motors and has shown the capability of producing 600W continuous power while achieving 1,600W Peak Power during running. The compact size of the motor controller, shown in Fig. 4.15 allows the ROA device to run untethered while blue tooth capabilities allow for control adjustments and data collection during use.

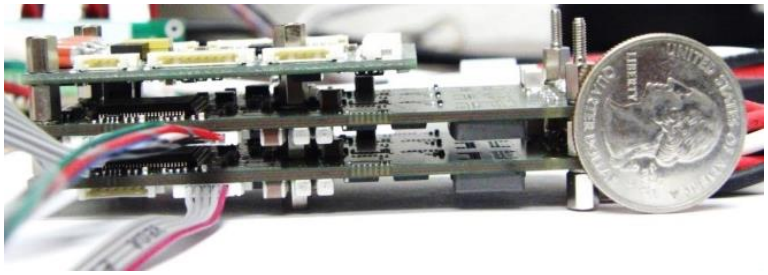

FIGURE 4.15: SPRINGACTIVE, INC. BRUSHED OR BRUSHLESS MOTOR CONTROLLER ELECTRONICS, SHOWN HERE IN A 2-AXIS CONFIGURATION WITH MODULAR MICROPROCESSOR BOARD.

The key technological achievements that make the performance specifications possible are the uniquely tuned actuator springs, the energy store and release actuation scheme, and our continuous (non-state based) gait controllers [14], [16]–[21]

FIGURE 4.16: 3D MODEL OF THE RUGGEDIZED ODYSSEY ANKLE.

The only way to achieve higher peak power output from a mechanical system than what can be accomplished with the motor drive alone, is to intelligently use springs [11], [12]. A model of the current Ruggedized Odyssey Ankle (ROA) is illustrated in Figure 4.16 and the final design specifications are listed in Table 4.1.

TABLE 4.1: MEASURED DEVICE SPECIFICATION FOR THE RUGGEDIZED ODYSSEY ANKLE.

Parameter	Value
Mass of Device (kg)	2.3
Maximum Dorsiflexion (deg)	26
Maximum Plantarflexion (deg)	38
Peak Ankle Torque Output (Nm)	190
Peak Ankle Power Output (W)	1,100

4.4 DESIGN SAFETY

Safety for the amputee is an important parameter of the mechanical system design. Finite Element Analysis is done for each part based on the loads it will carry. For this device the largest forces acting on the parts will occur during running. This particular analysis is for a force four times the max body weight of 220 lbs. or 100 kg mass. This allows for 4000 N of force acting on the device from the amputee. Internal forces are created by the spring and the motor as torque is added to the ankle joint. These internal forces are about 6000 N.

Figure 4.17 and Fig. 4.18 show the effects of both the internal forces and the forces due to body weight acting on the main shell of the ankle device. Based on the body weight this part holds a Factor of Safety (FOS) of 4.4 while the internal forces yield a FOS of 1.7.

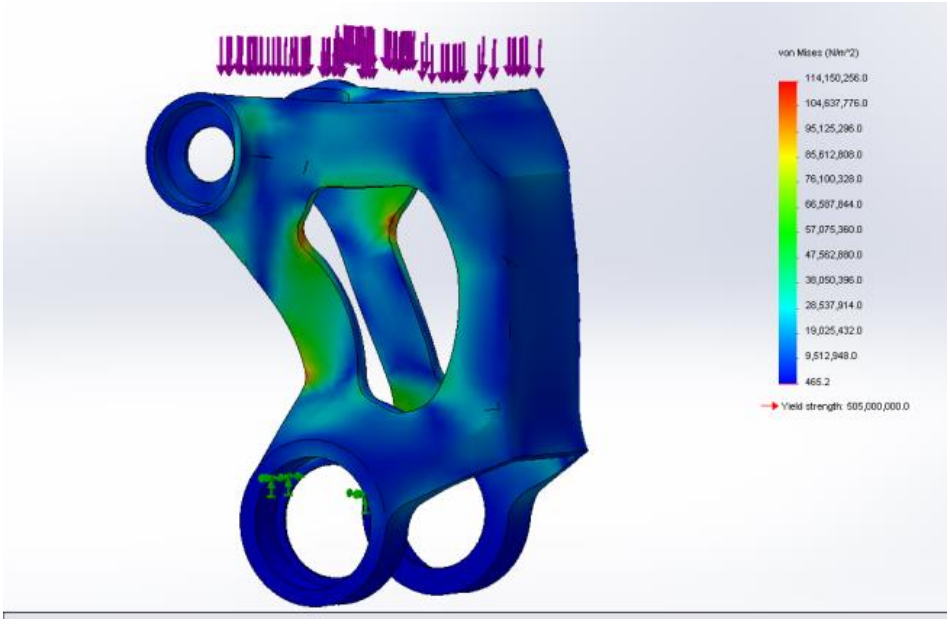

FIGURE 4.17: RUNNING BODY WEIGHT FOS (4.4).

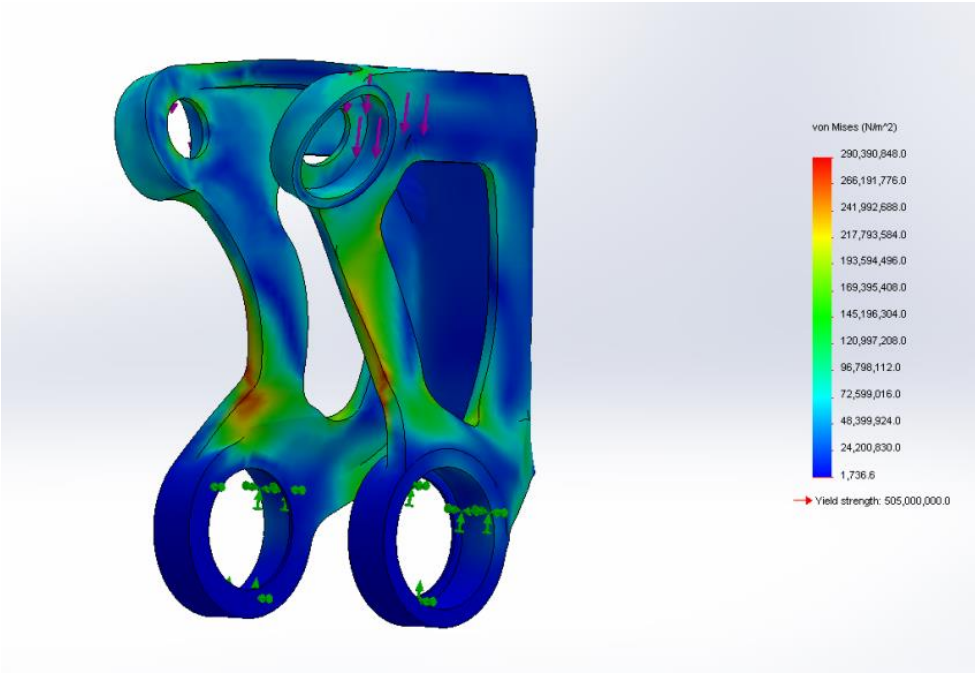

FIGURE 4.18: SPRING FORCES FOS (1.7).

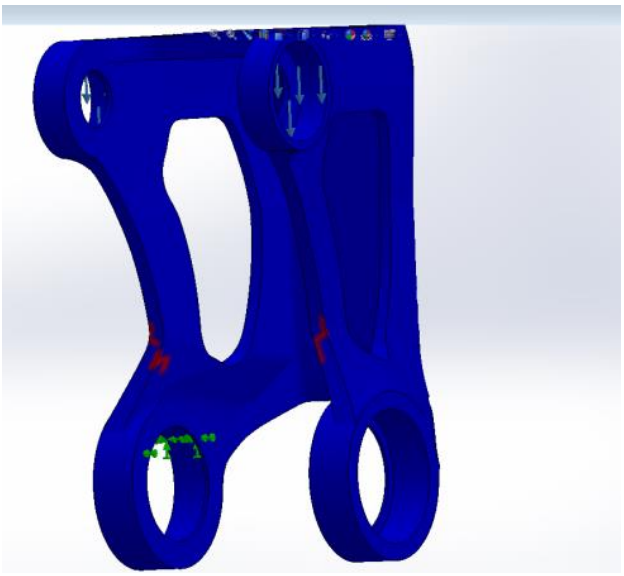

FIGURE 4.19: SPRING FORCES FOS (1.7) FAILURE POINT IN RED.

The analysis done in Fig. 4.19 show the main body and its predicted points of failure. In the figure these points are shown as red lines on top of the blue model. Knowing that this point is most likely to fail first, we are able to inspect this area often during testing to detect the early signs of fatigue. These failure points are given under exaggerated loading conditions and still show a FOS above 1.

TABLE 4.2: FACTORS OF SAFETY FOR STRUCTURAL MEMBERS.

Part	**FOS**
Body	1.7
Foot	1.7
Lever	2.7
Pulley Housing	3.8
Nut Housing	7

Each structural member is analyzed under the predicted maximum loading conditions to ensure safety of the design. Critical points on each part were also located for inspection purposes during human testing. Weight of the device is also an important parameter to the amputee. Most parts have been designed for minimum weight while still remaining near a factor of safety close to 2. Table 4.2 shows each part and its corresponding FOS under running conditions.

4.5 RESULTS

The ROA device is currently being tested on otherwise healthy, unilateral transtibial amputees. Our participant data is derived from sensors on the ROA device. An ankle encoder and a motor encoder are used to determine ankle position and a motor position. Spring deflection is calculated from the difference of the nut (motor) position with the ankle angle. Using Hooke's law the spring force is calculated. The spring and the nut velocities are then determined by numerical differentiation of position. Ankle moment was found by knowing the spring force and the spring's lever arm. The nut force was calculated by applying the ankle moment on the lever arm holding the roller screw nut. Power was then found by multiplying the spring and nut velocities with their corresponding force values. These two values of spring power and nut power combine to equate the ankle joint power for the ROA device [15], [43].

Ankle angle, ankle moment and ankle power were collected and compared to able-bodied data for different speeds of walking and running. The top three graphs in

Fig. 4.20 show able bodied data on a treadmill compared to over ground running of the ROA, both at 4 m/s. The middle three graphs compare treadmill running of the ROA device at speeds of 2.5 m/s with able-bodied data at 2.6 m/s. Walking speeds of the ROA device at 1.2 m/s are compared in the bottom three graphs to able bodied data at 1.6 m/s both performed on a treadmill. The moment and power amplitudes and curves delivered by the ROA are similar to the able bodied data.

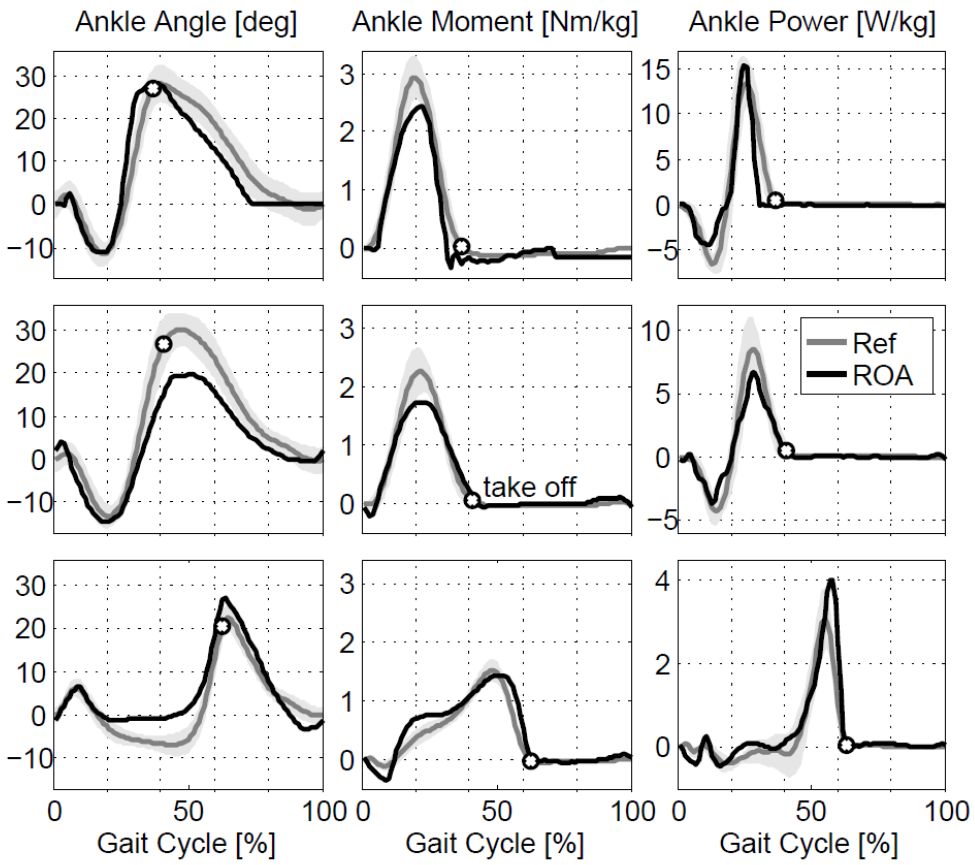

FIGURE 4.20: ANGLE, MOMENT AND POWER FOR ROA DEVICE DURING RUNNING AND WALKING COMPARED TO ABLE-BODIED DATA FROM GRIMMER ET AL. [12].

Ankle angle in the walking section does not show a good dorsiflexion correlation which may be due to a stiffer running spring in ROA device. This would mean during slower walking there is not enough torque from breaking energy to compress the spring but the motor does have enough power to provide a comparable push off.

Another way to evaluate ankle power and biomimetic gait was shown by Davis et al. using ankle angle and ankle torque in comparison [13]. The area under the ankle torque vs. ankle angle graph is positive energy added to the ankle in order to achieve proper push off. We use a similar method of ankle angle and ankle torque comparison to evaluate the energy at the ankle for amputees using the ROA device. This type of graph allows us to evaluate biomimetic behavior of the ankle prosthetic in relation to the proper ankle articulation as well as energy used for push off.

In Figure 4.21 the ankle moment vs. angle graph, shows a good shape correlation with able-bodied data. The area inside the curve demonstrates that positive energy is added to the ankle. The figure shows that our participant only achieved 17 degrees of plantarflexion at toe-off, while the able-bodied data show 24 degrees. There is also a steeper climb in moment during rollover with only half the dorsiflexion as the able-bodied data. This correlates well with the earlier assumption that the spring may be too stiff for these walking speeds. Although the peak moment value is similar to able-bodied data the stiff spring would have been evident in an early heel rise. It is worth noting that the data in Fig. 4.21 are at 1.2 m/s on ROA and 1.6 m/s for able-bodied.

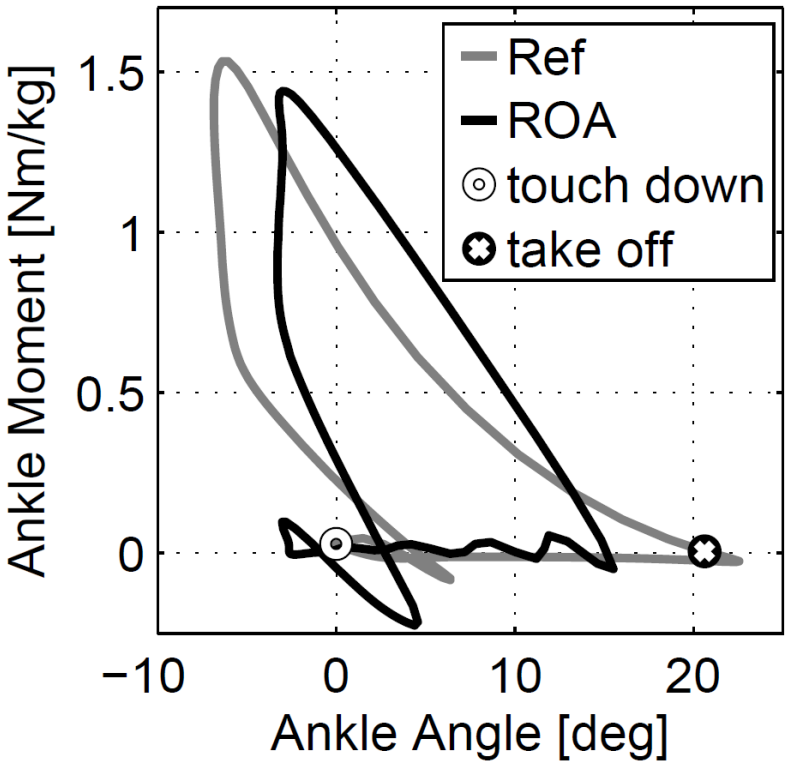

FIGURE 4.21: ANKLE MOMENT VS. ANKLE ANGLE FOR ABLE-BODIED DATA AT 1.6 M/S [12] AND DATA COLLECTED FROM THE ROA ON ONE SUBJECT AT 1.2 M/S.

Testing shows power amplification of the ROA device during walking gaits. This data is from a 73 kg user at a self-selected 1.2 m/s for walking gait. Peak moment about the ankle during walking of 110 Nm was found. Peak power at the ankle is illustrated in Fig. 4.22 showing 4 W/kg while the motor only peaked at 1.5 W/kg during the step. These results demonstrate that the input mechanical power from the motor to the output ankle power yield a power amplification factor of 2.6.

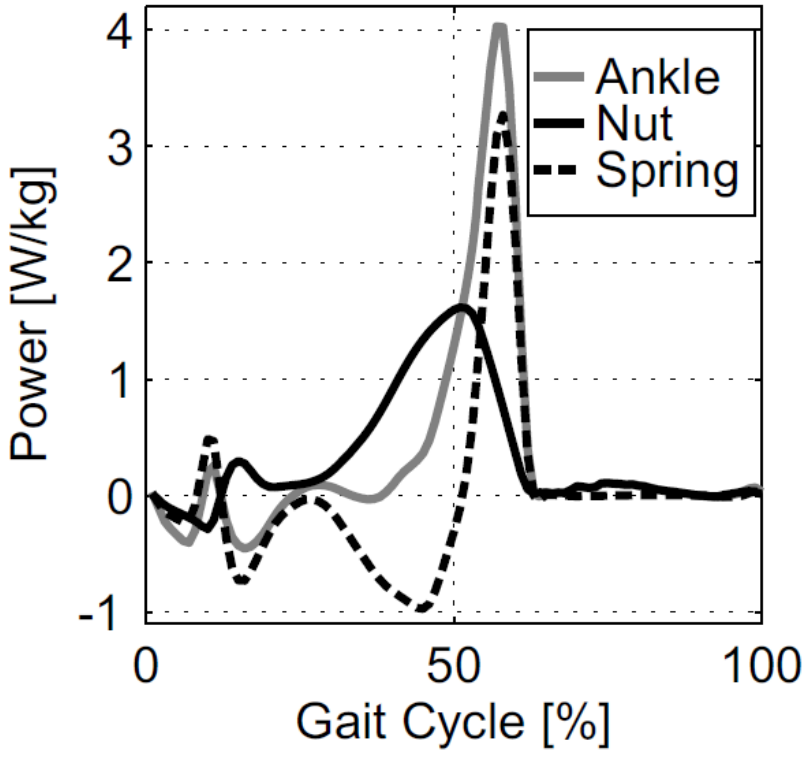

FIGURE 4.22: NORMALIZED ANKLE, SPRING AND NUT MECHANICAL POWER OUTPUT FOR 1.2 M/S WALKING. MAXIMUM NUT POWER OUTPUT (1.5 W/KG) IS AMPLIFIED (FACTOR 2.6) BY THE SPRING TO ACHIEVE A MAXIMUM ANKLE OUTPUT OF 4 W/KG.

Also shown in Fig. 4.22, during early stages of rollover (≈25-35% gait cycle) the ankle power is almost neutral supporting the hypothesis that the spring energy is mainly coming from the motor input for this section of gait. After 35% gait the ankle power is increasing due to motor input before the spring returns the energy it has stored. This may be improved with a softer spring if slow walking is the end goal.

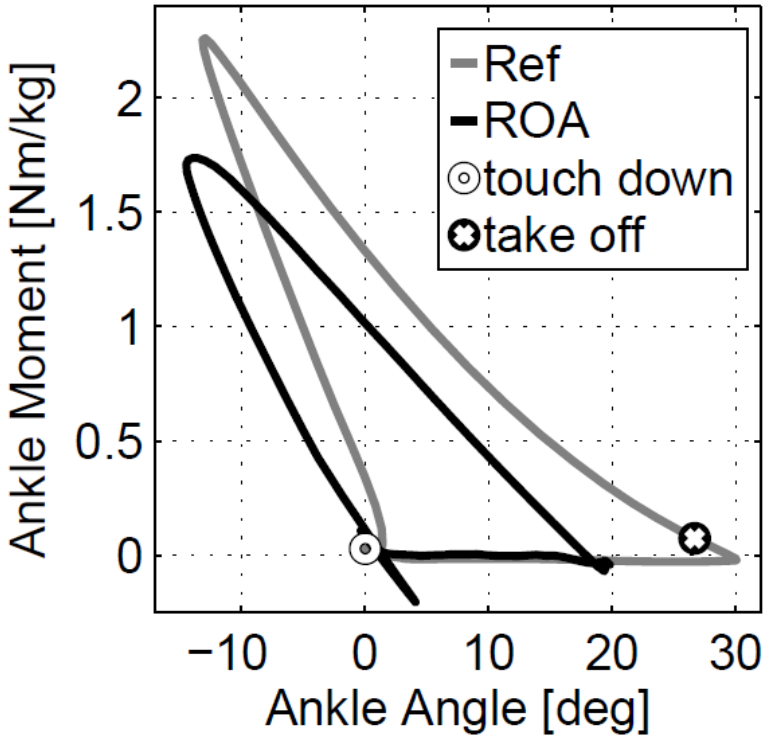

FIGURE 4.23: ANKLE MOMENT VS. ANKLE ANGLE FOR ABLE-BODIED DATA AT 2.55 M/S [12] AND DATA COLLECTED FROM THE ROA ON ONE SUBJECT AT 2.5 M/S.

The ROA running ankle angle, shown in Fig. 4.20, does not reach the values of plantarflexion that the able bodied data shows for similar speeds of running. Also shown in Fig. 4.20 and Fig. 4.23, the ankle moment is just shy of the able bodied data by about 1 Nm/kg. Although the moment and power of the ROA device is shy of able bodied data the overall shape of the angle, moment, and power curves are comparable.

This would suggest that the device needs to be better tuned for this user by shifting the actuator position surface (see Fig. 4.4). By shifting the surface, the shape of the ankle characteristic curves will stay the same but the amplitudes will increase better reaching these peak values of angle, moment and power at the ankle.

Testing shows power amplification of the ROA device during running gaits. This data is from a 73 kg user at a self-selected 2.5 m/s for running gait. Peak moment about the ankle during running of 130 Nm was measured. Peak power at the ankle is illustrated in Fig. 4.24 showing 7.5 W/kg while the motor only peaked at 2.7 W/kg during the step. These results demonstrate that the input mechanical power from the motor to the output ankle power yield a power amplification factor of 2.8.

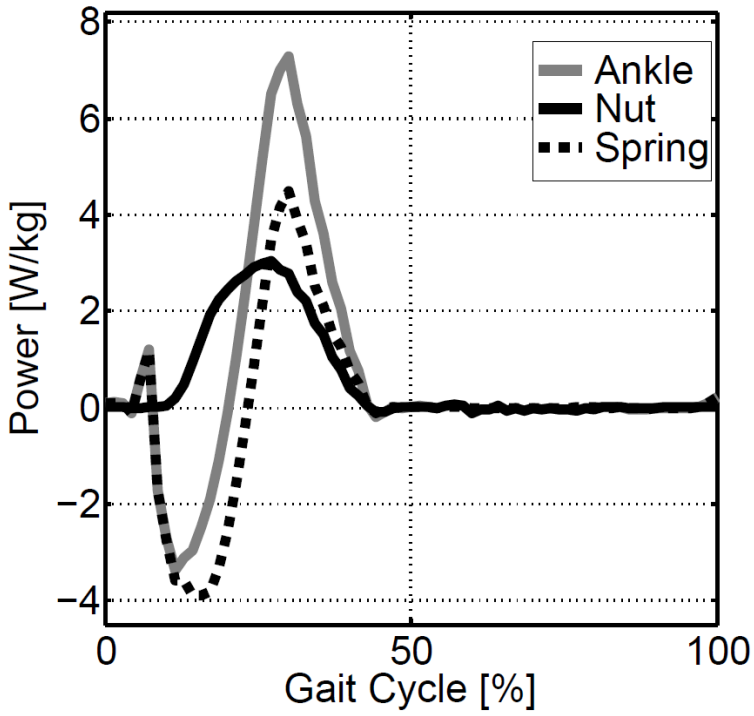

FIGURE 4.24: NORMALIZED ANKLE, SPRING AND NUT MECHANICAL POWER OUTPUT FOR 2.5 M/S RUNNING. MAXIMUM NUT POWER OUTPUT (2.7 W/KG) IS AMPLIFIED (FACTOR 2.7) BY THE SPRING TO ACHIEVE A MAXIMUM ANKLE OUTPUT OF 7.5 W/KG.

The ROA running ankle angle, shown in Fig. 4.20, reaches the values of plantarflexion that the able bodied data shows for similar running speeds. In Fig. 4.20 and Fig. 4.25, the ankle moment is just shy of the able bodied data by about 0.5 Nm/kg. Although the moment and power of the ROA device is shy of able bodied data the overall shape of the angle, moment, and power curves are comparable.

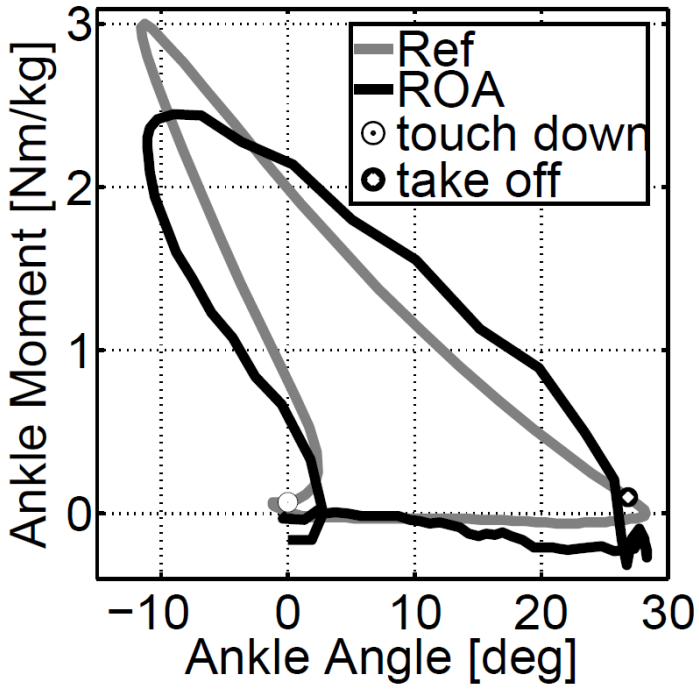

FIGURE 4.25: ANKLE MOMENT VS. ANKLE ANGLE FOR ABLE-BODIED DATA AT 4 M/S [12] AND DATA COLLECTED FROM THE ROA ON ONE SUBJECT AT 4 M/S.

The ROA device was also able to achieve sprinting with data showing peak moment of 190 Nm. In order to provide full powered running, the system was able to amplify the peak motor power of 3.5 W/kg during the sprint by 4.3 to reach peak ankle power of 15 W/kg as shown in Fig. 4.26.

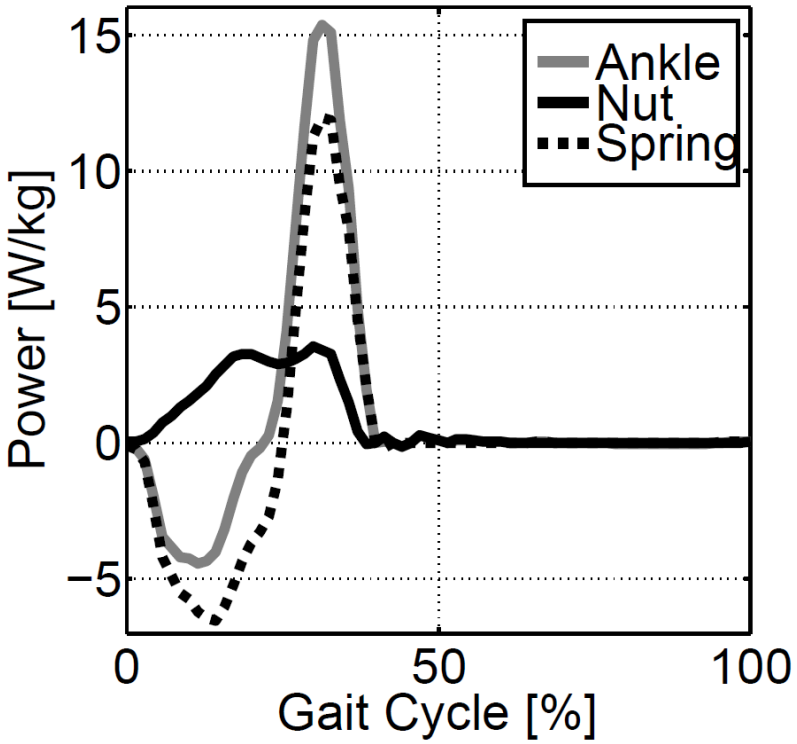

FIGURE 4.26: NORMALIZED ANKLE, SPRING AND NUT MECHANICAL POWER OUTPUT FOR 4 M/S RUNNING. MAXIMUM NUT POWER OUTPUT (3.5 W/KG) IS AMPLIFIED (FACTOR 4.3) BY THE SPRING TO ACHIEVE A MAXIMUM ANKLE OUTPUT OF 15 W/KG.

During sprinting the energy was calculated by numerically integrating the power curves. Figure 4.27 illustrates that the user stores substantial braking energy (60 J) into the spring element during early stance in the sprinting step. The motor adds 83 J of positive energy such that a total of 143 J of energy are released during push-off. The spring stores 60 J of energy and returns 60 J of energy to the user with the assumption that the metal spring is highly efficient. The total positive energy at the ankle is 88 J slightly greater than the positive energy of 83 J supplied by the motor. Slight numerical errors when integrating over the gait cycle may contribute to the small discrepancy of 5 J.

A motor spring system that allows for energy storage creates a very efficient system [113]. Without the spring, a motor only system would have to supply an additional 60 J of work. A passive spring system is not effective as well. It would store 60 J of work and return the energy but the ankle energy would remain at 0 J over the entire gait cycle. The 60 J of work at push off is not enough for high speed running.

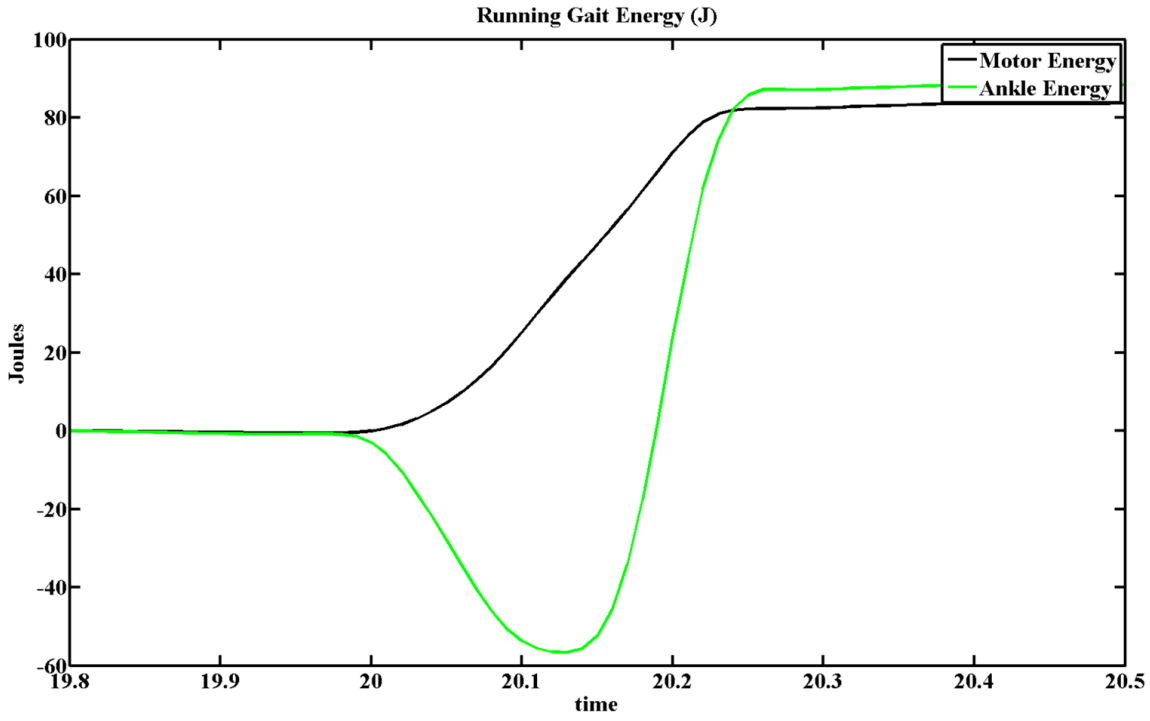

FIGURE 4.27: NORMALIZED MOTOR AND ANKLE ENERGY FOR SPRINTING GAIT. ENERGY STORAGE IN A SPRING (60 J) DECREASES ENERGY NEEDED FROM THE MOTOR (83 J) TO ACHIEVE 143 J AT PUSH OFF.

In addition to level ground, even terrain walking and running ruggedized testing of the ROA device was done on uneven trails allowing the person to walk up and down steep slopes and easily traverse difficult terrain. Figure 4.28 illustrates how this testing allowed the ankle to move through maximum angles of dorsiflexion and plantarflexion while navigating obstacles and providing the user with a powered gait.

FIGURE 4.28: 73KG USER RUGGEDIZED TESTING.

4.6 DISCUSSION

As speed is increased, it is expected that the peak moment increases and the moment and power curves are shifted left, earlier in the gait cycle. The actual curves are shifted correctly but the peak values are shy of the average able bodied gait data.

The angle discrepancy is attributed to the actuation surface (Fig. 4.4) not being properly tuned to our participant during this particular session. While the generic actuation surface works well for most individuals, fine tuning can be accomplished by shifting and scaling the surface at various walking speeds. Another artifact that suggests additional tuning of the surface is required is the oscillations seen in the data from take-off to touch down of Fig. 4.21. The toe oscillates in the swing phase if excessive energy remains in the spring when the user lifts the foot.

The ROA ankle is able to produce large peak power at push off shown in the top graphs in Fig. 4.20. The ROA has a compliant actuator that stores energy during the stance phase of gait. The tuned spring and continuous controller allow peak output power to be efficiently amplified when compared to the peak motor power input. Correct timing and amplification allow the ROA to reach output requirements of a running gait.

4.7 CONCLUSION

The ROA device represents a leap forward in powered ankle prosthesis technology. Initial testing shows a strong correlation with able-bodied kinematics and kinetics for both walking and running conditions. This single motor system is the first to demonstrate kilowatt levels of ankle power to support amputee running gait.

There is an increasing trend for the development of bionic prosthetic devices driven by advances in motor, battery, sensor, and material technology as well as a growing demand for better functionality from the amputee population. This research/product development area is poised for steep growth as these supporting technologies continue to evolve. It is of critical importance to gain a scientific understanding of how these systems affect the amputee population and what group of amputees will benefit the most.

Now that practical powered ankle prostheses exist, meaningful research can be conducted on a variety of biomechanical metrics. Preliminary research suggests that these systems can reduce metabolic cost, increase self-selected pace, and reduce ground reaction forces on the healthy limb [114]. The degree at which these benefits are realized will depend highly on the control system, device weight, and actuation strategy. Additionally, these systems return a functioning antagonistic monoarticular ankle joint actuation to an amputee. Greater benefit would be expected if these concepts are extended to include the bi-articular structures coupling the knee and the ankle joint [115].

Future improvements may include an additional degree of freedom to allow inversion and eversion at the ankle. This type of 2 DOF ankle will need continued advancement in control schemes and smart use of mechanisms to insure amputee stability and confidence during gait. Achievements have been made in peripheral nerve interface and the possibility for their control of prosthetic devices should also be explored allowing the amputee to have more ownership and agency over the ROA device behavior.

CHAPTER 5

ACTIVELY PASSIVE JOINTS

Many different types of mechanisms have been used to develop joint actuators. One specific example of joint actuators are those found in ankle prosthetics. Some of these ankle systems are powered in that they use motors to achieve desired output [51], [53], [65], [116]–[118]. Other systems use a tuned mechanism to create a passive joint that does not require motors to achieve its desired performance [36], [119]. Each mechanism, either powered or passive, has a joint stiffness at each specific joint angle that corresponds with its motion and behavior [13]–[15], [11]. This stiffness can be controlled, or forced in powered systems, to simulate able bodied joint behavior [9], [10], [16]–[19]. Stiffness can also be uncontrollable but predetermined from optimally designed passive systems [20]–[22].

There are advantages and disadvantages to both powered and passive joint mechanisms. A passive joint is beneficial when the joint requirements are predictable and constant. The passive joint can be optimally designed and requires no power during use. Powered joints are advantages for dynamic situations with changing load requirements in order to interact with an unknown environment. Powered joints in prosthetics are limited by weight and size and battery capabilities. Passive prosthetic joints are usually designed for a specific situation and are not optimized for all the demands of human locomotion.

While using the application of an ankle joint prosthesis, a method for decoupling the joint stiffness from the joint position in any robotic joint is proposed. The advantage of this is to combine the optimization of passive system design and natural mechanism characteristics with a powered system. By using the preprogrammed powered system to adjust the mechanism stiffness at specific times, a joint can naturally (uncontrolled) achieve desired performance during use. Small adjustments are made to optimize the passive behavior. By only using a powered system to make slight adjustments to a passive mechanism the power and weight requirements should be much lower than in a fully powered joint mechanism.

The ideal scenario for this application is for systems with cyclical behavior where different desired joint stiffness is predictable. A powered ankle prosthetic applied to walking gait dynamics is such a case.

5.1 DECOUPLING STIFFNESS FROM POSITION

5.1.1 Mechanism Description

Joint stiffness can be described as the change in joint moment with respect to the change in joint angle ($\frac{\Delta M}{\Delta \theta}$). To develop a method for decoupling the joint stiffness and joint position, a simple mechanism with a spring attached to a lever arm is used. Figure 5.1 shows the details of this mechanism as applied to an ankle prosthetic device. The purpose of this mechanism is to show how the moment vs. ankle angle graph changes when the spring connection at (x2, y2) position is adjusted without changing the instantaneous joint moment about the ankle joint.

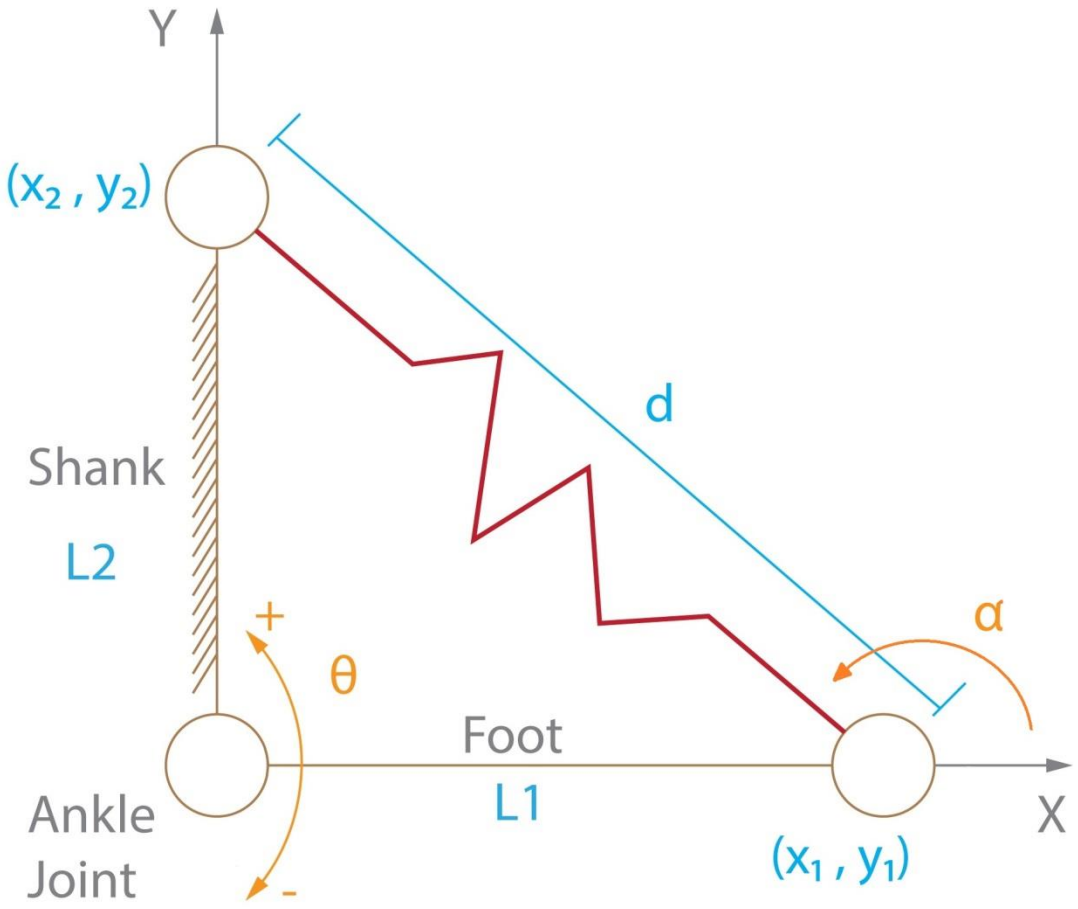

FIGURE 5.1: PROSTHETIC ANKLE JOINT MECHANISM REPRESENTED BY A LINEAR SPRING AND LEVER ARM.

Figure 5.1 shows the mechanism where L1 is the foot and L2 is the shank. Links L1 and L2 join at the origin which is the ankle joint. The points (x1, y1) and (x2, y2) are the spring connections and the distance between them is described by the variable d. For ankle angle, the zero degree position is the positive x-axis and ankle angle is described by θ, with dorsiflexion being positive and plantar flexion being negative.

In order to see the change in a moment vs ankle angle graph, a method for finding moment for every angle in this particular mechanism is established. The *L1* linkage is of constant length which makes it easy to find the (*x1*, *y1*) position for every angle (θ) of the foot. Equations (5.1) – (5.4) use these two spring connection points, spring stiffness (*K*), and spring free length (d_0), to solve for the spring angle (α) and the components of force (*F*) from the spring displacement. Equation (5.5) is the (*x*, *y*, *z*) components of any vector (*r*) that connects the origin with the force vector from the spring. Equation (5.6) uses the cross product (*r* x *F*) to calculate the moment (*M*) that the combined force components create at a distance (|*r*|) from the origin.

$$d = \sqrt{(y2 - y1)^2 + (x2 - x1)^2} \tag{5.1}$$

$$\alpha = 180 - \tan^{-1}\frac{y2 - y1}{x2 - x1} \tag{5.2}$$

$$|F| = K\,(d - d_0) \tag{5.3}$$

$$F = [\,|F|\cos(\alpha)\,, |F|\,\sin(\alpha)\,, 0\,] \tag{5.4}$$

$$r = [\,x1\,, y1\,, 0\,] \tag{5.5}$$

$$\mathrm{M} = (\mathrm{x1})|\mathrm{F}|\sin(\alpha) - (\mathrm{y1})|\mathrm{F}|\cos(\alpha) \tag{5.6}$$

The (x1, y1) points are dependent on the angle (θ) of the foot and therefore the moment is also a function of the foot angle. Equation (5.7) shows the moment can also be written as function of spring stretch, spring stiffness, and the perpendicular distance (r_p) the spring is from the ankle joint.

$$M = K\,(d - d_0)\,r_p \tag{5.7}$$

By making adjustments to the mechanism at the (*x2*, *y2*) spring connection point the spring stretch and the perpendicular distance will both be affected. If moment (M) is to remain the same during these adjustments then the spring stretch ($d - d_0$) and perpendicular distance (r_p) need to be changed inversely proportional to each other keeping Eq. (5.7) constant.

The goal is to keep the moment constant while adjusting the mechanism configuration. The stiffness of the mechanism is dependent on the mechanism configuration therefore by changing the configuration the stiffness changes also. This change in stiffness causes no change in ankle position because the moment about the ankle during the change remains constant.

5.1.2 Calculations

Consider the force vector applied at the (*x1*, *y1*) joint from the spring. For the ankle joint to have the same moment at different (*x2*, *y2*) positions the component of the spring force vector perpendicular to the *L1* link (foot) must remain the same. Figure 5.2 below shows the scaled force vectors (blue) from spring stretch for 10 different (*x2*, *y2*) positions that will produce a constant moment. This means that these 10 positions lie on the constant moment path for this specific ankle angle.

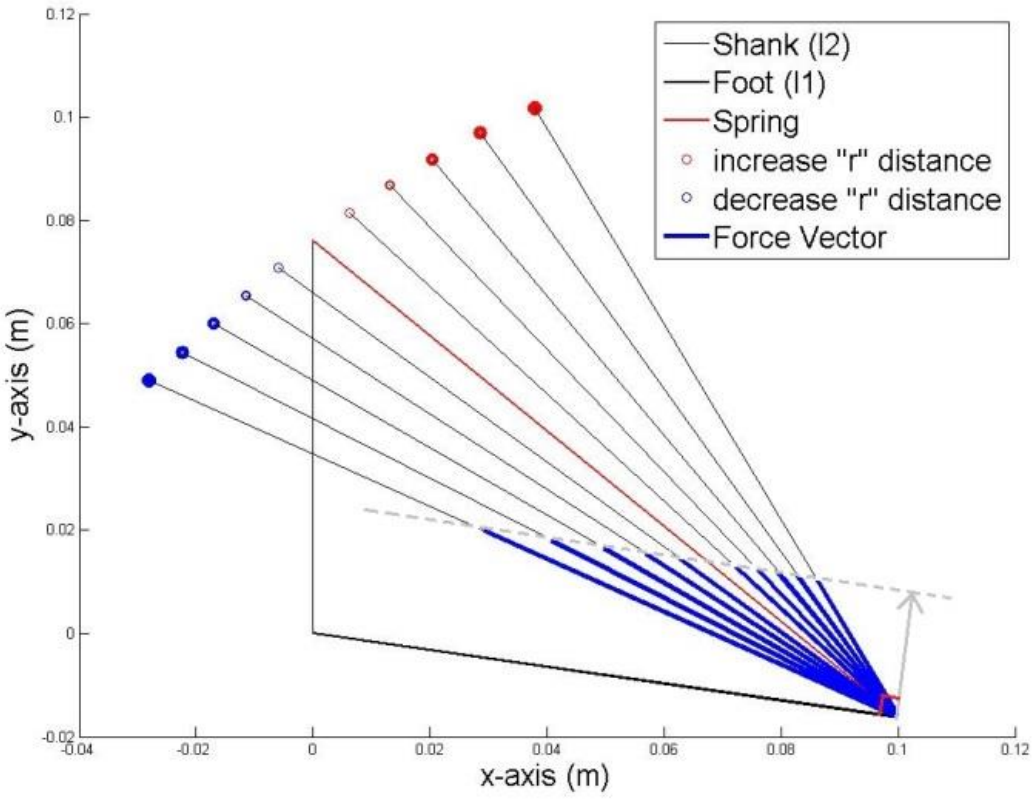

FIGURE 5.2: FORCE VECTOR COMPARISON FOR 10 JOINT POSITIONS.

To follow the moment curve produced by able bodied gait, a connection is found between the desired stiffness at a particular gait percent and where to move the *(x2, y2*) position to achieve that stiffness.

This means that at a specific ankle angle and moment there is an (*x2, y2*) position that will allow the ankle to naturally achieve the proper increase or decrease in moment as it travels through its normal ankle angles. For each consecutive ankle angle and corresponding moment the constant moment path is calculated. At the intersection of one constant moment path with the next (assuming it exists) is the position where the spring (*x2*, *y2*) coordinates can be placed and produce the proper torsional stiffness.

Figure 5.3 shows the constant moment paths for two spring positions with unique ankle moment and angle requirements. These two paths intersect at a position that will give the spring mechanism the proper torsional stiffness. If all the mechanism adjustments follow a constant moment path then the mechanism stiffness is always adjusting without changing the ankle angle during the adjustment.

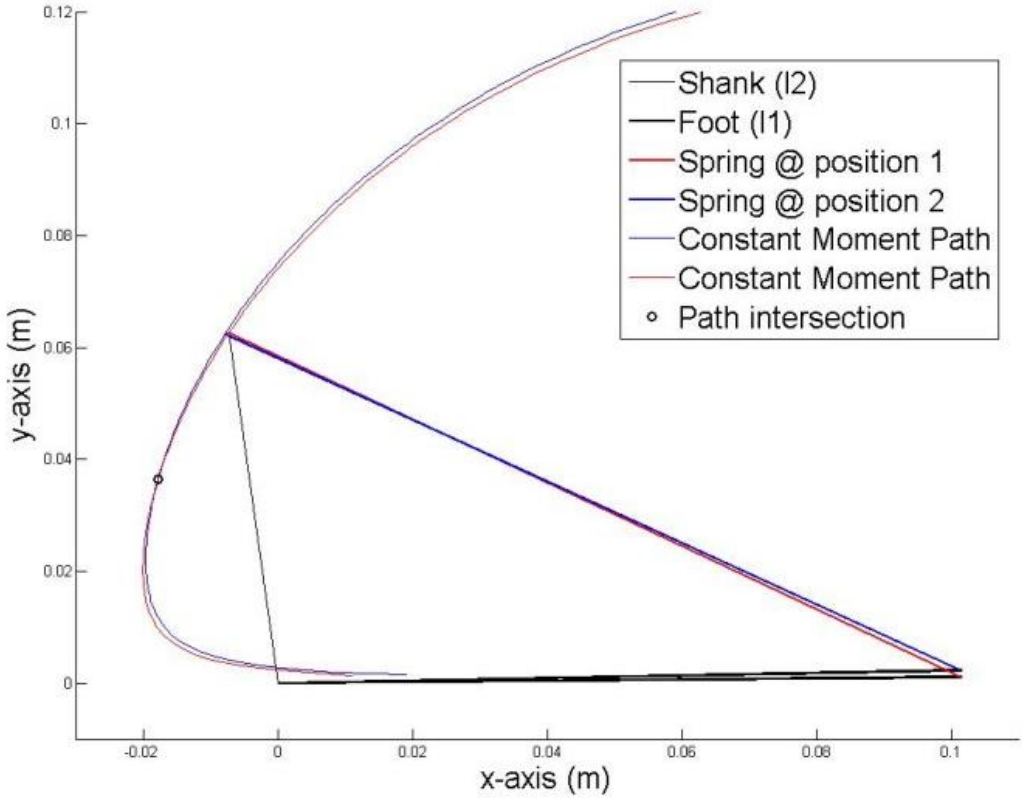

FIGURE 5.3: CONSTANT MOMENT PATH INTERSECTIONS FOR 2 ANKLE POSITIONS.

One method for finding this shared (*x2*, *y2*) point for two ankle moments and corresponding positions is to model the two force vectors as wrenches sharing an (*x*, *y*) coordinate. In this way $\$_1$ becomes $\{\mathscr{L}_1, \mathscr{M}_1, 0; 0, 0, \mathscr{P}_1\}$ and $\$_2$ becomes $\{\mathscr{L}_2, \mathscr{M}_2, 0; 0, 0, \mathscr{P}_2\}$ as shown in Fig. 5.4. In both wrenches coordinates $\mathscr{N} = \mathscr{P} = \mathscr{Q} = 0$ for this planar mechanism.

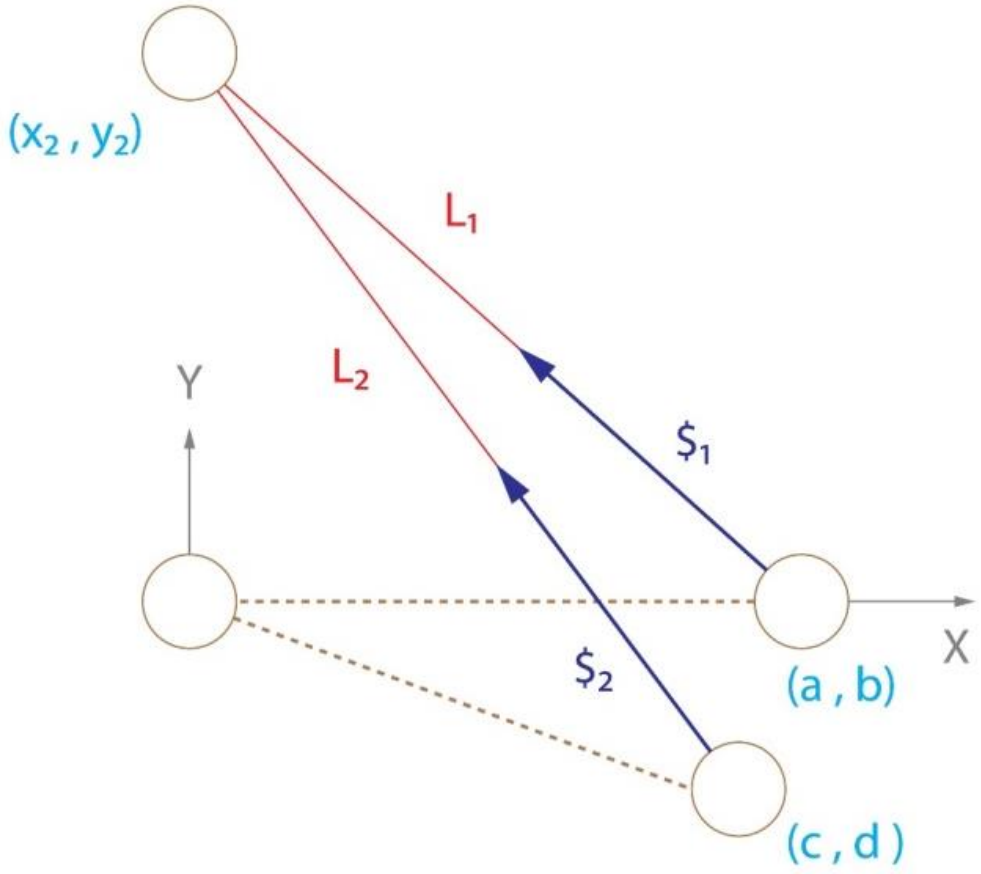

FIGURE 5.4: SCREW REPRESENTATION OF ANKLE KINEMATICS.

The unknowns in Fig. 5.4 include the (*x2, y2*) coordinates, and the $\mathscr{L}$ and $\mathscr{M}$ direction coordinates along with distance L_1 and L_2 between points (*x1, y1*) and (*x2, y2*). The given variables include the moment coordinate $\mathscr{R}$ and the (*x1, y1*) coordinates represented as either (*a, b*) or (*c, d*). Each screw can provide 4 equations:

$$\mathscr{R} = \mathscr{M}\mathsf{x}_1 - \mathscr{L}\,\mathsf{y}_1 \tag{5.8}$$

$$\mathscr{R} = \mathscr{M}\mathsf{x}_2 - \mathscr{L}\,\mathsf{y}_2 \tag{5.9}$$

$$L_n{}^2 = (x_2 - x_1)^2 + (y_2 - y_1)^2 \tag{5.10}$$

$$\mathscr{L}^2 + \mathscr{M}^2 = [(L_n - d_0)K]^2 \tag{5.11}$$

In Eq. (5.11), d_0 is the free length of the spring and K is the spring stiffness. Equations (5.8) and (5.9) can be combined to find $\mathscr{L}$ and $\mathscr{M}$ as functions of the point (*x2, y2*). Substituting these new values along with Eq. (5.10) into Eq. (5.11) creates two equations, one from each screw, with the variables *x2* and *y2* being the only unknowns. Equation (5.12) is the general representation of these two equations.

$$\left[\mathrm{R}\left(\frac{1-\frac{x_2}{x_1}}{\frac{y_1}{x_1}x_2 - y_2}\right)\right]^2 + \left[\mathrm{R}\left(\frac{1}{x_1} + \frac{y_1}{x_1}\left(\frac{1-\frac{x_2}{x_1}}{\frac{y_1}{x_1}x_2 - y_2}\right)\right)\right]^2 = \left[\left(\sqrt{(x_2 - x_1)^2 + (y_2 - y_1)^2} - d_0\right)K\right]^2 \tag{5.12}$$

5.1.3 Actively Changing Mechanism

To analyze a mechanism that can decouple joint stiffness from position, the first step is to show the base moment vs ankle angle graph for the simple mechanism. Then by choosing a specific angle of the foot and adjusting the (*x2, y2*) coordinates in a constant moment path as described above, we can compare the adjusted mechanisms moment vs ankle angle graph with the original. The moment at the chosen angle should remain constant while the slope of the moment vs. angle line should change. An ankle angle range used in this analysis is comparable to able bodied gait data [9].

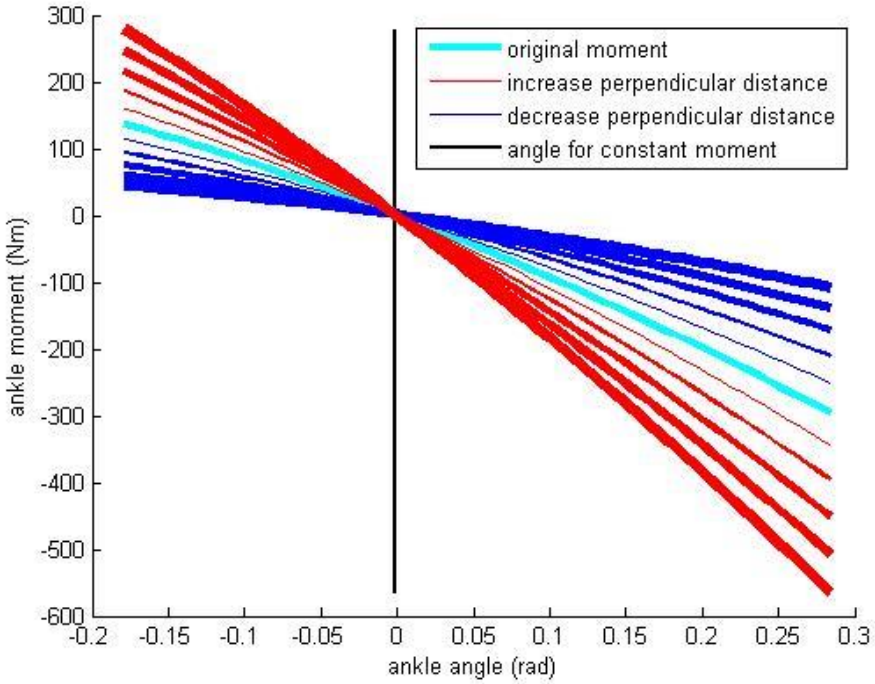

FIGURE 5.5: MOMENT VS ANKLE ANGLE LINES FOR CHANGING (X2, Y2) POSITION AT CONSTANT ANKLE ANGLE OF 0 RAD.

Figure 5.5 shows the progression of the moment curve as (*x2*, *y2*) coordinates are gradually changed to keep the constant moment about a chosen ankle angle of zero degrees. The torsional stiffness is described as the derivative of the moment profile with respect to the angle. The progression of the blue and red moment profile lines show that the slope and therefore the torsional stiffness at this specific angle is changed while keeping a constant moment. How far the mechanism is adjusted determines how stiff or soft the mechanism will feel without changing the ankle's instantaneous position.

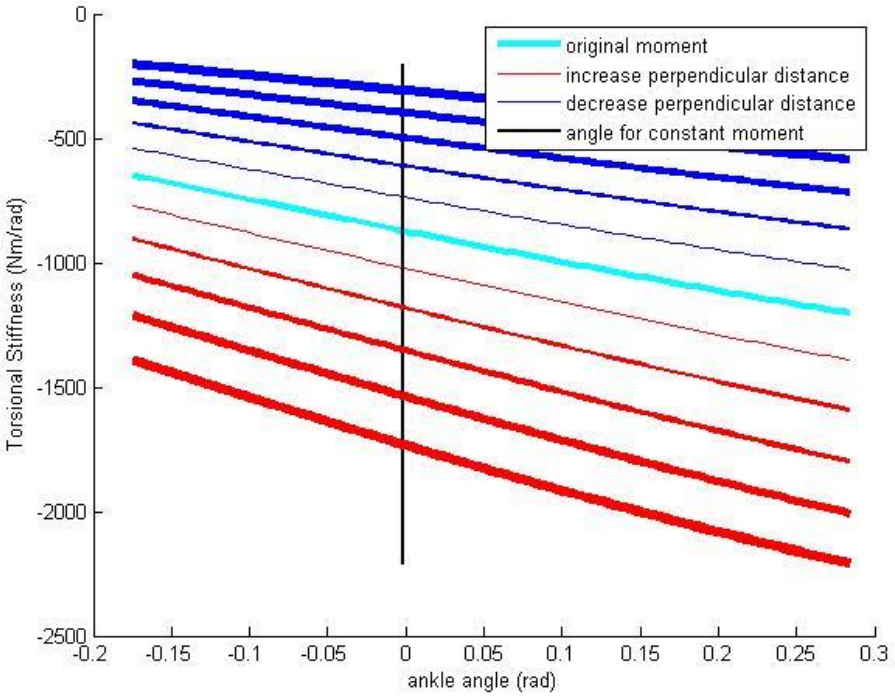

FIGURE 5.6: CHANGING OF TORSIONAL STIFFNESS FOR DIFFERENT (X2, Y2) VALUES AT 0 ANKLE ANGLE.

As the (*x2*, *y2*) coordinates are adjusted at an ankle angle of 0 degrees, Fig. 5.6 shows how the stiffness is increased and decreased proportionally with the increase and decrease of the spring's perpendicular distance from the origin. Figure 5.7 shows that a different ankle angle can also be chosen with similar results.

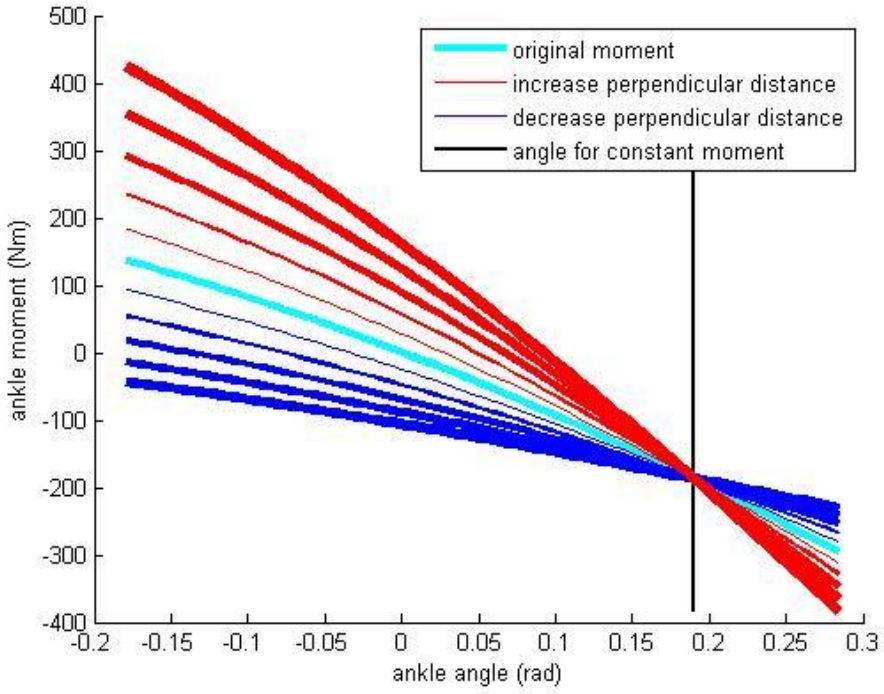

FIGURE 5.7: MOMENT VS ANKLE ANGLE LINES FOR CHANGING (X2, Y2) POSITION WITH CONSTANT ANKLE MOMENT AT 80% GAIT CYCLE.

Using this method any ankle angle, or gait cycle percentage, can be chosen and the mechanism can adjust the torsional stiffness at that point without changing the moment. By keeping ankle moment constant, the ankle position, at that instant, will remain the same also, thus decoupling the stiffness from position in a joint mechanism.

5.2 CONSTANT MOMENT PATH

Equation (5.12) from both screws were numerically solved to find the shared (*x2, y2*) value for each pair of ankle moments and angles in an able bodied gait cycle. Once all the (*x2, y2*) points were found for one gait cycle, the path was created to show where the end of the spring will need to travel to achieve all stiffness values during gait. This is shown in Fig. 5.8 where the blue points are the specific, calculated (*x2, y2*) points.

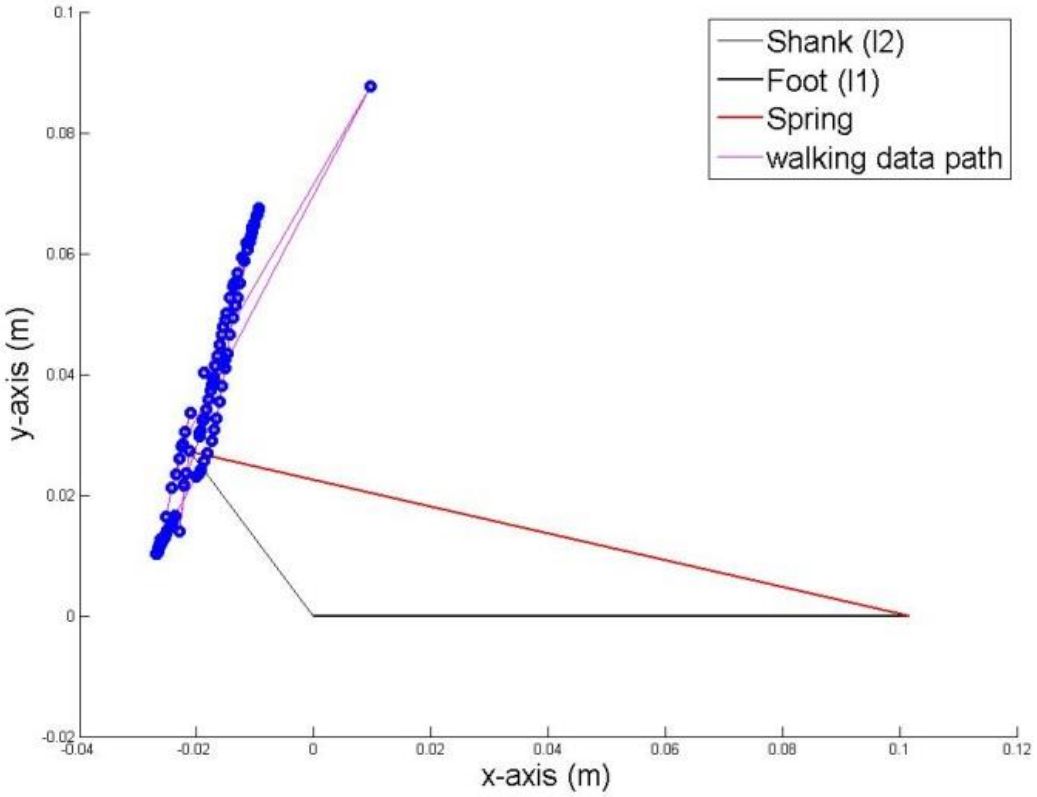

FIGURE 5.8: COORDINATES OF (X2, Y2) POSITIONS FOR ONE GAIT CYCLE.

The resulting path is highly encouraging, due to its linear nature. It suggests that the required motion of such an ankle actuator may only require one motor. It is also important to note that the one extraneous point above all the rest occurs during the swing phase and can be ignored for this analysis.

Once this path was found the resulting moment vs gait percent was calculated based on the new (*x2*, *y2*) points to see how well it matches the original data. Figure 5.9 shows the new data compared with the ankle moment data from able bodied walking.

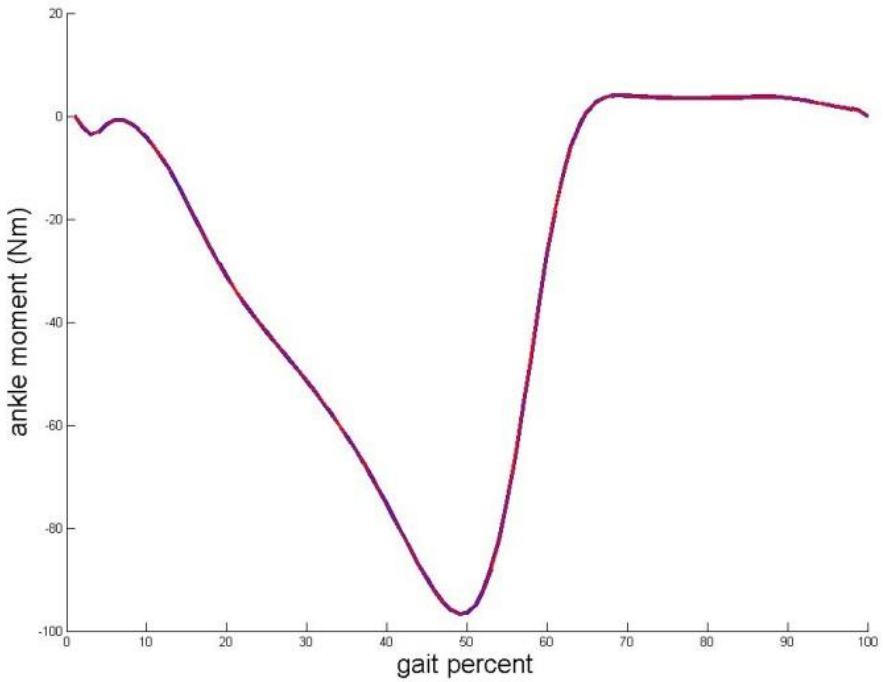

FIGURE 5.9: ANKLE MOMENT FROM WALKING DATA (BLUE) COMPARED WITH MECHANISM (RED).

The two data sets in Fig. 5.9 line up directly. This is to be expected as it proves the math and the method to be correct. In application the points are nearly linear and need to be represented in a linear manner if expected to predict their performance when reached by a linear actuator.

Two different methods are explored, fitting the data with a line and fitting the data with a circle. The reason to test a circle fit is that if the path can be appropriately mimicked with a circle of constant radius this will allow any axial force to be carried by a link on a radial bearing instead of on a linear bearing and rail. The path fitting is focused on the section of data involved with the loading of the ankle from heel strike to toe off. The swing phase of gait can be optimized later for position, with near zero moment, to prepare the ankle angle for the next heel strike.

A linear least squares fit was used to fit the new (*x2, y2*) positions to a line. Each data point was then adjusted to be on the line at a point closest to its original position. Some data points were slightly adjusted further along the new line in order to achieve the best performance. Using these fitted (*x2, y2*) positions, a moment curve was created using the able bodied ankle angle path. Figure 5.10 shows the linear fit (in black) to the (*x2, y2*) data points (blue circles).

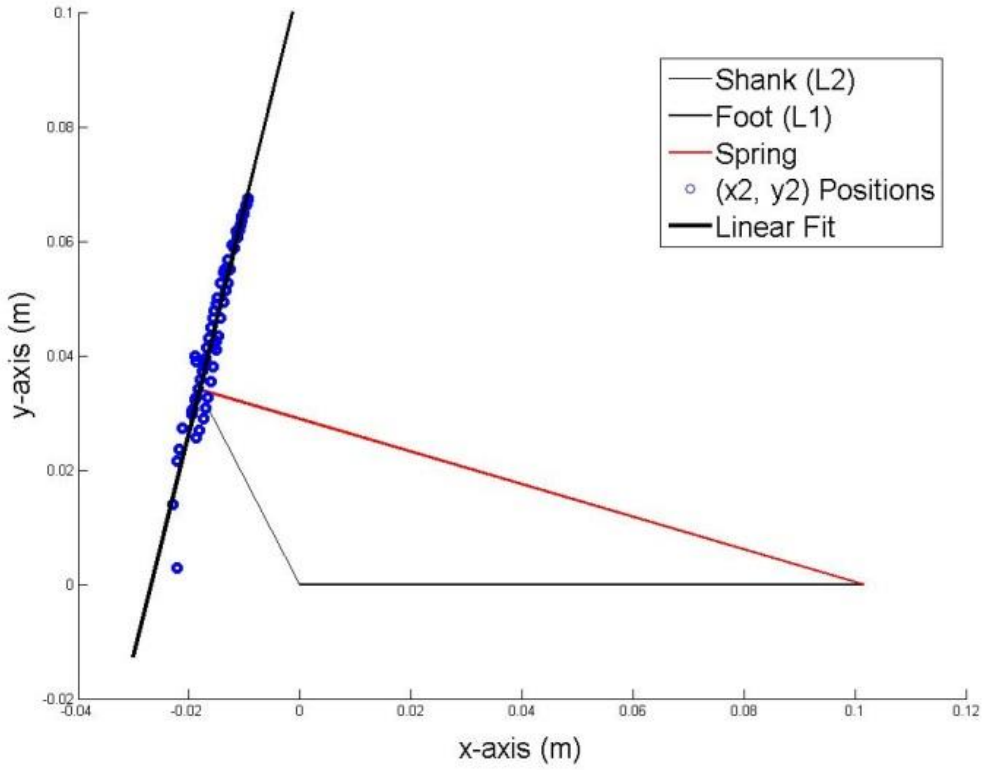

FIGURE 5.10: LINEAR FIT OF (X2, Y2) DATA POINTS, LINE SLOPE = 3.934, LINE Y-INTERCEPT = 0.105m.

A non-linear least squares fitting method was then used to fit the new (*x2*, *y2*) positions along a circular path [120]. This method returns a circle center and radius of best fit. Each data point was then moved towards or away from the circle center until it lies on the new circle path. Some data points were slightly adjusted further along the circle in order to achieve the best performance. Figure 5.11 shows the circular fit (black) to the (*x2*, *y2*) data points (blue circles). Using these fitted (*x2*, *y2*) positions a moment curve was created using the able bodied ankle angle values.

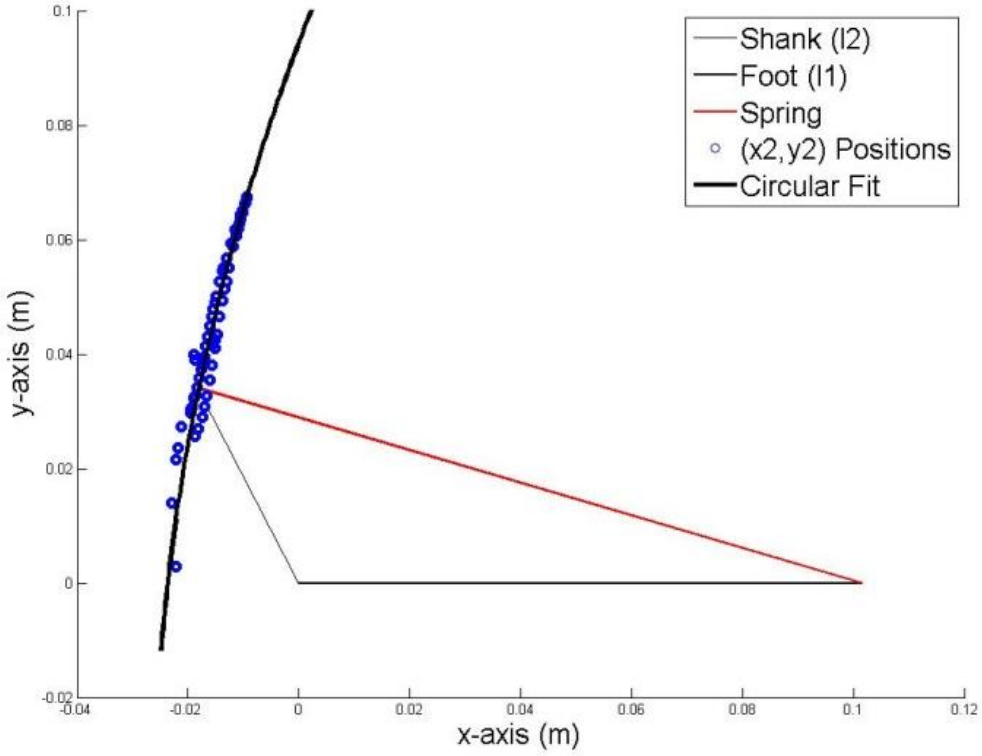

FIGURE 5.11: CIRCULAR FIT OF (X2, Y2) DATA POINTS, CIRCLE CENTER AT (0.358, -0.045), WITH RADIUS OF 0.384m.

Figure 5.12 shows the corresponding ankle moment curve from both the linear fitted data path and circular fitted data path compared with able bodied moment. The circular path results show improvements over the linear fit in matching able bodied data. Although some variations from able bodied gait moment data exist, the overall shape and path resemblance are highly correlated. Further adjustments in radius or circle center can be made in order to provide a closer fit to the moment path but may be at the cost of additional energy into the system and less natural stiffness from the mechanism configuration.

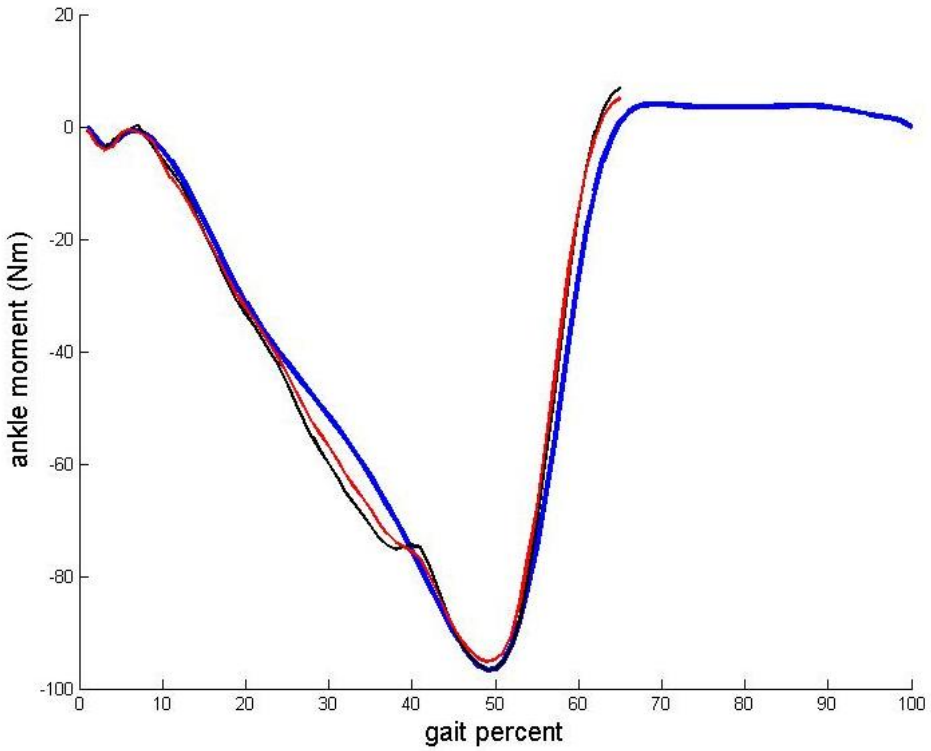

FIGURE 5.12: MOMENT VS GAIT PERCENT FROM LINEAR FIT (BLACK) AND CIRCULAR FIT (RED) COMPARED TO ABLE BODIED DATA (BLUE).

Other optimization trials may be achieved when considering fitting the moment data rather than the constant moment path calculations. By using the constant moment path predictions as a starting point it is hypothesized that the energy to achieve the correct moment path is minimized. Further analysis and testing has been completed and described in the following sections.

5.3 SIMPLIFY PATH

To minimize the movement of the mechanism, six different torsional stiffness values (slopes *1-5*, *A*) were chosen to fit the ankle moment vs. ankle angle graph. Figure 5.13 shows how the different values for stiffness chosen fit to the general shape of the able bodied data. The goal is to adjust the mechanism stiffness only four times (positions *A-D*) allowing the ankle to passively meet the required moments and positions similar to able-bodied data. The mechanism used to reach these six stiffness values is called a quasi-stiffness mechanism.

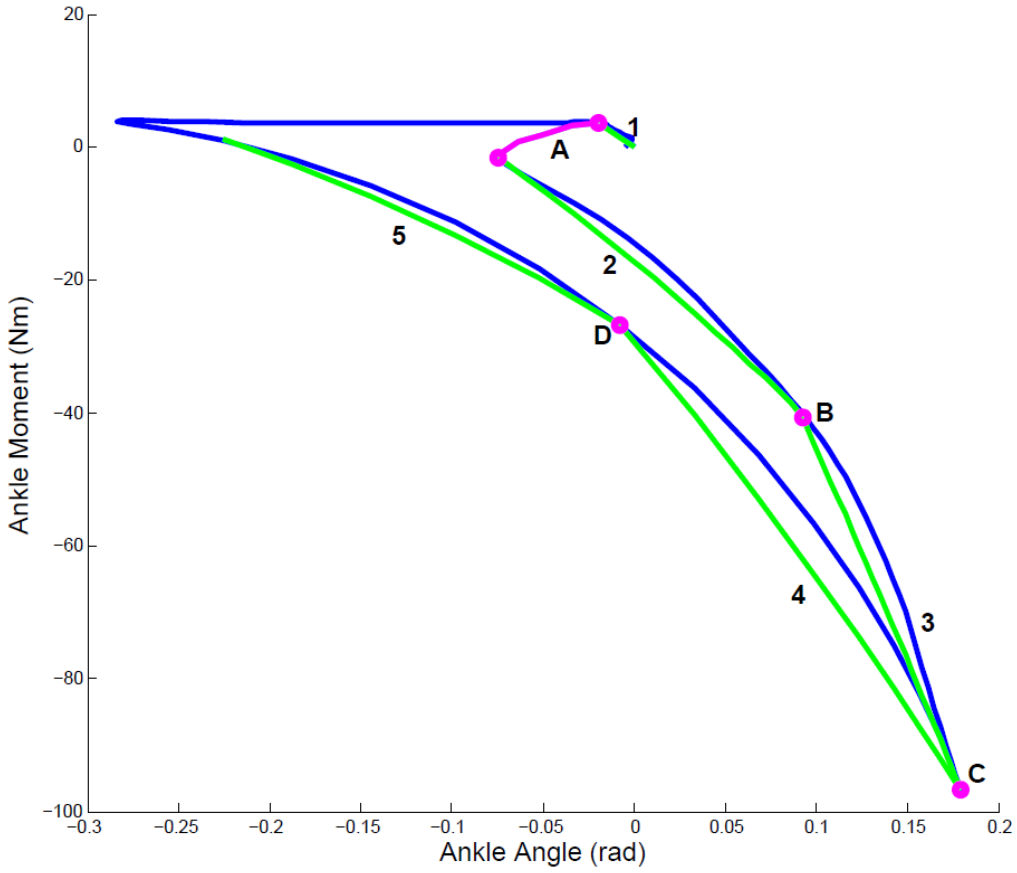

FIGURE 5.13: ANKLE MOMENT VS ANKLE ANGLE SHOWING 6 DIFFERENT QUASI-STIFFNESS VALUES REQUIRED.

Each quasi-stiffness values are chosen by using the constant moment paths of a starting and ending ankle moment and angle set from able bodied data then finding where these two paths intersect. If the mechanism (*x2*, *y2*) position is at this intersection, then the ankle will start with the correct moment and as the ankle progresses to the ending ankle angle it will naturally reach the chosen ankle moment as well. This process can then be repeated by following one constant moment path until it reaches the intersection of the next constant moment path associated with each new stiffness. This process is repeated along paths *1*, *2*, *3*, *4*, and *5*. Along path *A*, it is not possible to follow a constant moment path as both the position and moment are varying.

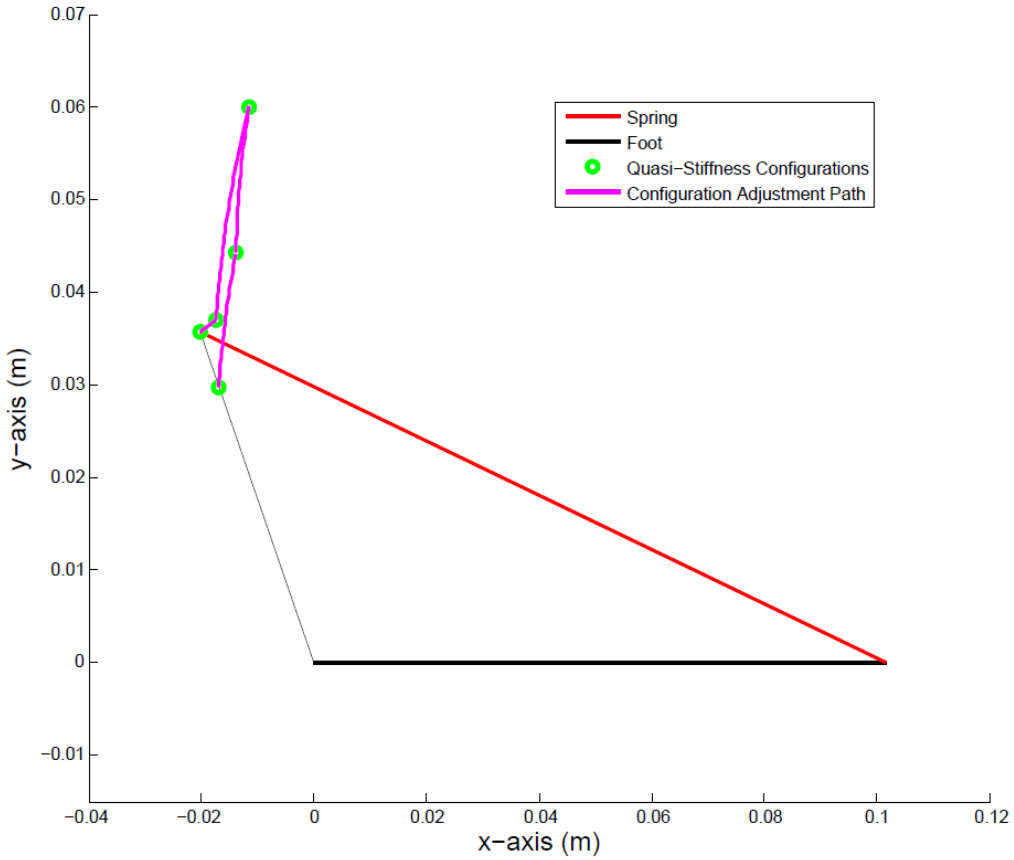

FIGURE 5.14: SHOWING THE FOOT AND SPRING WITH THE MECHANISM CONFIGURATIONS AND PATHS FOR CHANGING CONFIGURATIONS.

This method was used to find the mechanism quasi-stiffness configurations and configuration adjustment paths to reach the stiffness values shown in Fig. 5.13. The resulting 5 configurations and 4 adjustment paths are shown along with the spring and foot mechanism in Fig. 5.14. The green circle locations in Fig. 5.14 are the configurations which behave as shown in Fig. 5.13. Each purple path is the transition path from one configuration of the mechanism to another. The transition point (each green point in Fig. 5.14) is along a constant moment path which will not change the ankle angle or moment during its transition. The mechanism then holds its position with a new stiffness which connects ankle moments and ankle angles along the green lines in Fig. 5.13.

There are two mechanisms that can be changing at different times. The foot or ankle mechanism changes angle and moment as shown in Fig. 5.13. The green paths (Paths *2, 3, 4,* and *5*) in Fig. 5.13 follow constant stiffness paths where the moment and ankle angle change at a fixed rate given by the stiffness.

The second mechanism or "adjustment mechanism" is used to adjust the spring point (*x2, y2*) so that the mechanism is tuned for a different stiffness. For example, the quasi-stiffness is changed at Point *B* in Fig. 5.13 by changing the adjustment mechanism following the Path *B* shown in Fig. 5.15. The mechanism is held constant at Point *3* as shown in Fig. 5.15 as the ankle or foot moves along the constant stiffness Path *3* as shown in Fig. 5.13.

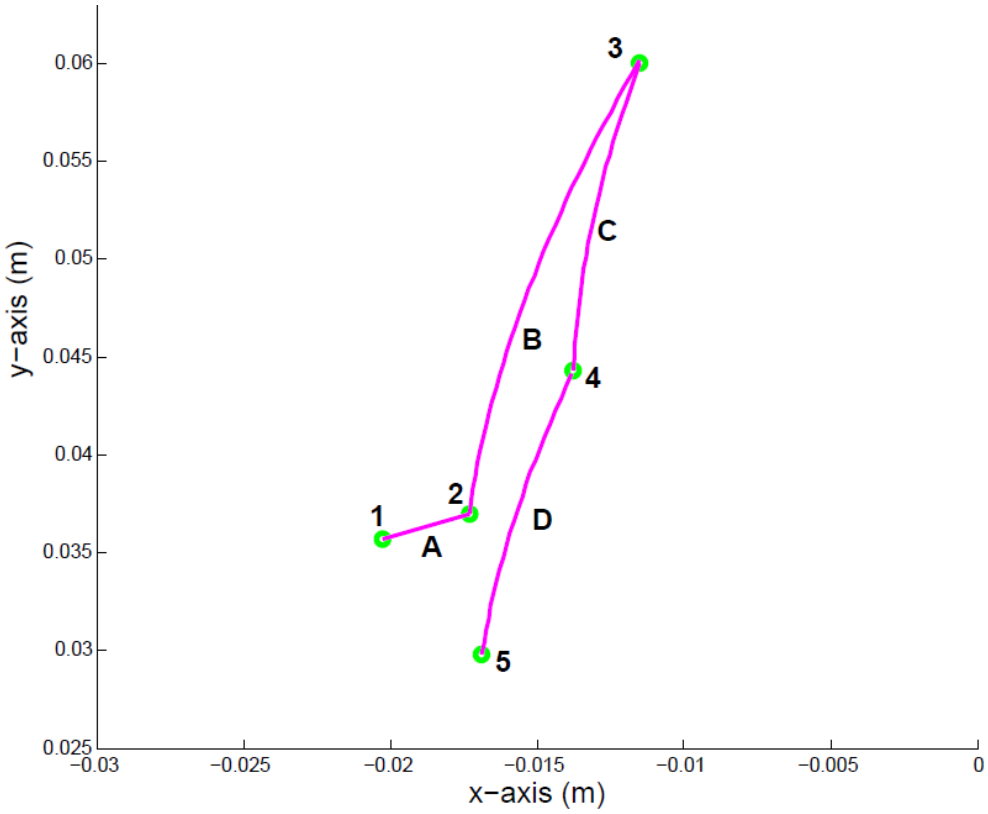

FIGURE 5.15: SHOWING THE PATH OF (X2, Y2) IN ORDER TO REACH THE QUASI-STIFFNESS RANGES.

This paragraph is a restatement of the previous paragraph for more clarity. The quasi-stiffness configurations and adjustment paths are shown in Fig. 5.15 labeled to show how each section is correlated to Fig. 5.13. The points shown as *A*, *B*, *C*, and *D* in Fig. 5.13 are the mechanism transition points where the mechanism is to transition between two stiffness values. Section *A* in Fig. 5.13 is a stiffness value that is not

'naturally' achievable by the mechanism being used. Energy is released during section *A* which can be used to adjust the stiffness to meet slope *2*. As the mechanism transitions form configuration *1* to configuration *2* all the required moment and angle values are reachable as the energy is released at a predetermined rate. Each mechanism configuration will result in a passive ankle system until the next stiffness value is required. The transition paths will then be the only times this mechanism may require power in order to change stiffness.

5.4 RESULTS

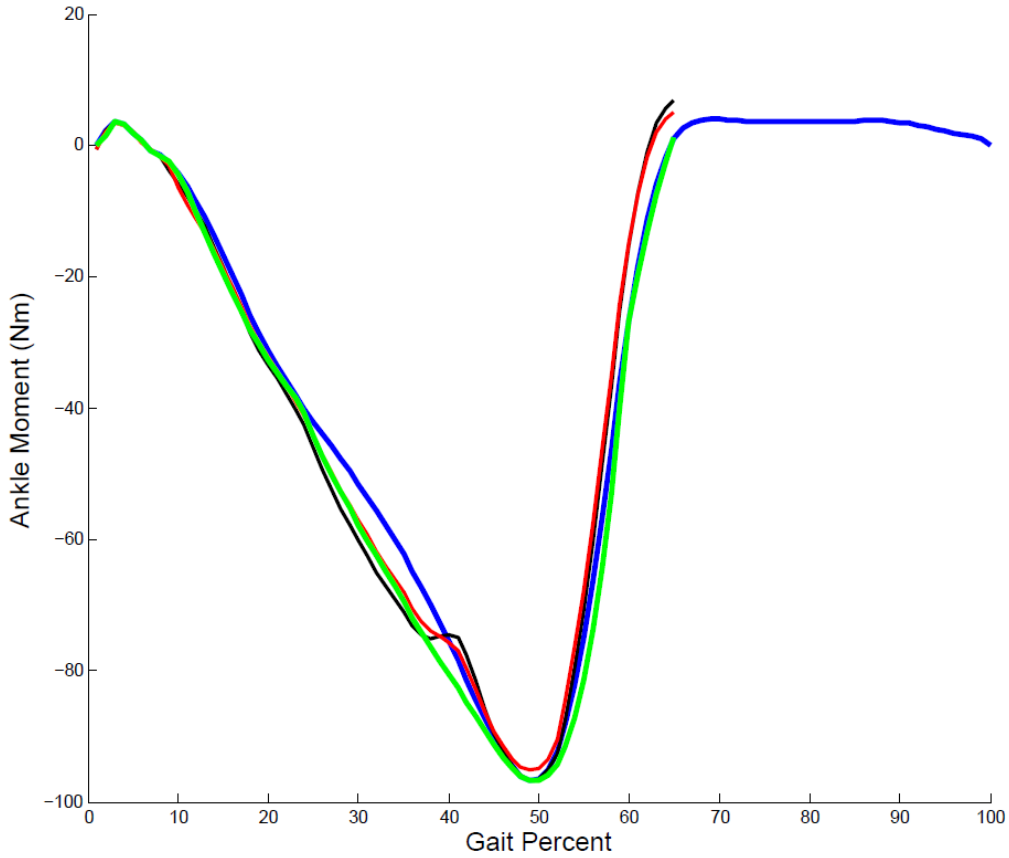

FIGURE 5.16: MOMENT VS GAIT PERCENT FROM LINEAR FIT (BLACK) AND CIRCULAR FIT (RED) AND QUASI-STIFFNESS FIT (GREEN) COMPARED TO ABLE BODIED DATA (BLUE).

Three cases are compared. In case *1*, the "adjustment mechanism" follows a linear path shown in Fig. 5.10. In case *2*, the "adjustment mechanism" follows a circular path shown in Fig. 5.11. In case *3*, the "adjustment mechanism", follows the path shown in Fig. 5.15. In the quasi-stiffness case, the mechanism is allowed to hold position during points *1-5* and only adjust along paths *A-D* in Fig. 5.15. Using the three cases, the output moment during the stance phase of gait is shown in Fig. 5.16 for the three cases. A smooth ankle moment profile is created using the third case as shown in Fig. 5.16. The quasi-stiffness mechanism path provides a better fit to the able bodied moment data than the linear and the circular mechanism fit especially during push off. It is also noticeable that at around 40% gait of the moment profile, the path is much smoother for the quasi-stiffness mechanism when compared to the others, although it is still not exact. Overall the quasi-stiffness method has a smooth fit to able bodied data with only making four active adjustments.

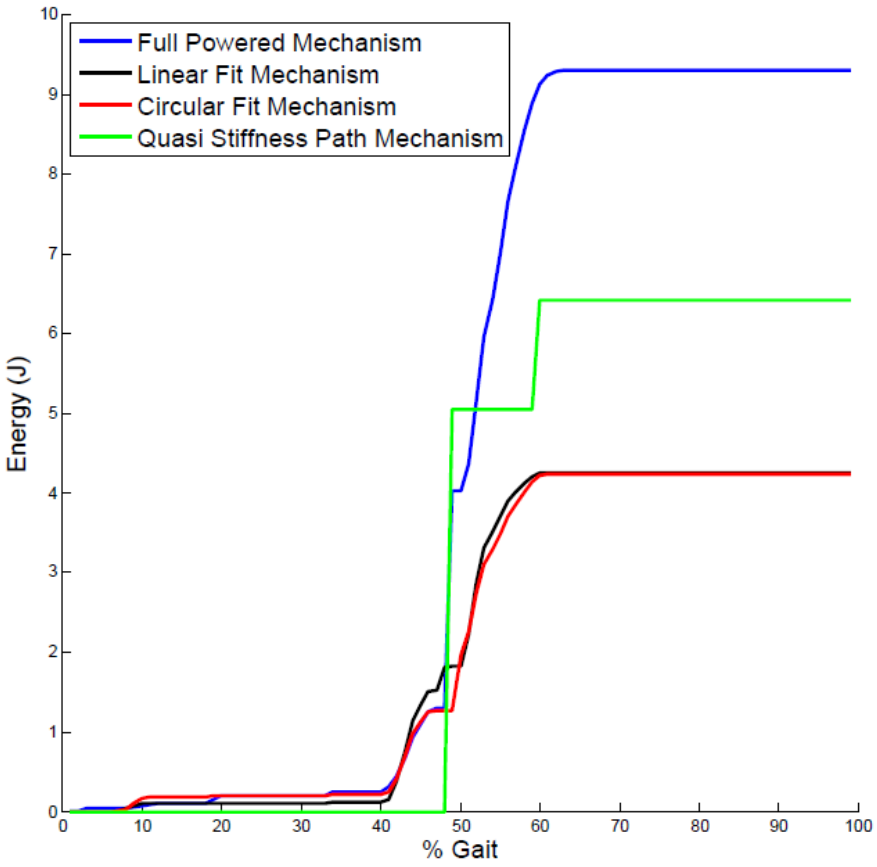

FIGURE 5.17: ENERGY VS GAIT PERCENT FROM LINEAR FIT (BLACK) AND CIRCULAR FIT (RED) AND QUASI-STIFFNESS FIT (GREEN) COMPARED TO FULL POWERED MECHANISM (BLUE).

To better compare the benefits of using each type of mechanism to achieve the same kinematics at the ankle joint, the energy used during the gait cycle was analyzed for each mechanism type. The adjustments that did not require additional energy from a motor were not included in this analysis. Energy was calculated from deflection of the spring during any required configuration changes. The accumulating energy values for each mechanism type are shown in Fig. 5.17 and are compared to a mechanism that is fully powered and can meet able bodied data exactly. In Fig. 5.17, the linear and circular

mechanisms use the least amount of energy and seem to be the best. Both the fully powered mechanism and the quasi-stiffness mechanism require large spikes in energy in order to match the able bodied data. This can result in large spikes in motor power needed to achieve such large increases in energy over a short amount of time. In reality the quasi-stiffness mechanism will adjust between configurations over more than 1 gait percent allowing the power spike to be less.

One of the advantages of the constant moment path adjustments is that even though there may be a higher power spike due to a rapid increase in energy required the amputee will not feel this power spike because the moment of the ankle is not affected during the spike. If the high power spike caused a spike in ankle moment the spike would be obvious in the ankle moment vs ankle angle graph shown previously or in the ankle energy comparison. This is important because the device can add appropriate power spikes necessary to change ankle kinematics without causing unwanted movement or torque through the prosthetic system onto the amputee's leg or socket connection.

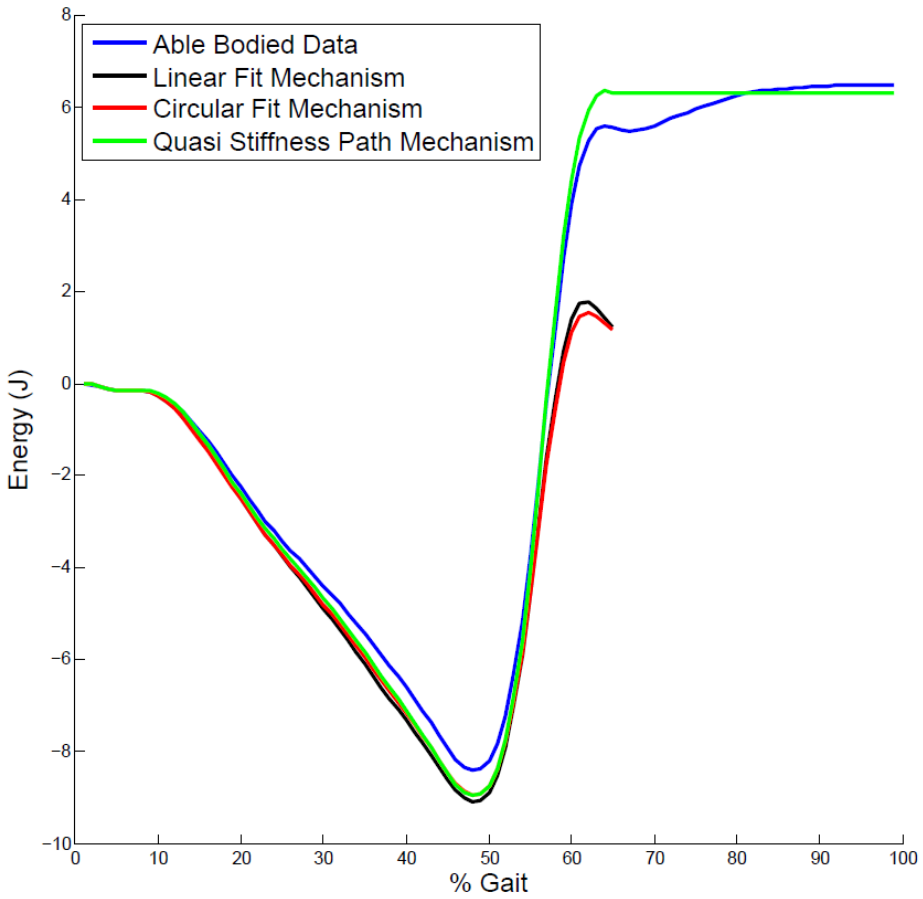

FIGURE 5.18: ANKLE ENERGY VS GAIT PERCENT FROM LINEAR FIT (BLACK) AND CIRCULAR FIT (RED) AND QUASI-STIFFNESS FIT (GREEN) COMPARED TO ABLE BODIED DATA (BLUE).

A common method for comparing prosthetic devices and their capability to produce able bodied kinematics is to show the energy and power output of the ankle when using the different devices. Figure 5.18 is a comparison of the 3 different mechanisms used in this analysis and how they match up to able bodied results. While the linear and circular mechanisms require less energy than the fully powered and quasi-stiffness mechanisms, they also do not allow the ankle to reach the required ankle energy values during gait. In Fig. 5.18 the energy produced by the quasi-stiffness mechanism is comparable to able bodied data.

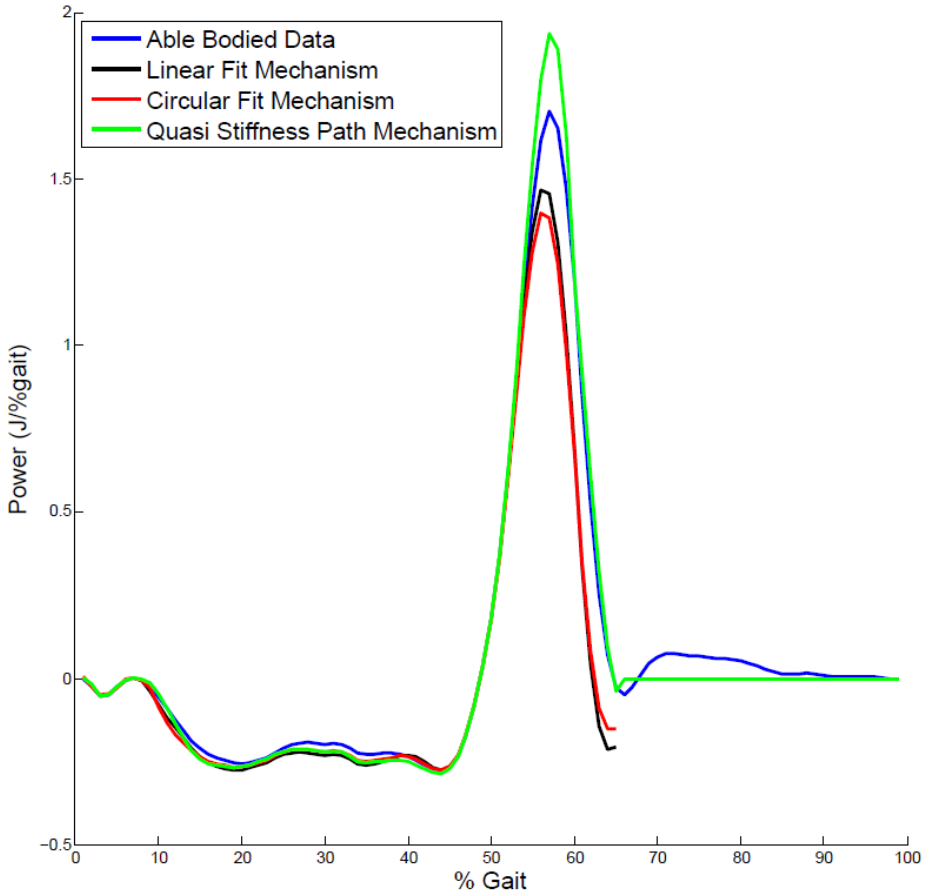

FIGURE 5.19: ANKLE POWER VS GAIT PERCENT FROM LINEAR FIT (BLACK) AND CIRCULAR FIT (RED) AND QUASI-STIFFNESS FIT (GREEN) COMPARED TO ABLE BODIED DATA (BLUE).

Figure 5.19 is a comparison of the power output at the ankle between the 3 mechanisms. In the early stages of gait all three mechanisms produce similar ankle power as able bodied gait. The deviation between mechanisms happens near the end of roll over where additional energy is necessary to assist in propelling the person through the gait cycle. While the linear and the circular mechanisms fall short of power and energy, the quasi-stiffness mechanism produced more power than necessary during the transition to push off. This would suggest that further optimization can be achieved and mechanism power can possibly be reduced further.

5.5 CONCLUSION

A simple spring and lever arm mechanism was used to develop a method for decoupling joint stiffness and instantaneous joint position. The method was analyzed while modeling the mechanism as a prosthetic ankle system using able bodied ankle kinematic data. The resulting method was then applied to a specific of a powered prosthetic ankle system. For this application, an appropriate moment path was created for each specific ankle angle through one gait cycle. The path data were then fit by a line and a circle to prove manufacturability and simplicity of design. The particular path solution presented in this work is not unique. There are other specific paths that can be explored and compared in terms of energy cost and desired output.

The able bodied data for ankle moment and ankle angle was then separated into multiple segments to represent quasi-stiffness values. Mechanism configurations were then connected using the constant moment paths in order to switch between stiffness values while adding energy without changing instantaneous ankle kinematics. The quasi-stiffness mechanism results, along with the linear and circular mechanisms, were compared to each other in terms of required energy. It was shown that the quasi-stiffness mechanism was able to produce power output at the ankle necessary to match the able bodied data.

Once a method for moving along the quasi-stiffness mechanism path is chosen, further optimization can be done in order to match able bodied data more exactly while optimizing power requirements of the motor. The methods used in this chapter were

demonstrated on a simple spring and lever arm but will be applied to ankle joints that are optimized for able bodied kinematics.

It is recognized and important to note that these results and analysis in the prosthetic field only represent one gait speed and level ground walking. The tools developed will be easily adapted to optimize for multiple speeds and gait dynamics.

CHAPTER 6

MECHANISM ENERGY SURFACES

A robot manipulator's own weight will create large joint torques on the motors. Passive, gravity compensation techniques are used to remove the torque added to each joint due to the mass. The following chapter describes a method to adjust passive gravity compensating mechanisms in order to compensate for joint torques caused by the weight plus additional end effector moments. If a robot end effector changes loads, the mechanism will adjust to the new weight. There will be physical limitations on each mechanism setting and the range of external moments that the passive joint will be able to compensate.

6.1 GRAVITY EQUILIBRATOR & PARAMETERS

This section explains the methods of conserving energy in gravity equilibrators and introduces a method of intersecting energy graphs that can be used to define equilibrator parameters. The main results will define the changes in equilibrator parameters that affect the joint moments.

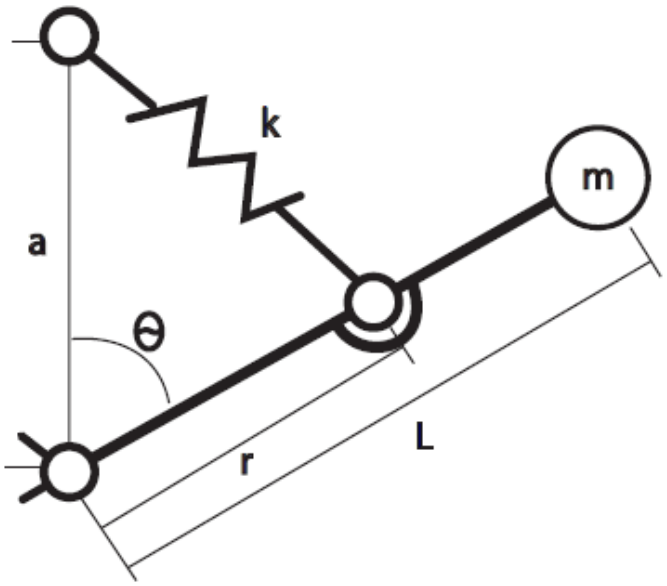

FIGURE 6.1: DR. HERDER'S BASIC GRAVITY EQUILIBRATOR SET UP [95].

Figure 6.1 defines the basic layout of a gravity equilibrator mechanism where a mass (*m*) subject to gravity is attached to an arm at distance '*L*' from the joint. The arm is being supported by a zero free length spring of stiffness value '*k*'. This spring is attached to the base at a distance '*a*' above the arm joint and attached to the arm at a distance '*r*' from the arm joint. A zero free length spring is a spring with no free length where the distance between end points is the actual spring deflection [95], [121]. In a gravity equilibrator the spring counters the effects of gravity on the mass, allowing the arm to remain stationary when placed at any value of θ. The design parameters when creating a gravity equilibrator system can be found by comparing the changes in energy as a function of the arm angle θ.

There are two energy equations involved with the gravity equilibrator system, the potential energy from the mass as its height changes and the potential energy in the spring as the spring displacement changes. These two equations are shown as Eq. (6.1) and Eq. (6.2) below.

$$E_m = mgh \tag{6.1}$$

$$E_s = \frac{1}{2}kd^2 \tag{6.2}$$

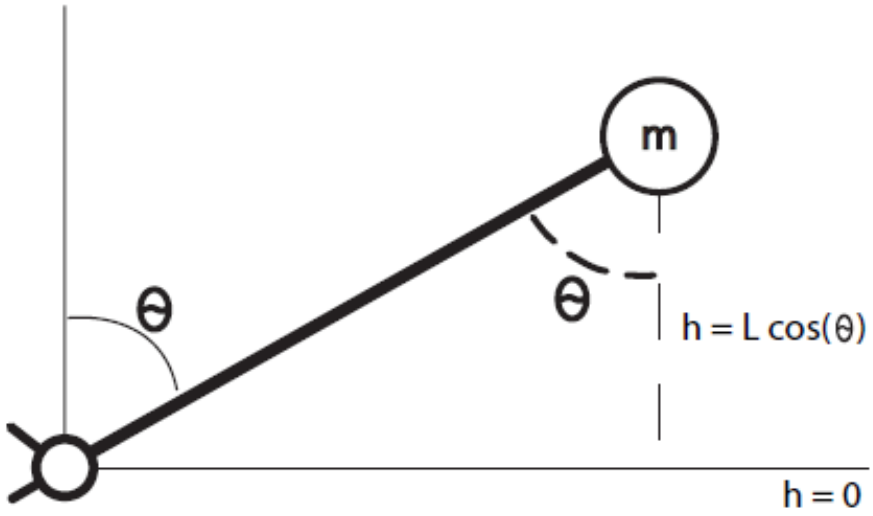

FIGURE 6.2: THE HEIGHT OF THE MASS FOR POTENTIAL ENERGY CALCULATIONS.

In Eq. (6.1) E_m is the potential energy of the mass and the value of gravity (g) is 9.81 $\frac{m}{s^2}$ with 'h' being defined as the height of the mass. In this case the height is measured from a reference point that can be arbitrarily chosen. The reference is chosen to be the arm pivot point as $h = 0$. Figure 6.2 shows how the height at any angle is equal to the arm length (L) multiplied by the cosine of the angle θ.

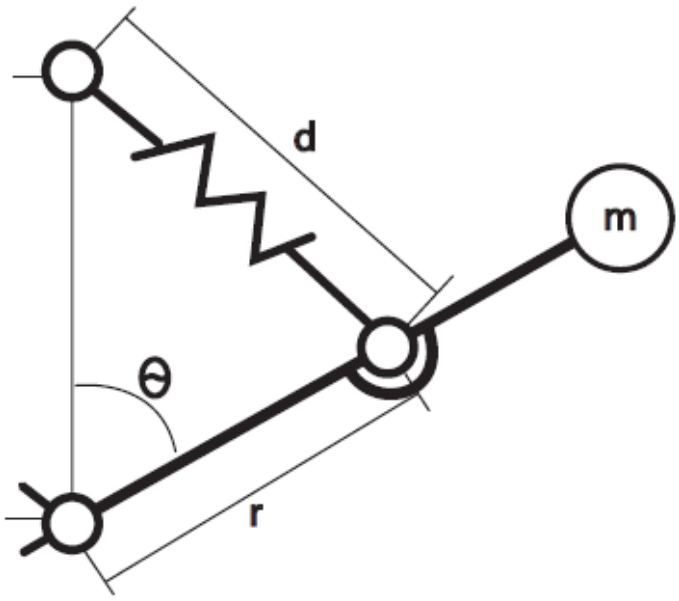

FIGURE 6.3: TRIANGLE (Δadr) USED FOR LAW OF COSINES IN EQ. (6.4).

In Eq. (6.2) E_s is the potential energy stored in the spring of stiffness 'k' with a spring displacement of 'd'. Fig. 6.3 and Eq. (6.3) show how the law of cosines is used to relate the spring displacement to the arm angle θ.

$$d^2 = a^2 + r^2 - 2ar\cos\theta \tag{6.3}$$

The potential energy of the mass as described in Eq. (6.1) is expanded using the definition of mass height from Fig. 6.2 to be a function of the equilibrator mechanism

design parameters. The expanded equation is given by Eq. (6.4). Also, the potential energy in the spring, as described in Eq. (6.2), is expanded with the law of cosines in Eq. (6.3) to be a function of the equilibrator mechanism design parameters and is given by Eq. (6.5).

$$E_m = mgLcos(\theta)) \tag{6.4}$$

$$E_s = \frac{1}{2}k(a^2 + r^2 - 2arcos(\theta)) \tag{6.5}$$

$$E_T = E_m + E_s = \frac{1}{2}k(a^2 + r^2) + (mgL - kar)cos(\theta) \tag{6.6}$$

$$mgL = kar \tag{6.7}$$

The total potential energy in the equilibrator mechanism is given by Eq. (6.6) by adding the two energy equations together. For the equilibrator system to be balanced, the total energy in the system must remain constant for all values of θ. From Eq. (6.6), the condition which removes any changes in the total energy due to changes in θ is when the mechanism parameters satisfy Eq. (6.7) [88], [89].

6.1.1 Energy Surface Intersections

A method for visualizing the requirements on the gravity equilibrator is to graph the two energy equations in the system as surface plots showing how the energy changes as a function of θ. Using the design condition from Eq. (6.7), the portions of Eq. (6.4) and Eq. (6.5) that change with θ are shown as surface plots in Fig. (6.4) and Fig. (6.5).

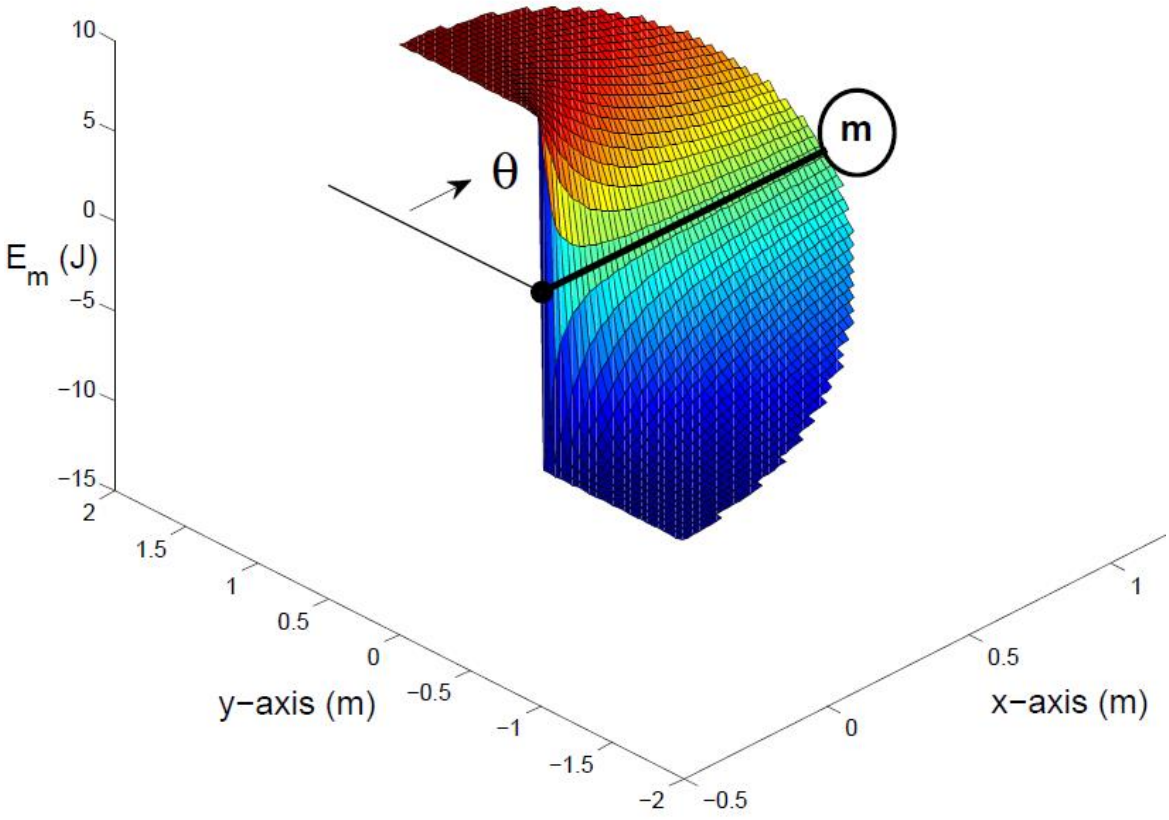

FIGURE 6.4: ENERGY OF MASS THROUGH ANGLE θ FROM 0 TO 180 DEG.

Fig. 6.4 is the potential energy from Eq. (6.4) plotted as a surface around the pivot point for each angle θ from 0 to 180 degrees. The x and y axis are actual distances measured in meters in the plane of the mechanism. The z-axis is the energy value for the (x, y) distance coordinates in the plane. The energy from 0 to 180 degrees is symmetric with the energy from 180 to 360 degrees and is greatest at 0 degrees and lowest at 180 degrees.

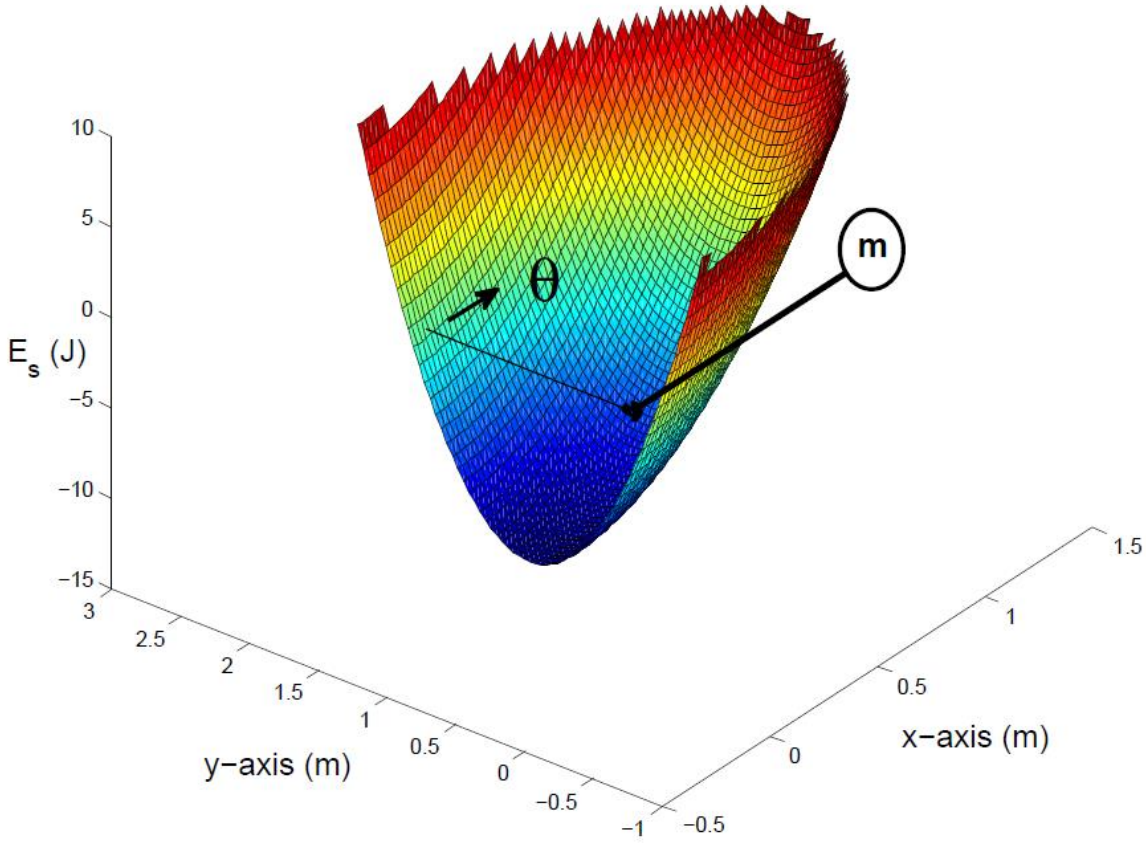

FIGURE 6.5: ENERGY BOWL FROM A ZERO FREE LENGTH SPRING ATTACHED AT DISTANCE A = 1 FROM THE ORIGIN DISPLACED THROUGH A RANGE OF 0-180 DEG. AROUND THE ATTACHMENT POINT.

Figure 6.5 is the surface plot of spring potential energy in Eq. (6.5) excluding the terms not influenced by θ. The plot is developed by choosing some arbitrary 'm', 'a', 'r', and 'L' distances and using Eq. (6.2) to define spring constant 'k'. In situations where the spring constant is not yet chosen the values of 'a', 'r', and 'k' can be adjusted in order to get a desired spring energy surface shape.

Once the potential energy due to gravity surface (Fig. 6.4) and the potential energy from the spring surface (Fig. 6.5) are created, they are combine to show how they interact with each other in Fig. 6.6.

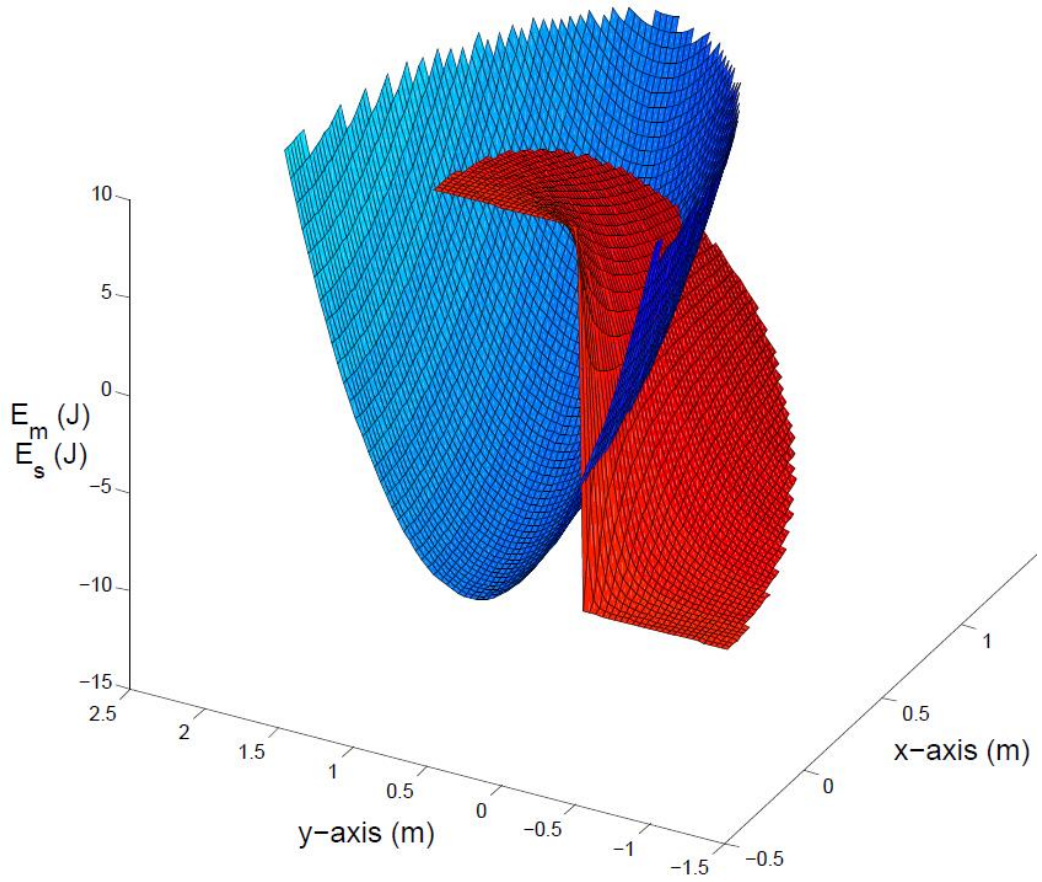

FIGURE 6.6: SPRING ENERGY SURFACE COMBINED WITH MASS POTENTIAL ENERGY SURFACE.

The idea of a gravity equilibrator is that the spring can be attached to the arm in a position where the change in spring energy will absorb any change in potential energy from the mass due to gravity as the arm moves. For this reason it is necessary to find where the two changes in energy will be the same throughout the arm's range-of-motion. Figure 6.7 shows where the spring potential energy surface intersects the negative of the mass potential energy surface to visualize the correct transfer of energy from one system to the other.

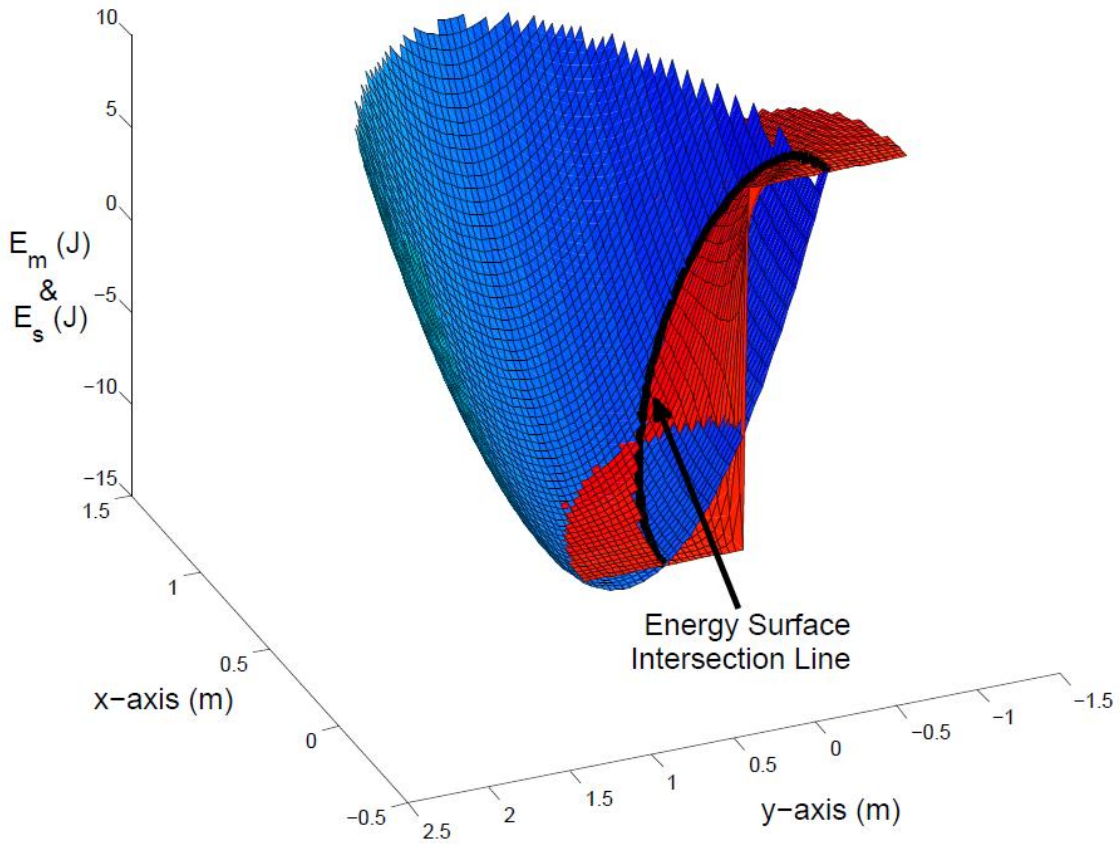

FIGURE 6.7: SPRING POTENTIAL ENERGY INTERSECTS WITH NEGATIVE OF GRAVITATIONAL POTENTIAL ENERGY, INTERSECTION SHOWN WITH BLACK LINE.

The black line in Fig. 6.7 indicates the intersection path of the two surfaces. This intersection can be changed as the values of '*a*', '*r*', and '*k*' from Fig. 6.1 are adjusted in relation to where the arm joint is positioned. The *x* and *y* axes on Fig. 6.7 are actual distance values that the spring is displaced or the arm is moved while the *z*-axis is a representation of the energy values at those specific locations. Figure 6.8 is the intersection of the energy surfaces projected onto the x-y plane showing where the spring and arm need to be connected. The spring attachment point at distance '*r*' from the arm pivot must follow the black line for the two energy surfaces to stay equal and opposite.

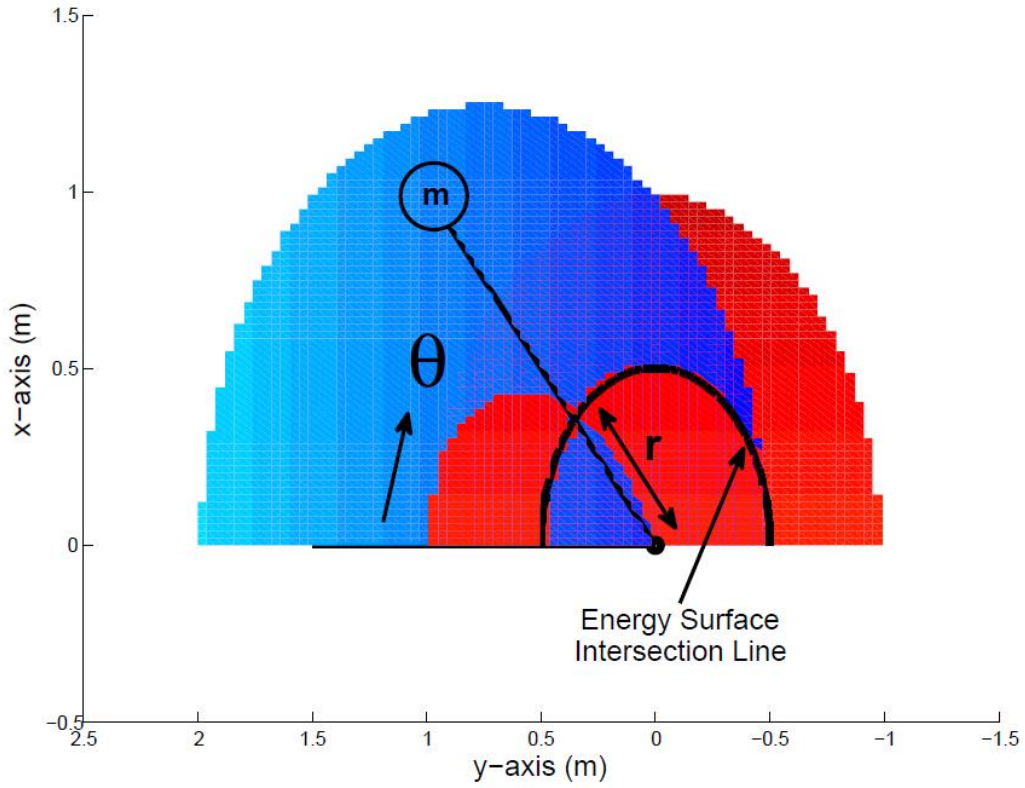

FIGURE 6.8: THE INTERSECTION OF THE ENERGY SURFACES PROJECTED ON THE X-Y PLANE.

6.1.2 Energy Amplitude Plots

For the example being analyzed, there is another way to visualize the solution to the intersecting energy surfaces. This is done by using the direct equations for potential energy and finding the spring attachment values that match the potential energy of the mass. Equations (6.4) and (6.5) are graphed together in Fig. 6.9 to show the comparison using specific values for '*a*', '*r*', and '*k*' so that the solution can be shown. For this example, we used $a = 0.75$ m, $r = 0.5$ m, and $k = 26.133$ N/m.

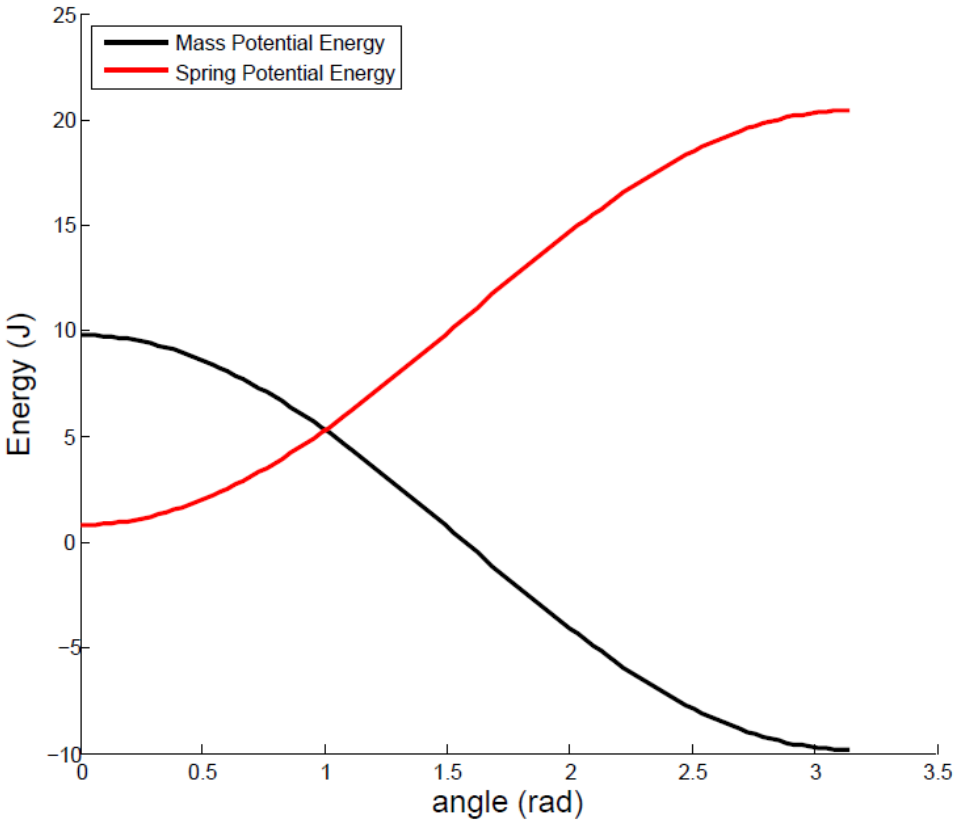

FIGURE 6.9: SPRING ENERGY AND MASS ENERGY FROM 0 TO 2π RADIANS.

Figure 6.9 also shows the actual values for spring and mass energy, but we are only concerned with the changes in energy for the specific range of motion. Therefore to show that the change of energy is equal and opposite, Fig. 6.10 shows the negative of the gravity energy while Fig. 6.11 shifts this negative energy up to lay underneath the spring potential energy for a perfect match.

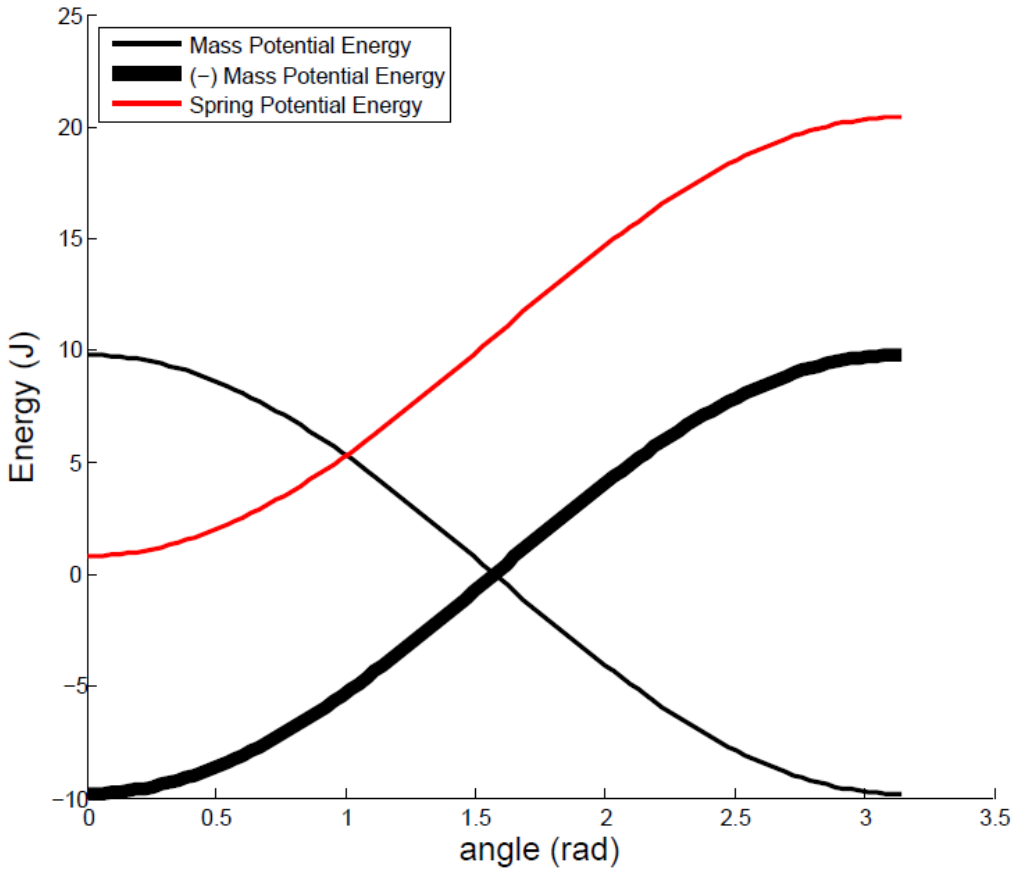

FIGURE 6.10: NEGATIVE OF THE GRAVITATIONAL POTENTIAL ENERGY.

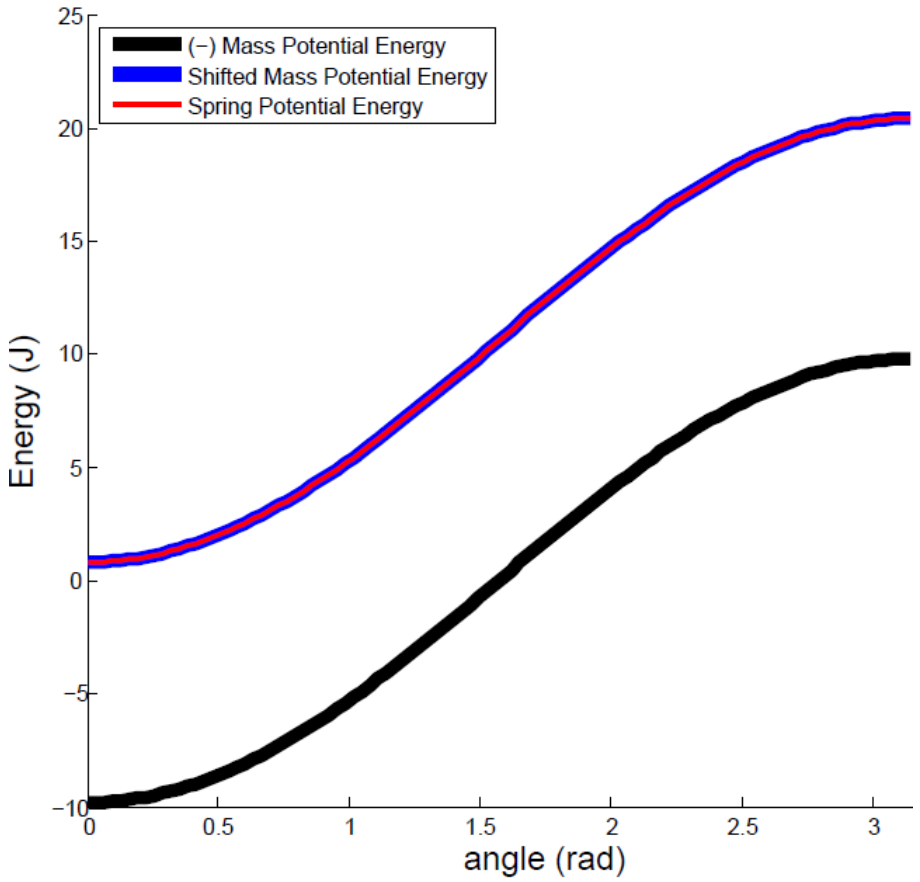

FIGURE 6.11: NEGATIVE GRAVITATIONAL ENERGY SHIFTED UP TO MATCH SPRING ENERGY.

6.1.3 Results: Changing Equilibrator Parameters

Figure 6.11 shows that for the specific mechanism parameter values of '*a*', '*r*', and '*k*' the spring absorbs the energy from the mass due to gravity for every position of the arm. While the values of the spring were pre-chosen in this case, it is important to define what happens to the curve as the parameters are adjusted. Figure 6.12 shows the changes in spring potential energy as the values for '*a*', '*r*', and '*k*' are adjusted.

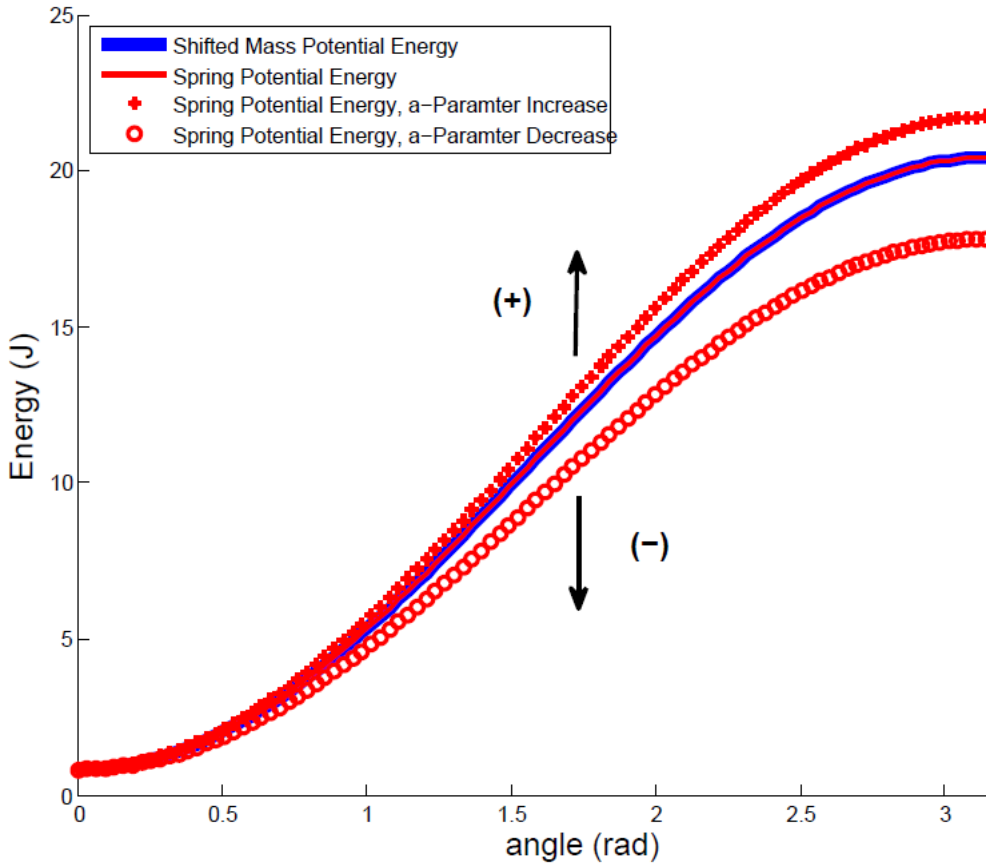

FIGURE 6.12: BEHAVIOR OF SPRING POTENTIAL ENERGY FOR DIFFERENT MECHANISM PARAMETERS.

In Fig. 6.12 for any increased value of '*a*', '*r*', or '*k*' the amplitude of the spring potential energy curve increases over the range of motion. Also, if any of the three parameter values are decreased, the amplitude will decrease over the range of motion. This can be important when designing a gravity equilibrator for a real task. There are many options for parameter values who's combination will satisfy the energy requirements. The appropriate design can meet the requirements for space or position while still having a combination of values that will match the gravitational potential energy change.

This method for matching the graphs is a method to find the mechanical properties of the spring necessary to create conservation of energy. Another important piece of information is the error involved in this creation. For the graphs to match, the derivative of the spring's potential energy needs to be the same as the derivative of the negative of the mass potential energy. This method of taking the derivative of each energy equation removes any difference or offset in the actual energy value stored in either energy source. Summing the derivative removes the need to make one of the energy curves negative and allows for a measurable error. The error is the difference between the transitory energy of each energy source.

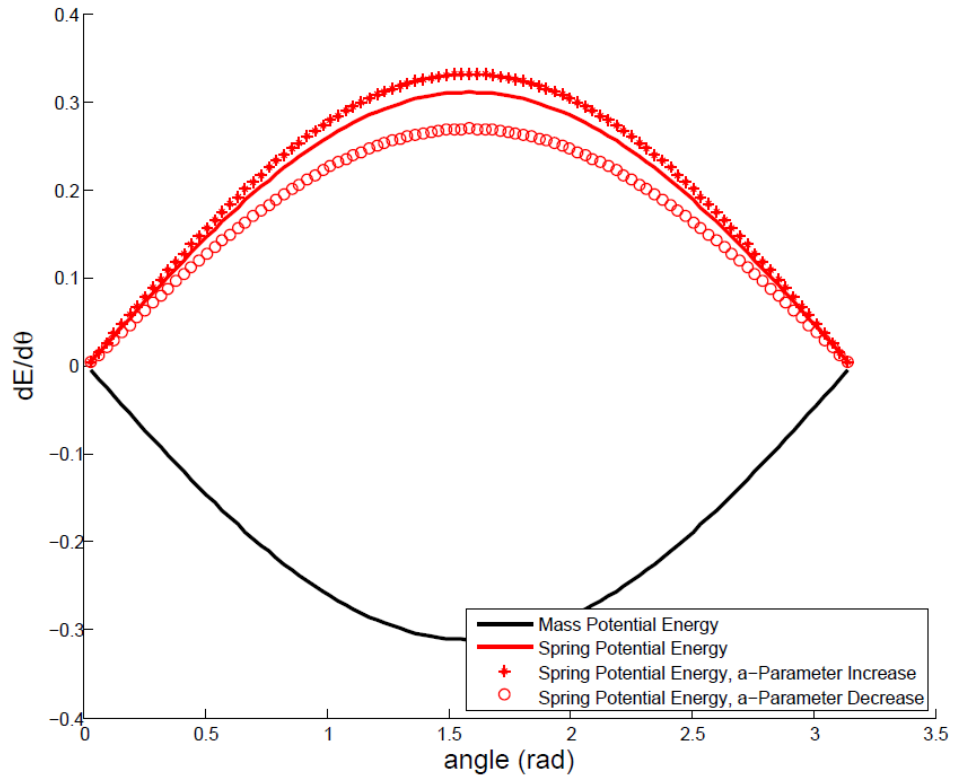

FIGURE 6.13: DERIVATIVE OF SPRING POTENTIAL ENERGY AND MASS POTENTIAL ENERGY CURVES.

Figure 6.13 is the derivative of the two potential energy curves in Fig. 6.9 along with the two additional curves in Fig. 6.12 from increasing and decreasing parameter values. Figure 6.13 has three representations of the spring potential energy. Fig. 6.14 is the result of adding each of the three spring potential energy curves individually with the mass potential energy curve in Fig. 6.13. The sum of the spring derivative with the mass potential energy derivative is used to compare the error values in the design.

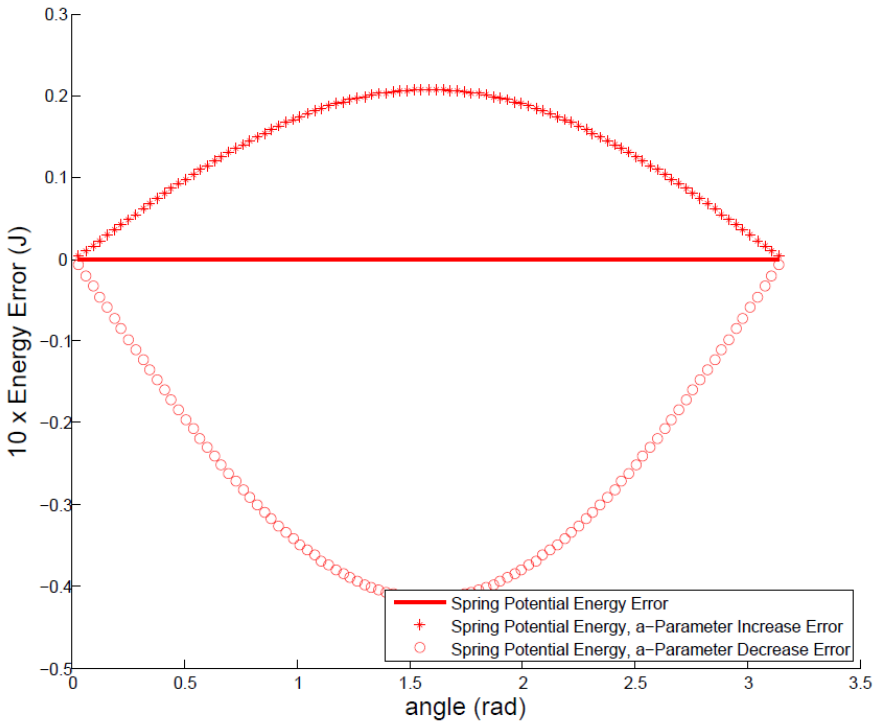

FIGURE 6.14: EXAGERATED ERROR BETWEEN ENERGY DERIVATIVES.

In Fig. 6.14, the error values were exaggerated by a factor of 10 to help visualize the small errors. An appropriate filter can be applied to the error data to allow for a specified cushion around the energy crossing line in an actual design.

If an error is introduced when building an equilibrator, it is helpful to determine what the error means in physical performance of the arm. The error values in energy differentiation are either positive or negative and have a specific magnitude. This error will determine the direction that the arm will want to move if started from rest at a specific angle and will describe the stiffness of the joint in each direction. We will later show that the stiffness for the mechanism can be positive or negative and the specific magnitude relates to the magnitude of the stiffness.

6.2 SPRING POTENTIAL ENERGY (ENERGY BOWL)

Work by Dr. Herder and others have presented methods for creating the basic equilibrator [89], [95], [96], [121], [122]. The mass on a lever arm is balanced against gravity by comparing its potential energy equation to the potential energy stored in the spring used to balance it. By changing parameters while using this method, the benefits of an active equilibrator system can be analyzed. This experiment uses a spring that is not of zero free length.

First the energy in the spring (E_s) is represented using Eq. (6.8) where 'k' is the spring stiffness and 'x' is the spring displacement from its neutral position. The energy equation is the same for tension and compression of the spring.

$$E_s = \frac{1}{2}kx^2 \tag{6.8}$$

Figure 6.15 is the graphical representation of Eq. (6.8) as the energy of a spring moving around a constant center location. The *z*-axis is the energy stored in the spring as it is displaced. Fig. 6.15 is a circular parabola due to the x^2 term in the energy equation. The *xy*-plane of the energy bowl defines the physical displacement values of one end of the spring while the other end is rigidly attached to the center *(0, 0)* position.

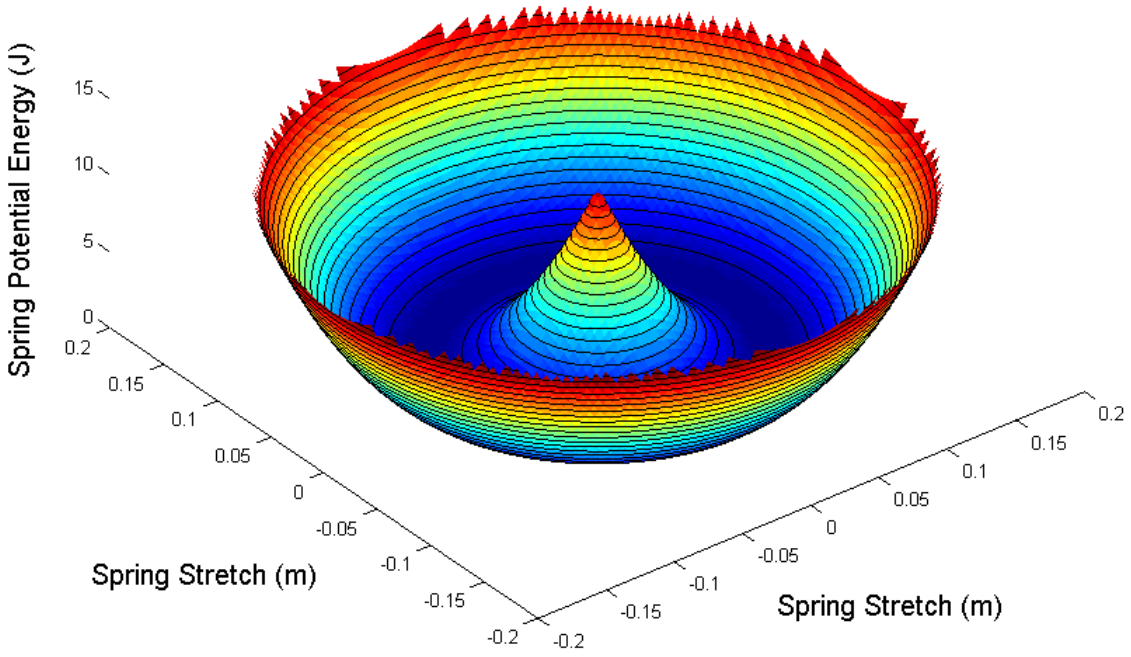

FIGURE 6.15: SPRING ENERGY BOWL OF STIFFNESS 'k'.

6.3 CONSTANT MOMENT PATH

A constant moment field was created to better understand the dynamics of a joint mechanism using energy surfaces. The potential energy (E_j) of a link rotating about a joint with constant moment (M) is modeled using Eq. (6.9) as the link is rotated through an angle (θ).

$$E_j = M\theta \tag{6.9}$$

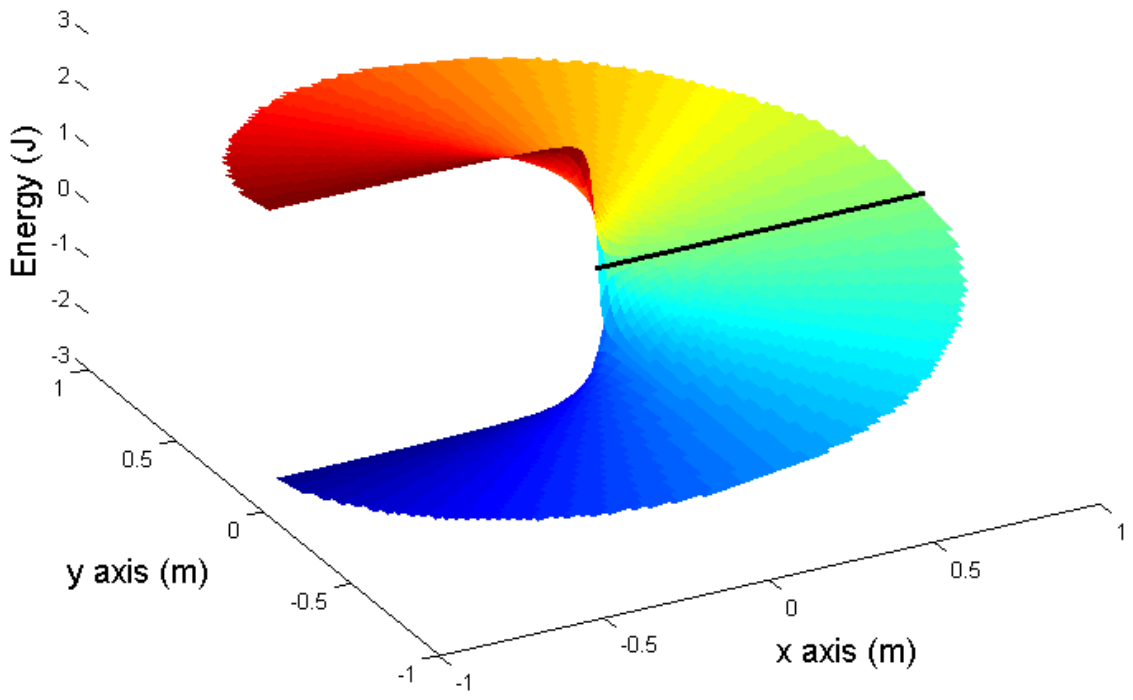

FIGURE 6.16: THE ENERGY HELICAL SURFACE OF A SPECIFIC MOMENT ROTATED THROUGH AN ANGLE OF -180 TO 180 DEGREES.

Figure 6.16 is the graphical representation of Eq. (6.9) with the link joint attached to the origin and the positive x-axis as a starting point for $\theta = 0$. The energy given by Eq. (6.9) creates a helical shaped energy surface spiraling around the joint with a constant pitch (see Fig. 6.16). The *xy*-plane coordinates represent distance from the joint and the *z*-axis is energy measured in Joules. Energy is constant for the helical surface at any distance from the joint for each specific angle. Note that from Eq. (6.9) the total energy is affected by changes in angle but the moment (M) stays constant and describes the slope of the energy surface.

Similar to Fig. 6.7, the negative of the potential energy from the constant moment field is used to find the equal and opposite energy slopes. If the negative potential energy values about the joint from the helical surface and the potential energy stored in the spring from the energy bowl are placed on the same graph there will be an intersection of the two surfaces, this is shown in Fig. 6.17. Projecting the intersection of the two surfaces onto the *xy*-plane shows a path that will cause the spring to store the same amount of energy it takes to move the arm, by θ, to that position. The purpose is then to create a mechanism that will force the spring attachment point to follow this path of intersecting surfaces as the link is rotated about the joint. The change in potential energy of the spring during rotation will then be equal and opposite of the change in energy from the moment about the joint creating a constant moment on the mechanism link for all θ.

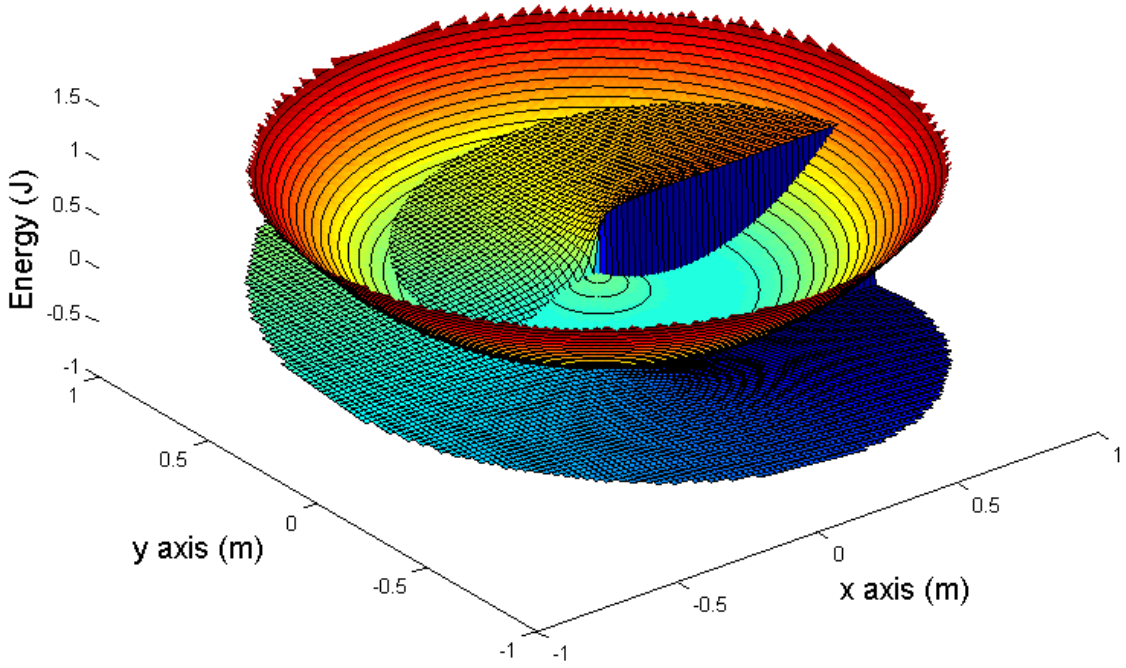

FIGURE 6.17: NEGATIVE HELICAL ENERGY SURFACE INTERSECTION WITH THE ENERGY BOWL.

While the intersection shown in Fig. 6.17 is for a specific moment about the joint, each moment will have its own specific energy path up the energy bowl. Also, each different moment has a path of linear progression up the energy bowl, linear with respect to theta with a slope of '*M*'. Five different moment values are used to create five energy helical paths intersecting the energy bowl. These paths are shown in Fig. 6.18 with blue being the lowest moment value and purple being the highest.

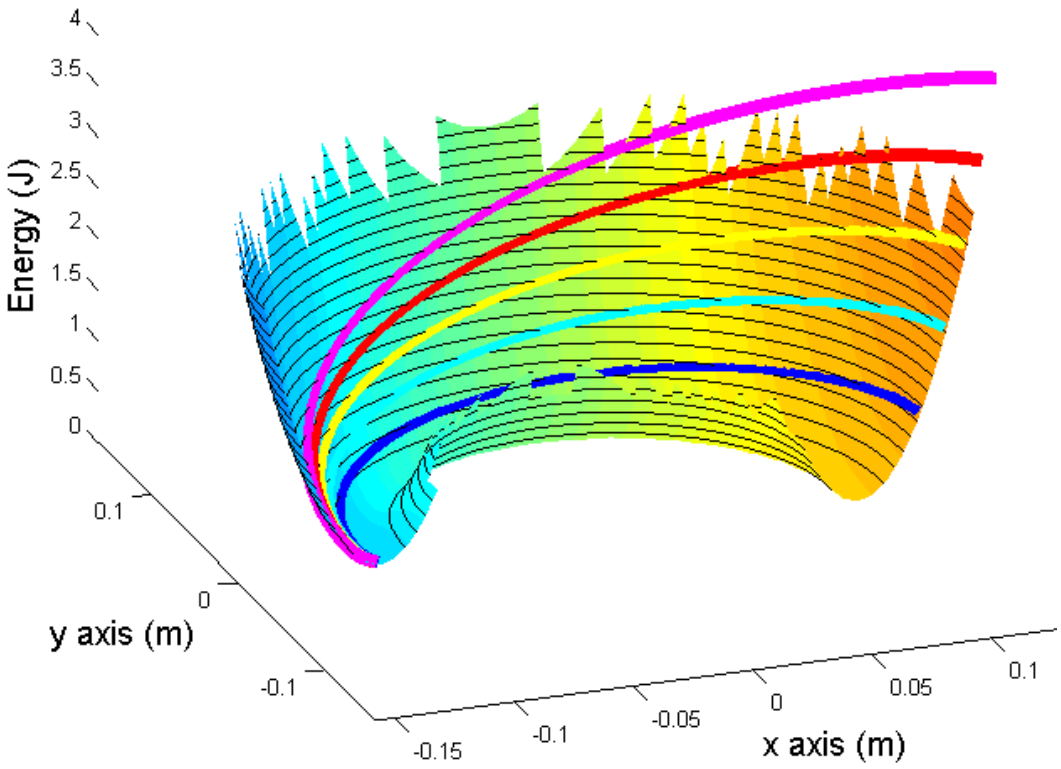

FIGURE 6.18: THE ENERGY HELIX OF FIVE DIFFERENT JOINT MOMENT VALUES INTERSECTING THE ENERGY BOWL.

These lines of intersecting surfaces in Fig. 6.18 are the constant moment paths that if the spring is forced to follow, the arm will be balanced for all θ positions. Once the constant moment path or balancing energy path is defined, the next challenge is to create a mechanism that will cause the spring to stretch along this correct path as it rotates.

It is important to note that if the internal energy slope of the mechanism matches the external energy slope, then the arm will not move, but if the external energy slope or

moment either increases or decreases slightly the arm will move in a certain direction. Thus to compensate for a changing environment, the internal mechanism will need to adjust so that the surfaces realign. If a motor is used to adjust for an increase in external energy, the motor path should act perpendicular to the constant moment paths. This will allow the mechanism to adjust for higher moments while still maintaining its current angular position.

6.4 HELICAL CIRCULAR FIT

6.4.1 Defining Circle Fit

Although there are many mechanisms that can be synthesized the following section will provide one method for fitting the constant energy path. The helical intersection can be approximated from above as a circle for small ranges of θ. A circular path can easily be created using a constant radius link rotating around a center point. In order to find an optimal center point, each section of the intersection path is used to calculate a relative circle center and radius. These center points are mapped onto the same graph for the different ranges of theta. Five circles that center along the 5 intersecting surface paths were mapped onto the energy bowl and are shown in Fig. 6.19. If an optimal range of motion is known this method of choosing a circle and circle center may be sufficient. For more general applications, a motor attached to the mechanism can be used to make adjustments to help fit the energy path of choice.

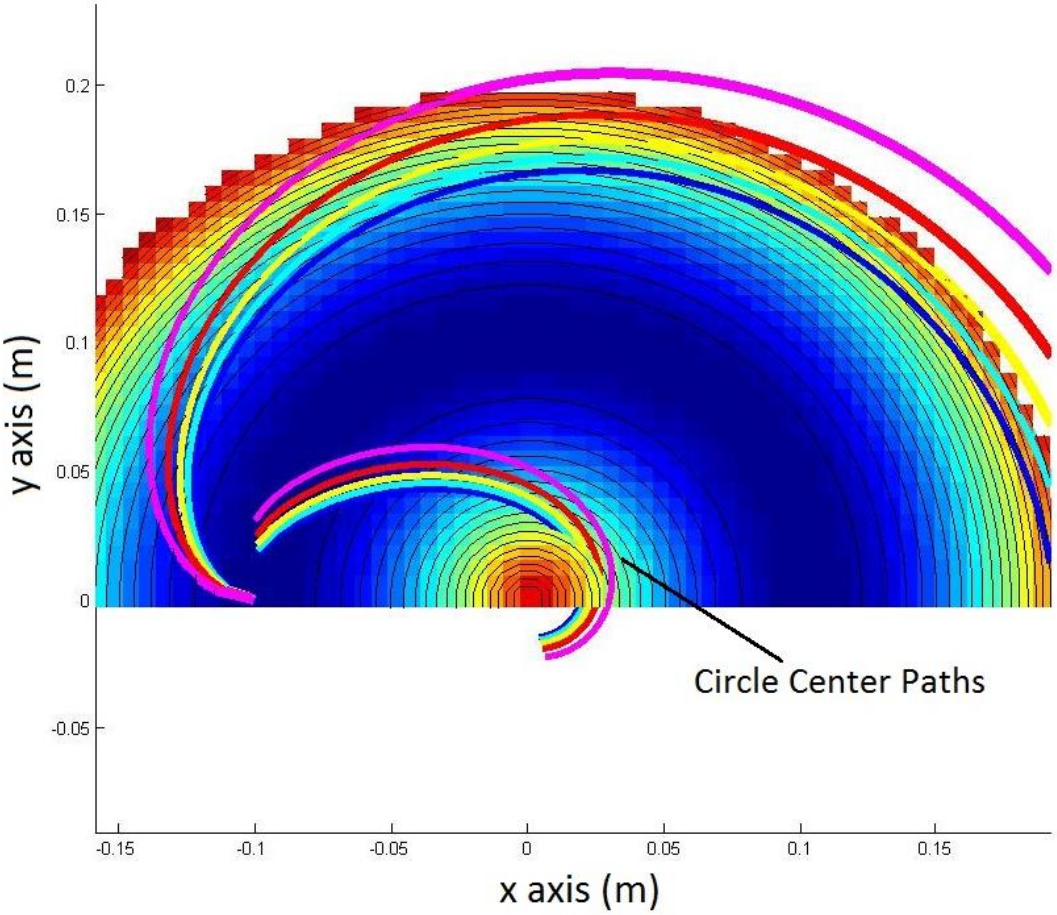

FIGURE 6.19: CIRCLE CENTER PATHS FOR 5 DIFFERENT MOMENTS.

These different paths could be better approximated if one center was chosen and a motor was placed on the link arm to make it longer and shorter as the moment at the joint changes. This fixed circle center approximation would have a fixed range of motion where the two paths overlap before needing adjusting. For purposes of this analysis, a circle was fit to the red moment path at a circle center that is predicted to fit a range of θ.

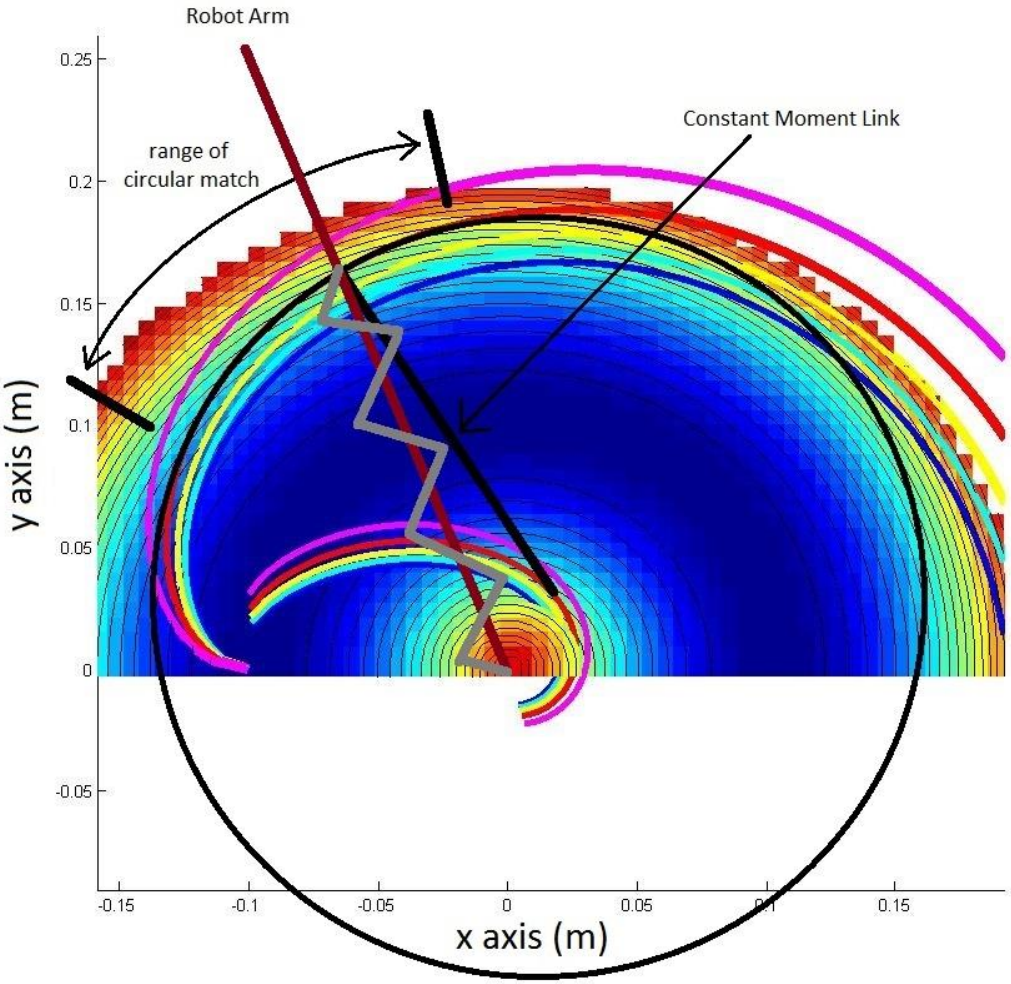

FIGURE 6.20: CIRCULARIZATION OF CONSTANT ENERGY PATH.

Figure 6.20 shows our new method of matching a circle to the intersecting path. The constant moment link in Fig. 6.20 forces the spring on the robot arm to follow the red constant moment path for this particular range of θ. The constant moment link is fixed at the base with a rotational joint and is attached to the robot arm with a linear slide bearing. The spring end is attached to the base of the robot arm and the distal end is attached to the constant moment link at the linear slide bearing. This configuration allows the constant moment link to stretch the spring as the robot arm rotates through θ.

6.4.2 Mechanism Build Version 1.0

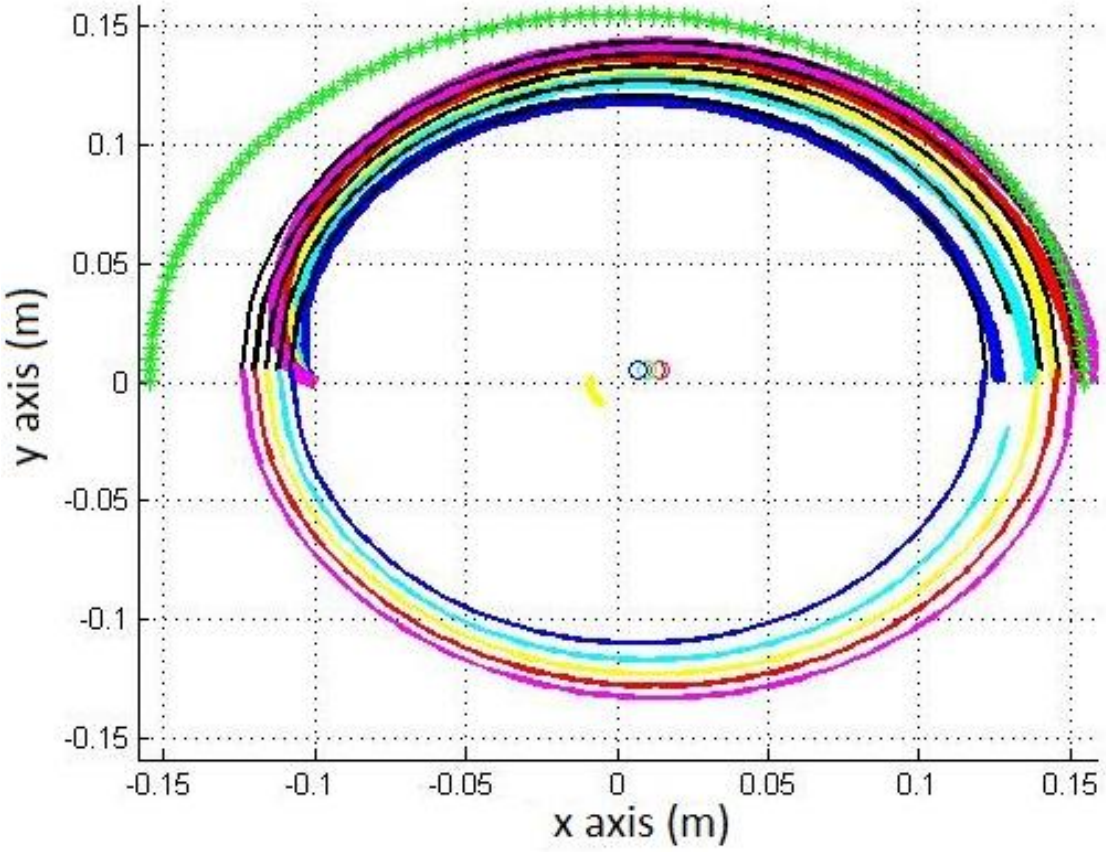

FIGURE 6.21: CIRCULARIZATION OF FIVE DIFFERENT ENERGY PATHS.

The actual mechanism was created so that the black circle representing the mechanism is able to cover about 60 degrees of a constant energy path. Figure 6.21 shows distinct values for center position and circle radius that were chosen to match the five different energy paths. The green half circle in Fig. 6.21 represents the physical limit of the spring on the mechanism and thus the limit of the spring energy bowl. Physical

limitations of the spring include maximum extension before deformation or maximum compression to reach solid length.

To analyze the behavior of this mechanism in relation to its energy paths the mechanism was designed and created to be adjustable and match the requirements of Fig. 6.21. Figure 6.22 is the first model created in solid works.

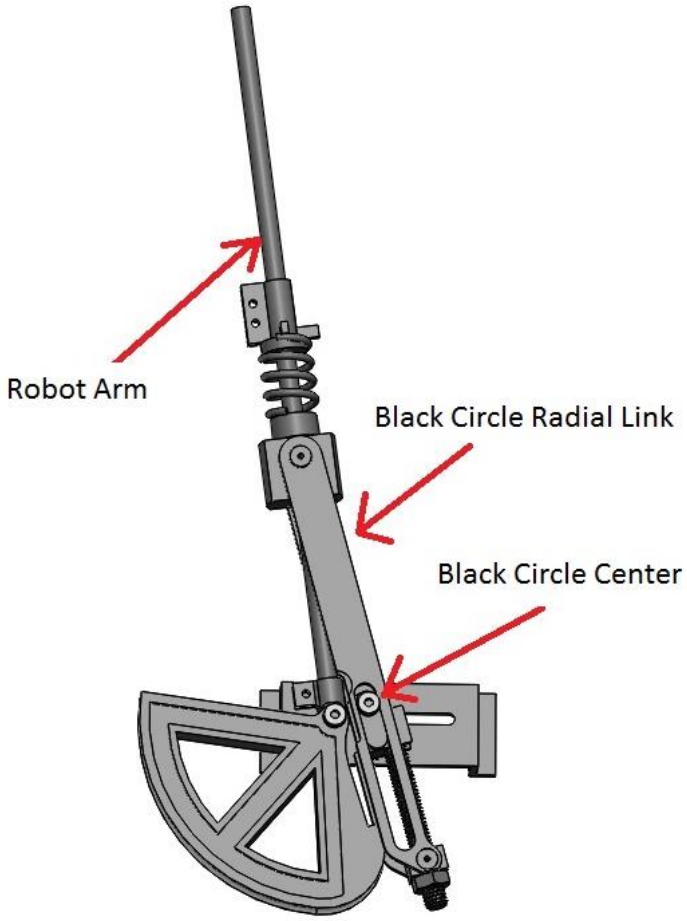

FIGURE 6.22: CONSTANT MOMENT MECHANISM VERSION 1.0.

A constant moment was applied to the mechanism by hanging a weight off the table with a pulley and using a second pulley to attach the tensile force to the arm keeping the constant force from gravity pulling at a constant distance around the joint of the robot arm. All the appropriate mechanism distances were measured to match Fig. 6.21 above. Figure 6.23 shows the actual mechanism made from 3D printed parts.

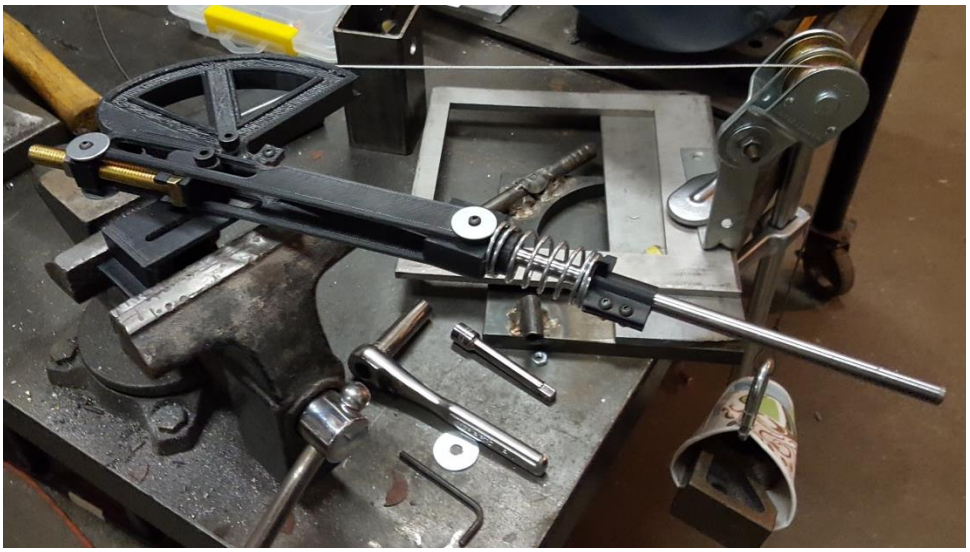

FIGURE 6.23: CONSTANT MOMENT MECHANISM VERSION 1.0.

While loaded with 2.95 lbs. to create a moment of 1Nm the mechanism performed as expected. It was easy to move and would stay where it was left for the range of motion predicted. The problem was that the mechanism design had too much friction. Theoretically this translates to a thick black line in Fig. 6.21 which will cover the energy curve and make up for any discrepancies in the mismatch of the curves. Although this friction can help a real robot account for slight mismatching in energy curves, this

friction does not help in understand the distinct behavior of the mechanism to intelligently design the energy curves and align the mechanism properly.

6.4.3 Mechanism Build Version 1.1

A second version of the mechanism was made with steel radial bearings and stronger supports to diminish any unwanted friction or mechanism bending. The main assembly is shown in Fig. 6.24 as a Solidworks model and Fig. 6.25 as the actual version. Again, it was built using 3D printed parts. Some main parts were machined out of 6061 Aluminum in order to support the energy changes.

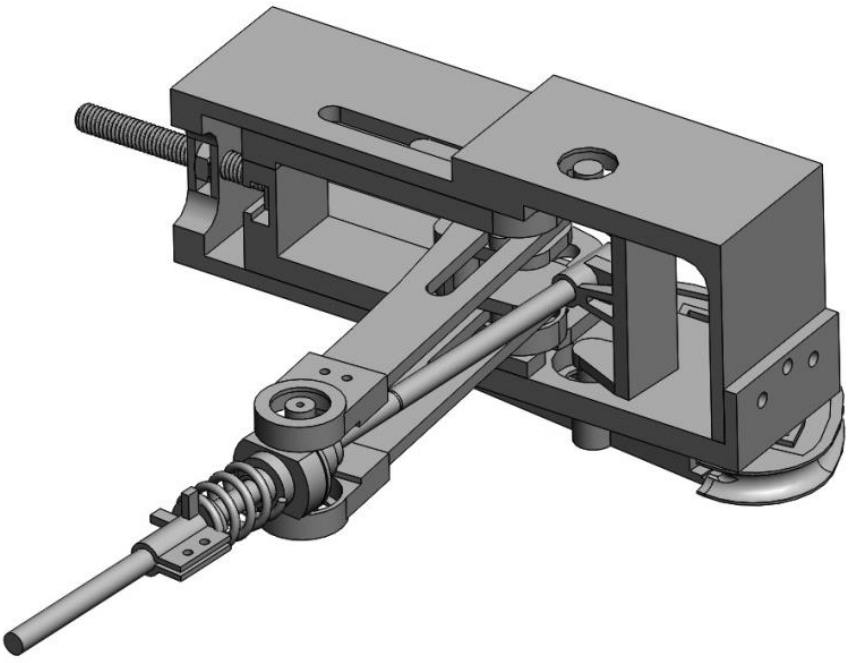

FIGURE 6.24: SOLIDWORKS MODEL OF CONSTANT FORCE MECHANISM VERSION 1.1.

FIGURE 6.25: ACTUAL CONSTANT FORCE MECHANISM VERSION 1.1.

6.4.4 Circular Prediction

This new design allowed for much smoother arm movements and more accurate testing of the constant moment energy path methods. The mechanism worked very well and even with a high moment created by the hanging weight, the mechanism was easy to rotate in the expected range of motion.

In this text for defining the mechanism, a clockwise motion in the mechanism is caused by the predesigned, constant moment field or hanging weight. A counter-clockwise motion in the mechanism is caused by the spring pushing on the radial arm. The maximum rotation of the mechanism in the counter-clockwise direction is defined as θ = 27 degrees while the maximum clockwise rotation of the mechanism is defined as θ = 157 degrees.

Mathematically, energy from the hanging weight is represented as the helical surface while the energy from the spring mechanism is represented by the black circle that forces the spring along a specific energy path across the energy bowl (see Fig. 6.20). For the motion of the arm to be non-existent the change in potential energy in the spring will need to be equal and opposite of the change in potential energy of the hanging mass at the arms current position.

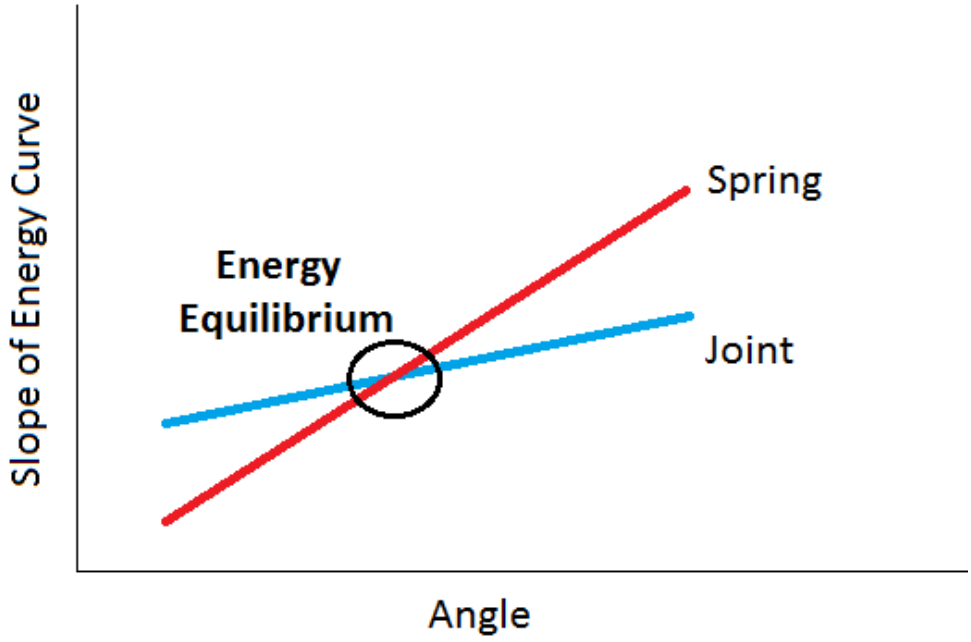

FIGURE 6.26: CONSTANT MOMENT ENERGY SLOPE (BLACK) COMPARED WITH SPRING MECHANISM ENERGY SLOPE (BLUE) VS. JOINT ANGLE.

It is important to determine what happens with the joint dynamics when one energy path has a higher energy slope than the other. Figure 6.26 is an example of an expected situation where the change in mechanism energy or spring energy crosses the change in energy created by the hanging weight on the robot arm with respect to joint angle θ. On one side of the crossing point the arm has higher energy slope and the other side the spring mechanism has a higher energy slope.

It seems counter intuitive that the magnitude of the energy values in each mechanism do not determine joint motion but that the difference in the slope of the two energy curves does. It is predicted that when the energy curve from the hanging mass has a greater slope (to the left of the intersection) the arm will move clockwise and when the energy curve from the spring mechanism has a greater slope (to the right of the intersection) the arm will move counter-clockwise. Combining these definitions, the point of intersection should be a stable equilibrium point. This mechanism is defined as stable because joint motion on either side of this angle will drive the arm back towards the equilibrium position.

The reciprocal of this definition is that if the energy slopes cross in the opposite direction, then to the left the mechanism will cause a counter clockwise arm rotation and to the right a clockwise arm rotation. The angle of equal slopes then becomes an equilibrium point but only marginally stable. These two equilibrium position types are both predicted to occur when testing the mechanism in Fig. 6.24 and Fig. 6.25.

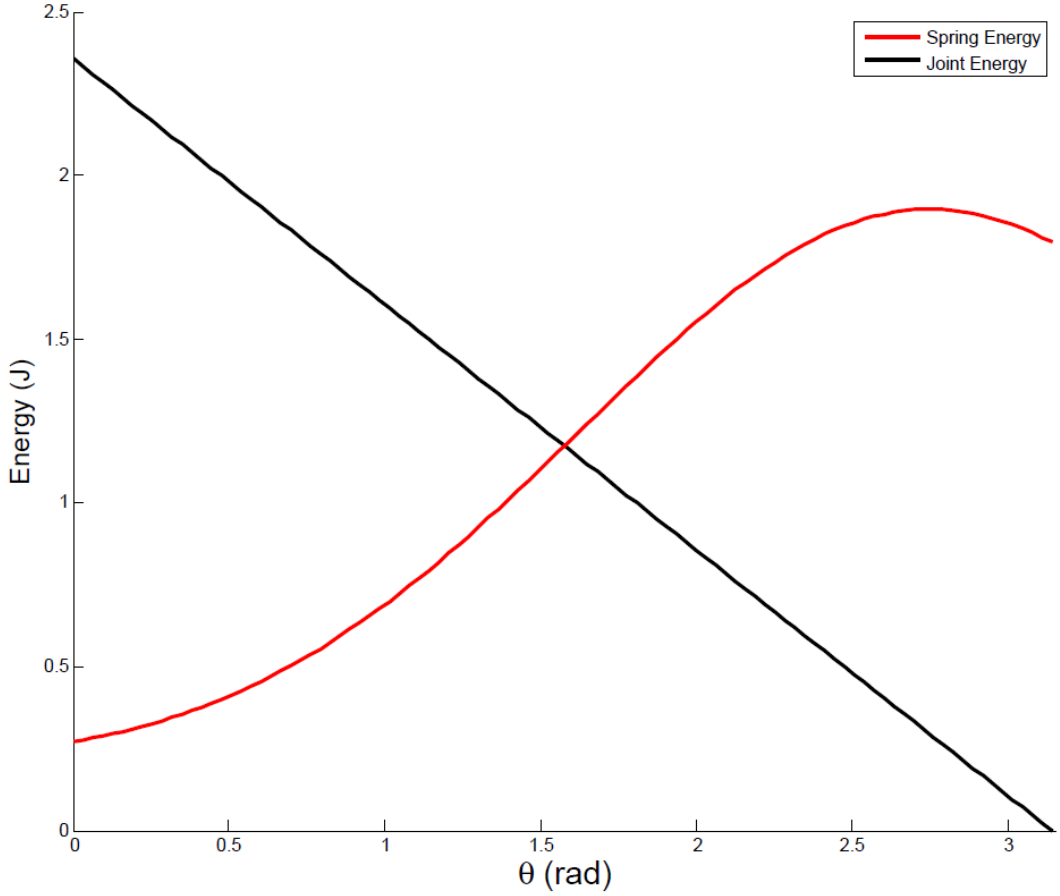

FIGURE 6.27: POTENTIAL ENERGY AT JOINT FROM HANGING MASS (BLACK) COMPARED WITH SPRING POTENTIAL ENERGY FROM MECHANISM CONFIGURATION (RED)

The mechanism configuration was adjusted by physically turning a nut on a bolt to move the "circle center" in Fig. 6.22 to represent the system defined in Fig. 6.20. The potential energy in the spring was calculated and compared to the potential energy of the joint from the hanging mass through a range of angles from 0 to 180 degrees, shown in Fig. 6.27.

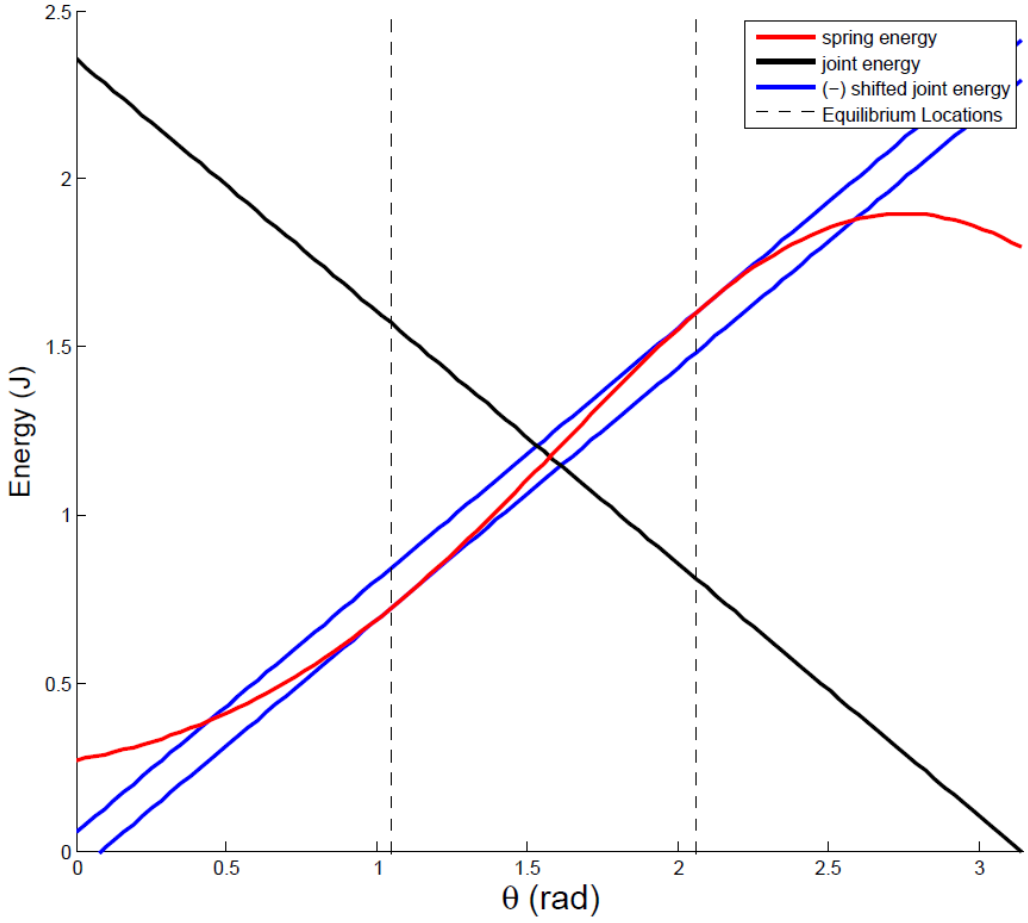

FIGURE 6.28: TRANSPOSED JOINT POTENTIAL ENERGY SHIFTED TO MATCH THE SPRING POTENTIAL ENERGY.

Figure 6.28 shows the transposed joint energy curve shifted up to align with the spring potential energy curve at the points where the slope is equal and opposite. The dashed lines in Fig. 6.28 show the angles where the matching slope values occur.

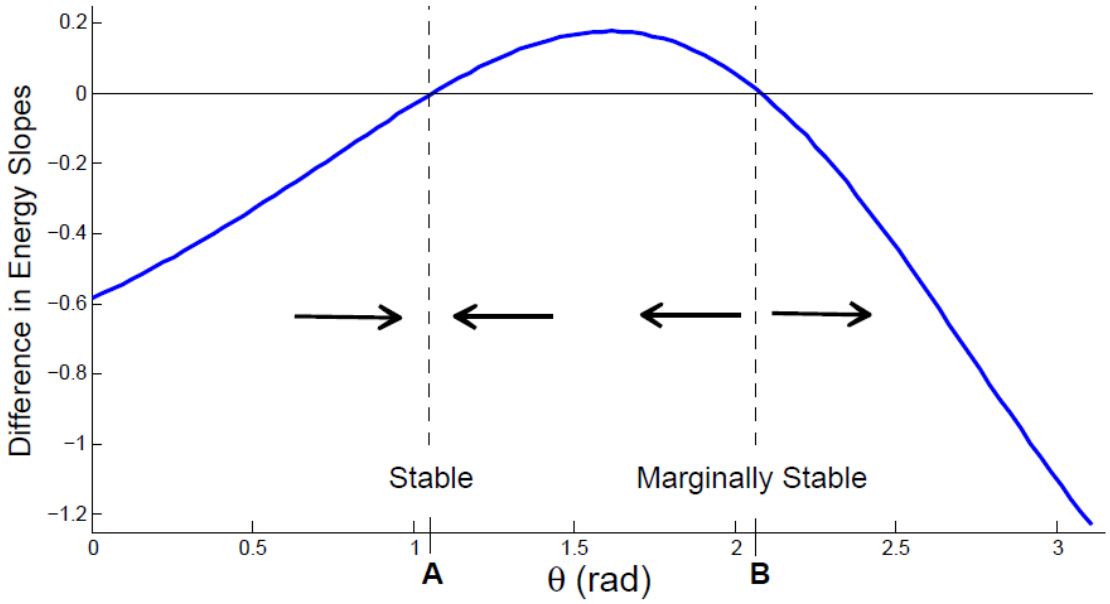

FIGURE 6.29: DIFFERENCE IN ENERGY CURVE SLOPES, POSITIVE MEANS THE SPRING POTENTIAL ENERGY SLOPE IS GREATER THAN THE MASS POTENTIAL ENERGY SLOPE. ANGLES A AND B ARE PREDICTED EQUILIBRIUM POINTS.

Figure 6.29 is the difference between the shifted, transposed mass potential energy slope from the spring potential energy slope over the range of angles. Points A = 60^o and B = 118^o are the angles at which the analysis predicts the mechanism equilibrium positions will occur. Joint position A is a stable equilibrium in that the energy slopes will direct the joint motion back towards position A as the joint is moved away. Joint position B is a marginally stable equilibrium angle where the joint will remain as long as it is unperturbed. The stiffness of the mechanism can also be predicted based on these energy slopes.

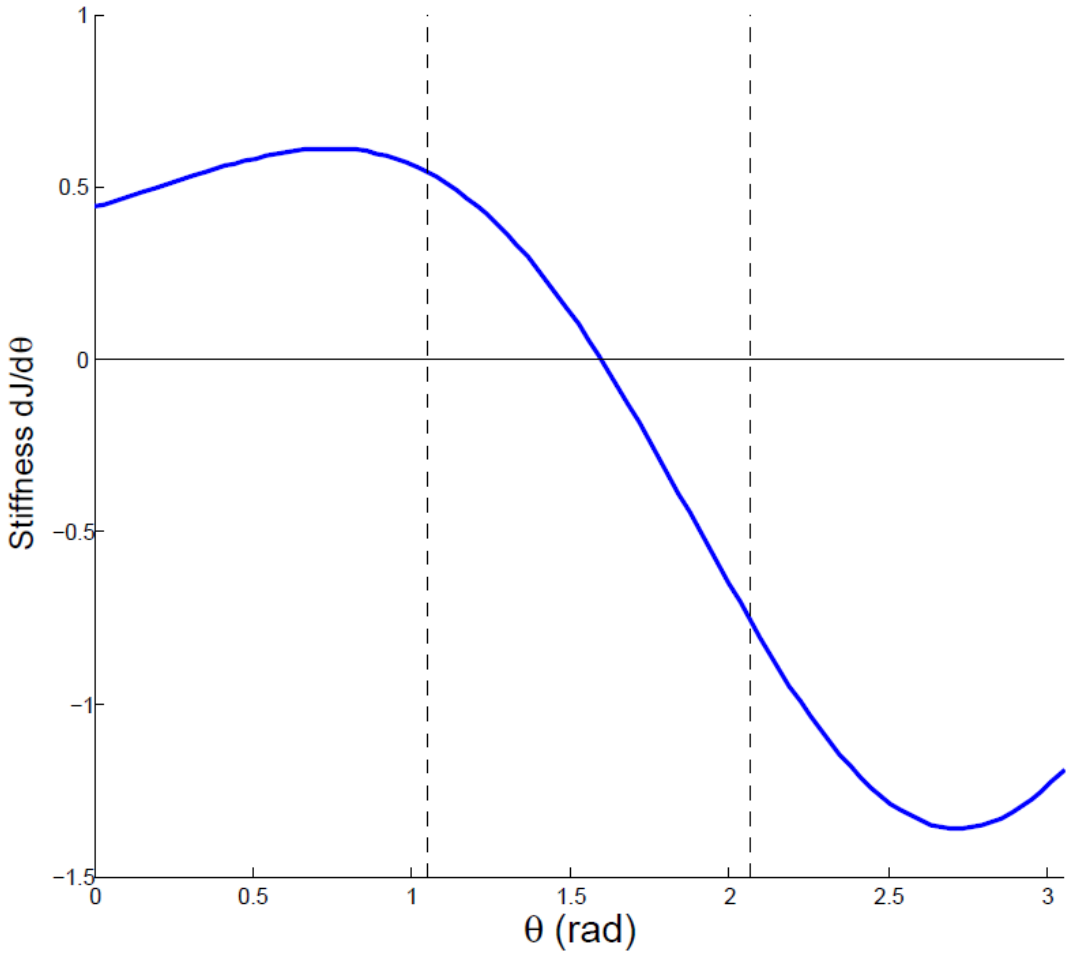

FIGURE 6.30: STIFFNESS OF THE MECHANISM FROM 0 TO 180 DEGREES.

Figure 6.30 is a representation of the stiffness for the joint mechanism through a range of θ values. In Fig. 6.30 a negative stiffness implies that the increase in moment will increase in the same direction as the joint motion. A positive stiffness value means that the change in moment at the joint will increase in opposition to the direction of joint motion.

6.4.5 Circular Fit Results

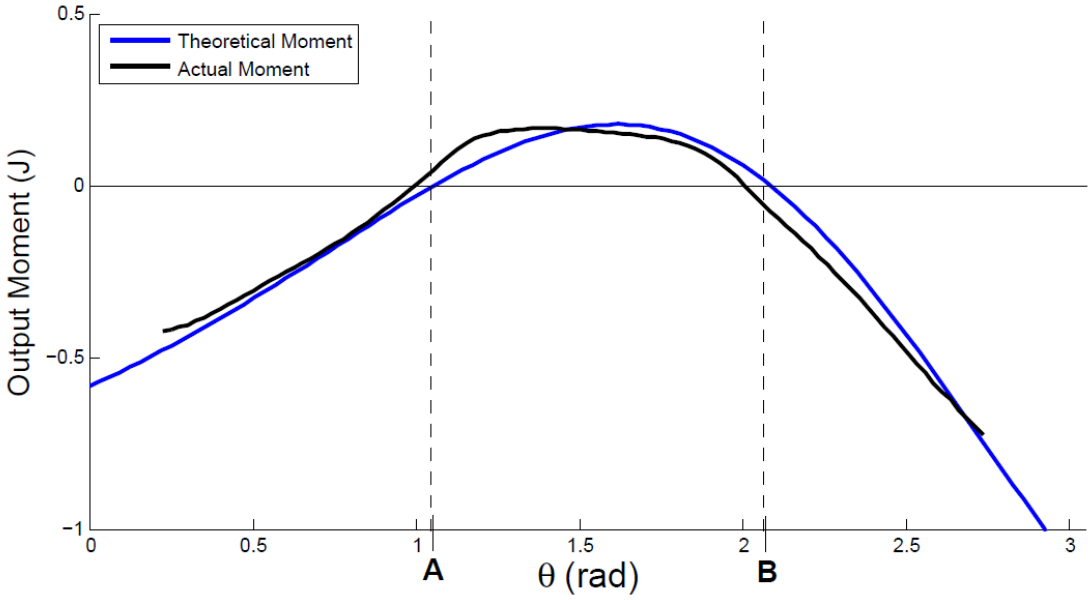

FIGURE 6.31: MECHANISM MOMENT RESULTS (BLACK) COMPARED WITH THE PREDICTED VALUES (BLUE).

The mechanism version 1.1 was set up with a specific configuration in order to test the behavior compared to the predicted values. Figure 6.31 shows the results for the mechanism where the moment is calculated over its entire range of motion. The testing results were filtered with a 3rd order polynomial least squares method. From the moment comparison that the results align well with the predicted values and the behavior of the mechanism was as predicted.

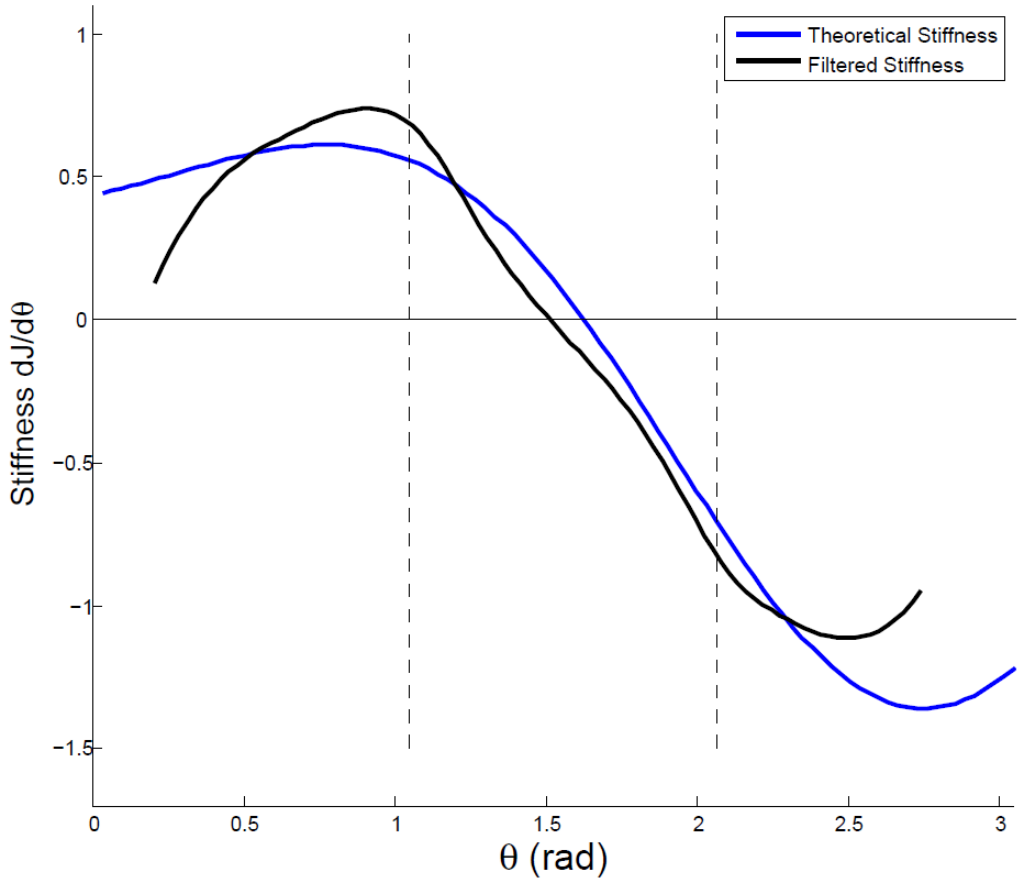

FIGURE 6.32: STIFFNESS VS. ANGLE THEORETICAL RESULTS (BLUE) COMPARED WITH ACTUAL RESULTS (BLACK).

Stiffness values for the joint were also predicted using the energy slopes. Figure 6.32 shows how the calculated stiffness values compare with the actual values found from testing. The test results for stiffness were also filtered using a 3rd order polynomial least squares method.

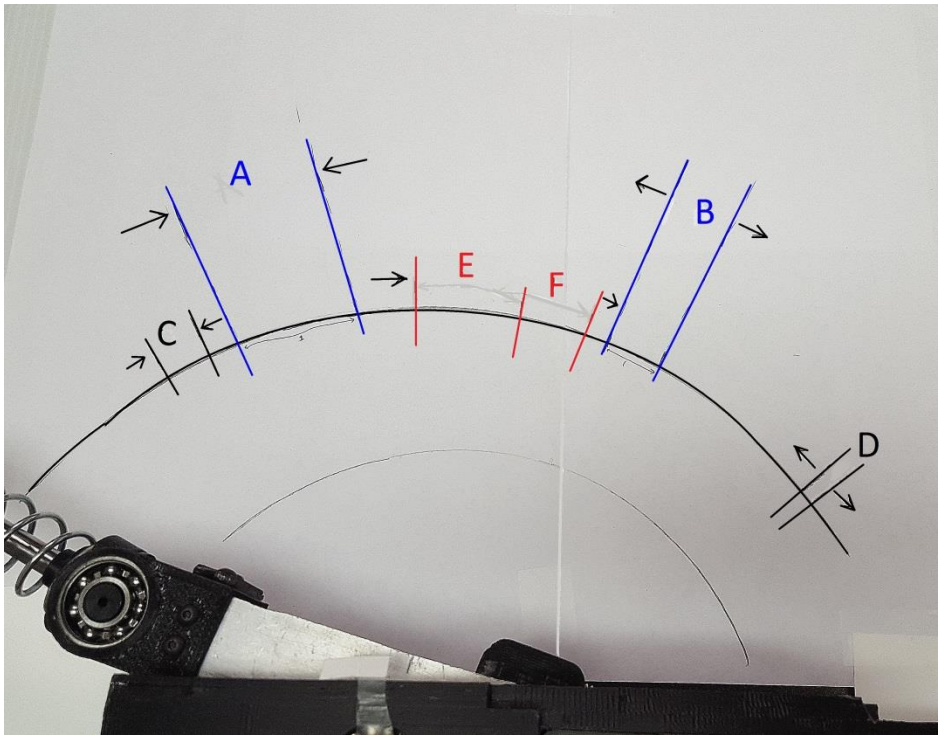

FIGURE 6.33: EQUILIBRIUM RESULTS FOR MECHANISM VERSION 1.1.

From testing the mechanism, equilibrium points are shown in Fig. 6.33 with a stable equilibrium point found at about 55-75 degrees, and a marginally stable equilibrium point at about 110-120 degrees. The testing results show the stable equilibrium at position 'A' and the marginally stable equilibrium at position 'B'. The predicted values of equilibrium occurred at 60 and 118 degrees, well within the testing results. The larger range of mechanism equilibrium behavior occurred due to slight friction in the system. As the difference in energy slopes become small the friction found in the mechanism can resist the small amounts of torque shown in the energy curves. In

between position *A* and *B* the torque values were so small that the friction was almost enough to mimic a larger equilibrator range. This may help in an actual robotic application where friction can make up for any slight discrepancies in joint construction or misalignment.

TABLE 6.1: PREDICTED LOCATION OF EQUILIBRIUM POSITIONS COMPARED WITH ACTUAL LOCATIONS.

Equilibrium Position	Circle Center (mm)	Stability	Predicted Location (Degrees)	Actual location (Degrees)
A	(19, 5)	Stable	60	59-75
B	(19, 5)	Marginally Stable	118	110-120
C	(12, 5)	Stable	52	53-57
D	(12, 5)	Marginally Stable	145	146-148
E	(8, 5)	CCW - Stable	76	81-x
F	(8, 5)	CW - Marginally Stable	76	x-101

Figure 6.33 also shows where the equilibrium points occurred for different mechanism configurations. These values are compared with the predicted values in Table 6.1. The mechanism center distance was adjusted in the *x*-direction to find the paired equilibrium positions: *A* with *B*, *C* with *D*, and *E* with *F*. The *x*-direction was adjusted to values of 8mm, 12mm and 19mm to produce the dynamic behavior shown in Fig. 6.34.

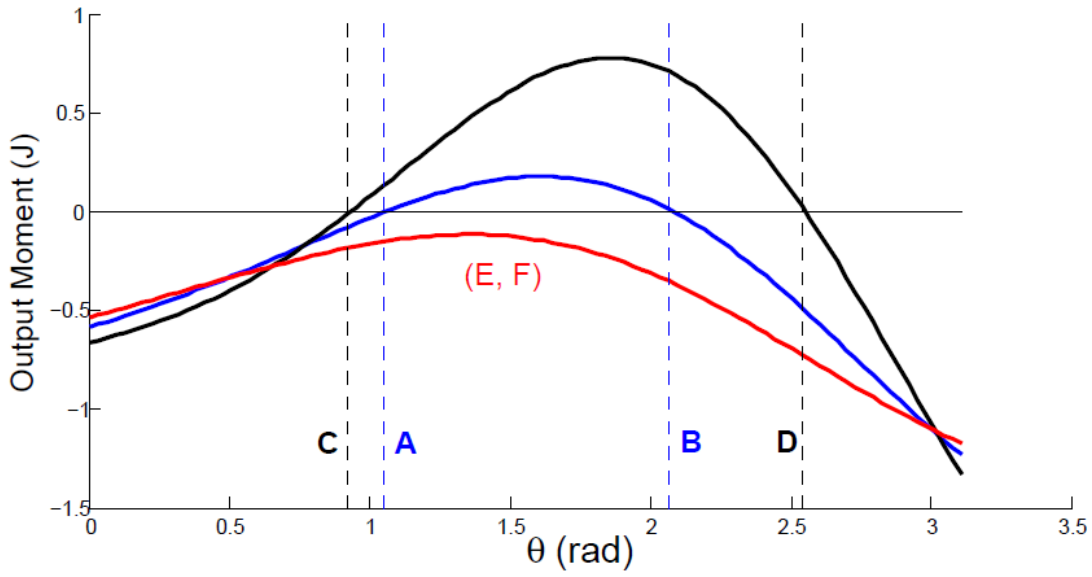

FIGURE 6.34: PREDICTED EQUILIBRIUM POSITIONS FOR MULTIPLE MECHANISM CONFIGURATIONS.

It is envisioned that the mechanism configuration can be easily adjusted by one small motor to achieve different equilibrium positions and different stiffness values. As the mechanism configuration is adjusted, the new predicted values of stable and marginally stable equilibrium are predicted in Fig. 6.34. The moment output of the mechanism will change as the mechanism is adjusted and so will the stiffness. By understanding these changes the mechanism can be tuned to specific applications. It also can predict and adjust the stiffness at that location.

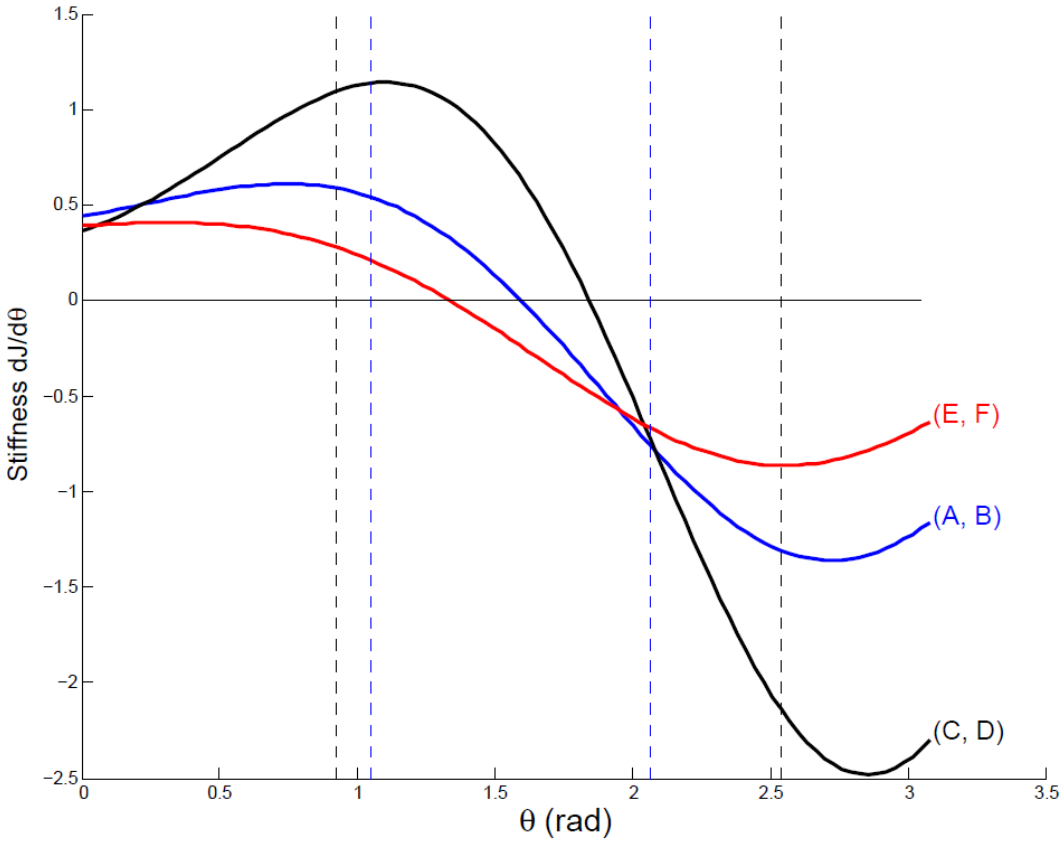

FIGURE 6.35: STIFFNESS CURVES FOR ADJUSTED MECHANISM PARAMETERS.

These values of stiffness in Fig. 6.35 show that the mechanism can be adjusted at both equilibrium positions to have more or less stiffness. The mechanism configuration for positions *E*, and *F* show the lowest values for stiffness and in Fig. 6.34 the moment value never reaches zero. This behavior is an example where the mechanism reduces the moment felt by the constant moment field. The joint arm is then very easy to move for the entire range of motion and has small values for stiffness. Equilibrium positions *C* and *D* have the most stiffness and is a good example of tuning both the negative and positive stiffness values to cause either greater stability (position *C*) or greater instability (position *D*).

6.5 CONCLUSION

The original work by Dr. Herder to create a constant force mechanism was expanded to define a new mechanism that can counteract a constant moment. Energy fields were defined and the intersection of the energy fields defined constant energy paths. We then looked at the derivative of the energy fields to determine when the system was in equilibrium and the slope of these curves defined the mechanism stiffness. Unique features include: the ability to adjust stiffness while not changing the moment and the ability to use a spring that has a length, not relying on a "zero free-length" spring.

In our new mechanism, the stable equilibrium points have a torsional stiffness associated with how hard it is to move the joint from the equilibrium position. This torsional stiffness does not have to be equal in both directions of rotation about the point. This stiffness is determined by the rate at which the difference of the energy slopes increase or decrease on either side of the equilibrium points.

Because the stiffness has to do with the rate of change of the total energy, the mechanism can be created to follow an almost constant energy. In this case with a zero stiffness or very low stiffness, the movement of the robot arm is very easy and soft even if there is a large load (weather the energy is small or large, the arm can be easily moved). For example, if the robot joint requires a large torque and therefore a large amount of energy to move, the mechanism can be adjusted to passively support most of the torque needed and reduce the energy required by a joint motor to change positions. If the passive mechanism is configured for a certain change in energy, then the torsional stiffness can be predicted and controllably tuned to behave in a predesigned way.

Another important attribute of this theory is that the equilibrium point itself can be changed. The black circle defined by the controlled mechanism in Fig. 6.20 can be moved and adjusted thus changing the energy slope crossing points (see Fig. 6.28). The mechanism adjusts the equilibrium position of the joint to be at the joint angles required for a desired end effector position.

The actuation allows a robot joint to have a way to actively adjust for changes in mass being manipulated by the end effector. This usually is the main reason for adding actuation to a equilibrator type mechanism. The results have verified how the joint stiffness can be changed and controlled for a desired behavior. The stiffness at the marginally stable equilibrium point is particularly important in creating a robot arm with tunable negative stiffness. This means that the energy can be stored at the equilibrium point and released quickly with an increase in moment supporting the joint motion.

Also, by combining the theory of decoupling joint stiffness from positon described in Chapter 5, the stiffness of any joint can be changed without changing its position. When making adjustments following this theory there will be no change in output as the mechanism makes the appropriate changes in configuration without changing the moment.

CHAPTER 7

CONCLUSION

7.1 SUMMARY

7.1.1 Passive Ankle System

A passive ankle-foot prosthesis was developed in order to provide able-bodied gait characteristics to amputees for slow to normal walking speeds. A novel mechanism was created to switch between two separate springs during the gait cycle. The design was built and functionality was tested showing the theoretically expected results to be correct.

7.1.2 Powered Ankle System

Walking and running able-bodied gait characteristics were achieved by a powered ankle-foot prosthetic. The design and actuation of the Ruggedized Odyssey Ankle was discussed. The ROA design was tested and results show that the design was able to supply the power necessary to achieve walking and running with a continuous transition between the two. A 4m/s sprinting gait was achieved while wearing the ROA device because of a 4x's power amplification from the motor input power to the ankle output power.

7.1.3 Actively Passive Joint

A simple spring and lever arm mechanism was used to develop a method for decoupling joint stiffness and instantaneous joint position. The method was created while modeling the mechanism as a prosthetic ankle system using able-bodied ankle kinematic data. The resulting method was then applied to a specific use as a powered prosthetic ankle system. For this application an appropriate moment path was created for each specific ankle angle through one gait cycle. The path data was then fit by a line and a circle to prove manufacturability and simplicity of design. The particular path solution presented in this work is not unique. There are other specific paths that can be explored and compared in terms of energy cost and desired output.

It is recognized and important to note that these results and analysis in the prosthetic field only represent one gait speed and level ground walking. The tools

developed will be easily adapted to optimize on multiple speeds and gait dynamics. The ankle joint stiffness was shown to successfully be controlled without any output change to ankle position.

7.1.4 Novel Stiffness Control

Gravity compensation methods were used to describe energy surfaces of a joint mechanism. The joint mechanism dynamic behavior was analyzed in comparison to the relationship of the energy surfaces. Desired joint moments and stiffness were achieved passively through intelligent selection of mechanism configurations. Adjustments to the mechanism configuration are able to change joint equilibrium positions, joint stiffness, and tune negative stiffness.

7.2 CONTRIBUTIONS

- Passive Prosthetic Ankle-Foot System for Walking Gait
- Powered Prosthetic Ankle-Foot System for Walking and Running
- Achieved tethered and untethered powered running at 4 m/s
- Achieved 4x's power amplification from motor to ankle during running
- Developed theory for decoupled stiffness and position in a joint robot system

- New unique mechanism is able to actively change stiffness between linear quasi-stiffness ranges of the ankle joint during the gait cycle without affecting ankle angle

- Developed theory for the application of an active gravity compensation system for defining dynamic behavior in robotic joints

- Mechanism is able to actively tune positive, equilibrium, and negative stiffness in joint systems

7.3 OTHER ACCOMPLISHMENTS

Work done with passive prosthetic systems has led to increased grant funding to create a quasi-active ankle foot prosthesis. Also, the development of the walk/run ankle-foot prosthesis led to the Ruggedized Odyssey Ankle design allowing running and walking on any terrain and was purchased by Ossur to become an affordable powered prosthetic option for amputees.

During the research presented the author has published work in journals and conferences and also achieved two different patents for novel robotic systems.

7.3.1 Papers Published

- A Joint Torque Augmentation Robot (JTAR) for Ankle Gait Assistance, ASME, 38th Mechanisms and Robotics Conference, 2014

- A Passive and Active Joint Torque Augmentation Robot (JTAR) for Hip Gait Assistance, ASME, 38th Mechanisms and Robotics Conference, 2014

- A Powered Prosthetic Ankle Joint for Walking and Running, BioMed Eng. OnLine, 2016

- A Passive Ankle-Foot Prosthesis with Energy Return to Mimic Able-Bodied Gait, ASME, 41st Mechanisms and Robotics Conference, 2017

- Decoupling Stiffness from Position in Joint Mechanisms: Applied to Powered Ankle Prosthesis, ASME, 41st Mechanisms and Robotics Conference, 2017

7.3.2 Patents

- Quasi-active Prosthetic Joint System – 9289316

- Joint Torque Augmentation System and Method For Gait Assistance – 9662262

7.4 FUTURE WORK

Future work will include the analysis and comparison of the energy an ankle-foot prosthetic will use when designed with the theory found in Chapter 5. Further optimization will be done to decrease the number of times the motor will need to make stiffness adjustments in order to lower the power necessary for the joint to reach specific moments along the chosen path. The idea will also be extended to a quasi-active ankle

prosthetic where only the points reachable with a defined power limit will be used to achieve as much moment as possible. The constant moment method of decoupling stiffness and joint position will allow the quasi-active ankle to profit from the natural mechanism stiffness saving power instead of using power to force or mimic joint stiffness. Eventually these concepts will be applied to a 2-DOF ankle-foot prosthesis that will allow for inversion eversion during gait.

Chapter 5 and Chapter 6 theory for intelligently adjusting and choosing mechanism configurations will be applied to multi-joint robotic limbs. The methods will be further optimized for changes in end effector loads. Tunable stiffness values for multi-joint robots will be explored for human machine interaction.

REFERENCES

[1] K. Ziegler-Graham, E. J. MacKenzie, P. L. Ephraim, T. G. Travison, and R. Brookmeyer, "Estimating the prevalence of limb loss in the United States: 2005 to 2050," *Archives of physical medicine and rehabilitation*, vol. 89, no. 3, pp. 422–429, 2008.

[2] H. Fischer, "A Guide to U.S. Military Casualty Statistics: Operation New Dawn, Operation Iraqi Freedom, and Operation Enduring Freedom." Congressional Research Service, 19-Feb-2014.

[3] D. J. Stinner, T. C. Burns, K. L. Kirk, and J. R. Ficke, "Return to duty rate of amputee soldiers in the current conflicts in Afghanistan and Iraq," *Journal of Trauma-Injury, Infection, and Critical Care*, vol. 68, no. 6, pp. 1476–1479, 2010.

[4] R. S. Gailey *et al.*, "Energy expenditure of trans-tibial amputees during ambulation at self-selected pace," *Prosthetics and Orthotics International*, vol. 18, no. 2, pp. 84–91, 1994.

[5] W. C. Miller, A. B. Deathe, M. Speechley, and J. Koval, "The influence of falling, fear of falling, and balance confidence on prosthetic mobility and social activity among individuals with a lower extremity amputation," *Archives of physical medicine and rehabilitation*, vol. 82, no. 9, pp. 1238–1244, 2001.

[6] W. C. Miller, M. Speechley, and B. Deathe, "The prevalence and risk factors of falling and fear of falling among lower extremity amputees," *Archives of physical medicine and rehabilitation*, vol. 82, no. 8, pp. 1031–1037, 2001.

[7] P. L. Ephraim, S. T. Wegener, E. J. MacKenzie, T. R. Dillingham, and L. E. Pezzin, "Phantom pain, residual limb pain, and back pain in amputees: results of a national survey," *Archives of physical medicine and rehabilitation*, vol. 86, no. 10, pp. 1910–1919, 2005.

[8] R. L. Waters, J. Perry, D. Antonelli, and H. Hislop, "Energy cost of walking of amputees: the influence of level of amputation," *J Bone Joint Surg Am*, vol. 58, no. 1, pp. 42–46, 1976.

[9] M. W. Whittle, *Gait analysis: an introduction*. Butterworth-Heinemann, 2003.

[10] A. H. Hansen, D. S. Childress, S. C. Miff, S. A. Gard, and K. P. Mesplay, "The human ankle during walking: implications for design of biomimetic ankle prostheses," *Journal of Biomechanics*, vol. 37, no. 10, pp. 1467–1474, Oct. 2004.

[11] J. A. Ward, T. G. Sugar, and K. W. Hollander, "Using the translational potential energy of springs for prosthetic systems," in *2011 IEEE International Conference on Control Applications (CCA)*, 2011, pp. 1461–1467.

[12] T. G. Sugar, K. W. Hollander, A. Boehler, and J. Ward, “Comparison and Analysis of a Robotic Tendon and Jackspring™ Actuator for Wearable Robotic Systems,” *J. Med. Devices*, vol. 7, no. 4, pp. 041003–041003, Sep. 2013.

[13] R. B. Davis and P. A. DeLuca, “Gait characterization via dynamic joint stiffness,” *Gait & Posture*, vol. 4, no. 3, pp. 224–231, May 1996.

[14] S. H. Collins and A. D. Kuo, “Controlled energy storage and return prosthesis reduces metabolic cost of walking,” *Power*, vol. 600, p. 800, 2005.

[15] M. Grimmer and A. Seyfarth, “Stiffness adjustment of a Series Elastic Actuator in an ankle-foot prosthesis for walking and running: The trade-off between energy and peak power optimization,” in *2011 IEEE International Conference on Robotics and Automation*, 2011, pp. 1439–1444.

[16] S. A. Migliore, E. A. Brown, and S. P. DeWeerth, “Biologically Inspired Joint Stiffness Control,” in *Proceedings of the 2005 IEEE International Conference on Robotics and Automation*, 2005, pp. 4508–4513.

[17] C. Li *et al.*, “Research and Development of the Intelligently-Controlled Prosthetic Ankle Joint,” in *2006 International Conference on Mechatronics and Automation*, 2006, pp. 1114–1119.

[18] R. Versluys, P. Beyl, M. V. Damme, A. Desomer, R. V. Ham, and D. Lefeber, “Prosthetic feet: State-of-the-art review and the importance of mimicking human ankle–foot biomechanics,” *Disability and Rehabilitation: Assistive Technology*, vol. 4, no. 2, pp. 65–75, Jan. 2009.

[19] A. H. Shultz, B. E. Lawson, and M. Goldfarb, “Running With a Powered Knee and Ankle Prosthesis,” *IEEE Transactions on Neural Systems and Rehabilitation Engineering*, vol. 23, no. 3, pp. 403–412, May 2015.

[20] K. Koganezawa and I. Kato, “Control aspects of artificial leg,” *IFAC Control Aspects of Biomedical Engineering*, pp. 71–85, 1987.

[21] Össur, “PROPRIO FOOT.” [Online]. Available: http://www.ossur.com/prosthetic-solutions/products/dynamic-solutions/proprio-foot. [Accessed: 10-Mar-2017].

[22] G.-P. Brüggemann, A. Arampatzis, F. Emrich, and W. Potthast, “Biomechanics of double transtibial amputee sprinting using dedicated sprinting prostheses,” *Sports Technol.*, vol. 1, no. 4–5, pp. 220–227, Jan. 2008.

[23] B. Vanderborght *et al.*, “Variable impedance actuators: Moving the robots of tomorrow,” in *2012 IEEE/RSJ International Conference on Intelligent Robots and Systems*, 2012, pp. 5454–5455.

[24] B. Vanderborght *et al.*, "Variable impedance actuators: A review," *Robotics and Autonomous Systems*, vol. 61, no. 12, pp. 1601–1614, Dec. 2013.

[25] M. D. Geil, "Energy Loss and Stiffness Properties of Dynamic Elastic Response Prosthetic Feet," *JPO: Journal of Prosthetics and Orthotics*.

[26] J.-M. Casillas, V. Dulieu, M. Cohen, I. Marcer, and J.-P. Didier, "Bioenergetic comparison of a new energy-storing foot and SACH foot in traumatic below-knee vascular amputations," *Archives of Physical Medicine and Rehabilitation*, vol. 76, no. 1, pp. 39–44, Jan. 1995.

[27] K. Schneider, T. Hart, R. F. Zernicke, Y. Setoguchi, and W. Oppenheim, "Dynamics of below-knee child amputee gait: SACH foot versus Flex foot," *Journal of Biomechanics*, vol. 26, no. 10, pp. 1191–1204, Oct. 1993.

[28] L. Torburn and J. Perry, "Below-knee amputee gait with dynamic elastic response prosthetic feet: A pilot study," *Journal of Rehabilitation Research & Development*, vol. 27, no. 4, p. 369, Fall 1990.

[29] S. S. Thomas, C. E. Buckon, D. Helper, N. Turner, M. Moor, and J. I. Krajbich, "Comparison of the Seattle Lite Foot and Genesis II Prosthetic Foot during walking and running," *JPO Journal of Prosthetics & Orthotics*, vol. 12, no. 1, pp. 9–14, 2000.

[30] "Flex-Foot Cheetah." [Online]. Available: https://www.ossur.com/prosthetic-solutions/products/sport-solutions/cheetah. [Accessed: 27-Jun-2017].

[31] Y. Zeng, "Design And Testing Of A Passive Prosthetic Ankle With Mechanical Performance Similar To That Of A Natural Ankle," 2013.

[32] Össur, "Pro-Flex." [Online]. Available: http://www.ossur.com/prosthetic-solutions/products/dynamic-solutions/pro-flex. [Accessed: 10-Mar-2017].

[33] E. Nickel, J. Sensinger, and A. Hansen, "Passive prosthetic ankle-foot mechanism for automatic adaptation to sloped surfaces," *Journal of Rehabilitation Research & Development*, vol. 51, no. 5, pp. 803–813, May 2014.

[34] A. H. Hansen and D. S. Childress, "Investigations of roll-over shape: implications for design, alignment, and evaluation of ankle-foot prostheses and orthoses," *Disability and Rehabilitation*, vol. 32, no. 26, pp. 2201–2209, Jan. 2010.

[35] A. Hansen, "Roll-over characteristics of human walking with applications for artificial limbs," Dissertation, Northwestern University, Evanston IL, 2002.

[36] R. J. Williams, A. H. Hansen, and S. A. Gard, "Prosthetic Ankle-Foot Mechanism Capable of Automatic Adaptation to the Walking Surface," *J Biomech Eng*, vol. 131, no. 3, pp. 035002-035002-7, Jan. 2009.

[37] B. Vanderborght, R. Van Ham, D. Lefeber, T. G. Sugar, and K. W. Hollander, "Comparison of Mechanical Design and Energy Consumption of Adaptable, Passive-compliant Actuators," *The Int'l Journal of Robotics Research*, vol. 28, no. 1, pp. 90–103, Jan. 2009.

[38] J. Pratt, B. Krupp, and C. Morse, "Series elastic actuators for high fidelity force control," *The Industrial Robot; Bedford*, vol. 29, no. 3, pp. 234–241, 2002.

[39] J. Realmuto, G. Klute, and S. Devasia, "Nonlinear Passive Cam-Based Springs for Powered Ankle Prostheses," *J. Med. Devices*, vol. 9, no. 1, pp. 011007-011007-10, Mar. 2015.

[40] S. Au, M. Berniker, and H. Herr, "Powered ankle-foot prosthesis to assist level-ground and stair-descent gaits," *Neural Networks*, vol. 21, no. 4, pp. 654–666, May 2008.

[41] F. Sup, A. Bohara, and M. Goldfarb, "Design and Control of a Powered Transfemoral Prosthesis," *The Int'l Journal of Robotics Research*, vol. 27, no. 2, pp. 263–273, Feb. 2008.

[42] M. Grimmer, M. Eslamy, and A. Seyfarth, "Energetic and Peak Power Advantages of Series Elastic Actuators in an Actuated Prosthetic Leg for Walking and Running," *Actuators*, vol. 3, no. 1, pp. 1–19, Feb. 2014.

[43] K. W. Hollander and T. G. Sugar, "Design of the robotic tendon," presented at the Design of Medical Devices Conference (DMD 2005), 2005.

[44] K. W. Hollander, R. Ilg, T. G. Sugar, and D. Herring, "An Efficient Robotic Tendon for Gait Assistance," *J Biomech Eng*, vol. 128, no. 5, pp. 788–791, Mar. 2006.

[45] M. A. Holgate, A. W. Bohler, and T. G. Suga, "Control algorithms for ankle robots: A reflection on the state-of-the-art and presentation of two novel algorithms," in *2008 2nd IEEE RAS EMBS International Conference on Biomedical Robotics and Biomechatronics*, 2008, pp. 97–102.

[46] M. A. Holgate, J. K. Hitt, R. D. Bellman, T. G. Sugar, and K. W. Hollander, "The SPARKy (Spring Ankle with Regenerative kinetics) project: Choosing a DC motor based actuation method," in *2008 2nd IEEE RAS EMBS International Conference on Biomedical Robotics and Biomechatronics*, 2008, pp. 163–168.

[47] M. A. Holgate, T. G. Sugar, and A. W. Bohler, "A novel control algorithm for wearable robotics using phase plane invariants," in *2009 IEEE International Conference on Robotics and Automation*, 2009, pp. 3845–3850.

[48] A. Saenz, "iWalk Presents World's First Actively Powered Foot and Ankle," *Singularity Hub*, 20-Jan-2010. .

[49] S. K. Au, H. Herr, J. Weber, and E. C. Martinez-Villalpando, "Powered Ankle-Foot Prosthesis for the Improvement of Amputee Ambulation," in *2007 29th Annual International Conference of the IEEE Engineering in Medicine and Biology Society*, 2007, pp. 3020–3026.

[50] S. Au, J. Weber, and H. Herr, "Powered ankle-foot prosthesis improved walking metabolic economy," *IEEE Transaction on Robotics*, vol. 25(1), pp. 51–66.

[51] J. K. Hitt, R. Bellman, M. Holgate, T. G. Sugar, and K. W. Hollander, "The SPARKy (Spring Ankle With Regenerative Kinetics) Project: Design and Analysis of a Robotic Transtibial Prosthesis With Regenerative Kinetics," *ASME 2007 International Design Engineering Technical Conferences and Computers and Information in Engineering Conference*, pp. 1587–1596, Jan. 2007.

[52] J. Hitt, T. Sugar, M. Holgate, R. Bellman, and K. Hollander, "Robotic transtibial prosthesis with biomechanical energy regeneration," *The Industrial Robot; Bedford*, vol. 36, no. 5, pp. 441–447, 2009.

[53] J. K. Hitt, T. G. Sugar, M. Holgate, and R. Bellman, "An Active Foot-Ankle Prosthesis With Biomechanical Energy Regeneration," *J. Med. Devices*, vol. 4, no. 1, pp. 011003-011003-9, Mar. 2010.

[54] F. Sup, H. A. Varol, and M. Goldfarb, "Upslope Walking With a Powered Knee and Ankle Prosthesis: Initial Results With an Amputee Subject," *IEEE Transactions on Neural Systems and Rehabilitation Engineering*, vol. 19, no. 1, pp. 71–78, Feb. 2011.

[55] F. Sup, H. A. Varol, J. Mitchell, T. J. Withrow, and M. Goldfarb, "Preliminary Evaluations of a Self-Contained Anthropomorphic Transfemoral Prosthesis," *IEEE/ASME Transactions on Mechatronics*, vol. 14, no. 6, pp. 667–676, Dec. 2009.

[56] A. H. Shultz, J. E. Mitchell, D. Truex, B. E. Lawson, and M. Goldfarb, "Preliminary evaluation of a walking controller for a powered ankle prosthesis," in *2013 IEEE international conference on robotics and automation (ICRA)*, 2013, pp. 4838–4843.

[57] P. Cherelle, G. Mathijssen, Q. Wang, B. Vanderborght, and D. Lefeber, "Advances in Propulsive Bionic Feet and Their Actuation Principles," *Advances in Mechanical Engineering*, vol. 6, p. 984046, Jan. 2014.

[58] P. Cherelle, V. Grosu, A. Matthys, B. Vanderborght, and D. Lefeber, "Design and Validation of the Ankle Mimicking Prosthetic (AMP-) Foot 2.0," *IEEE Transactions on Neural Systems and Rehabilitation Engineering*, vol. 22, no. 1, pp. 138–148, Jan. 2014.

[59] P. Cherelle, K. Junius, V. Grosu, H. Cuypers, B. Vanderborght, and D. Lefeber, "The AMP-Foot 2.1 : actuator design, control and experiments with an amputee," *Robotica*, vol. 32, no. 08, pp. 1347–1361, Dec. 2014.

[60] P. Cherelle, V. Grosu, M. Cestari, B. Vanderborght, and D. Lefeber, "The AMP-Foot 3, new generation propulsive prosthetic feet with explosive motion characteristics: design and validation," *BioMedical Engineering OnLine*, vol. 15, pp. 21–36, Dec. 2016.

[61] G. Mathijssen, P. Cherelle, D. Lefeber, and B. Vanderborght, "Concept of a series-parallel elastic actuator for a powered transtibial prosthesis," *Actuators*, pp. 59–73, 2013.

[62] J. Zhu, Q. Wang, and L. Wang, "PANTOE 1: Biomechanical design of powered ankle-foot prosthesis with compliant joints and segmented foot," in *2010 IEEE/ASME International Conference on Advanced Intelligent Mechatronics*, 2010, pp. 31–36.

[63] J. Zhu, Q. Wang, and L. Wang, "On the Design of a Powered Transtibial Prosthesis With Stiffness Adaptable Ankle and Toe Joints," *IEEE Transactions on Industrial Electronics*, vol. 61, no. 9, pp. 4797–4807, Sep. 2014.

[64] J. Zhu, Q. Wang, and L. Wang, "Effects of toe stiffness on ankle kinetics in a robotic transtibial prosthesis during level-ground walking," *Mechatronics*, vol. 24, no. 8, pp. 1254–1261, Dec. 2014.

[65] M. Grimmer, "Powered Lower Limb Prostheses," Ph.D. Thesis, Technische Universität, Darmstadt, 2015.

[66] C. Everarts, B. Dehez, and R. Ronsse, "Variable Stiffness Actuator applied to an active ankle prosthesis: Principle, energy-efficiency, and control," in *2012 IEEE/RSJ International Conference on Intelligent Robots and Systems*, 2012, pp. 323–328.

[67] K. W. Hollander, T. G. Sugar, and D. E. Herring, "Adjustable robotic tendon using a'Jack Spring'/spl trade," in *Rehabilitation robotics, 2005. icorr 2005. 9th international conference on*, 2005, pp. 113–118.

[68] T. G. Sugar, K. W. Hollander, A. Boehler, and J. Ward, "Comparison and Analysis of a robotic tendon and jackspring™ actuator for wearable robotic systems," *Journal of Medical Devices*, vol. 7, no. 4, p. 041003, 2013.

[69] L. C. Visser, R. Carloni, R. Ünal, and S. Stramigioli, "Modeling and design of energy efficient variable stiffness actuators," in *2010 IEEE International Conference on Robotics and Automation*, 2010, pp. 3273–3278.

[70] L. C. Visser, R. Carloni, and S. Stramigioli, "Energy-Efficient Variable Stiffness Actuators," *IEEE Transactions on Robotics*, vol. 27, no. 5, pp. 865–875, Oct. 2011.

[71] A. Jafari, N. Tsagarakis, B. Vanderborght, and D. Caldwell, "Minimizing energy consumption through optimal mechanical design and stiffness regulation," in *Workshop for Young Researchers on Human-Friendly Robotics*, 2009.

[72] A. Jafari, N. G. Tsagarakis, B. Vanderborght, and D. G. Caldwell, "A novel actuator with adjustable stiffness (AwAS)," in *2010 IEEE/RSJ International Conference on Intelligent Robots and Systems*, 2010, pp. 4201–4206.

[73] A. Jafari, N. G. Tsagarakis, and D. G. Caldwell, "AwAS-II: A new Actuator with Adjustable Stiffness based on the novel principle of adaptable pivot point and variable lever ratio," in *2011 IEEE International Conference on Robotics and Automation*, 2011, pp. 4638–4643.

[74] R. Van Ham, B. Vanderborght, M. Van Damme, B. Verrelst, and D. Lefeber, "MACCEPA, the mechanically adjustable compliance and controllable equilibrium position actuator: Design and implementation in a biped robot," *Robotics and Autonomous Systems*, vol. 55, no. 10, pp. 761–768, Oct. 2007.

[75] B. Vanderborght, N. G. Tsagarakis, R. V. Ham, I. Thorson, and D. G. Caldwell, "MACCEPA 2.0: compliant actuator used for energy efficient hopping robot Chobino1D," *Auton Robot*, vol. 31, no. 1, p. 55, Jul. 2011.

[76] G. K. Klute, J. Gorges, K. Yeates, and A. D. Segal, "Variable Stiffness Prosthesis to Improve Amputee Coronal Plane Balance," in *American Academy of Orthotists and Prosthetists*, 2015.

[77] S. Wolf and G. Hirzinger, "A new variable stiffness design: Matching requirements of the next robot generation," in *2008 IEEE International Conference on Robotics and Automation*, 2008, pp. 1741–1746.

[78] L. Flynn, J. Geeroms, R. Jimenez-Fabian, B. Vanderborght, N. Vitiello, and D. Lefeber, "Ankle–knee prosthesis with active ankle and energy transfer: Development of the CYBERLEGs Alpha-Prosthesis," *Robotics and Autonomous Systems*, vol. 73, pp. 4–15, Nov. 2015.

[79] S. Pfeifer, A. Pagel, R. Riener, and H. Vallery, "Actuator With Angle-Dependent Elasticity for Biomimetic Transfemoral Prostheses," *IEEE/ASME Transactions on Mechatronics*, vol. 20, no. 3, pp. 1384–1394, Jun. 2015.

[80] J. Sun and P. A. Voglewede, "Powered Transtibial Prosthetic Device Control System Design, Implementation, and Bench Testing," *J. Med. Devices*, vol. 8, no. 1, pp. 011004-011004-8, Dec. 2013.

[81] J. Sun, “Powered transtibial prosthetic device control system design, implementation and testing,” Masters Thesis, Marquette University, 2012.

[82] A. LaPre and F. Sup, “Redefining Prosthetic Ankle Mechanics,” in *IEEE International Conference on Rehabilitation Robotics*, 2013.

[83] G. Tonietti, R. Schiavi, and A. Bicchi, “Design and Control of a Variable Stiffness Actuator for Safe and Fast Physical Human/Robot Interaction,” in *Proceedings of the 2005 IEEE International Conference on Robotics and Automation*, 2005, pp. 526–531.

[84] R. Schiavi, G. Grioli, S. Sen, and A. Bicchi, “VSA-II: a novel prototype of variable stiffness actuator for safe and performing robots interacting with humans,” in *2008 IEEE International Conference on Robotics and Automation*, 2008, pp. 2171–2176.

[85] K. Hain, “Grundlagen der Landtechnik,” 1952, pp. 3, 38.

[86] K. Hain, “Feinwerktechnik,” 1954, pp. 58, 88.

[87] K. Hain, “Spring Mechanisms,” in *Spring Design and Application*, New York: N. P. Chironis. McGraw-Hill, 1961, pp. 268–275.

[88] G. J. Walsh, D. A. Streit, and B. J. Gilmore, “Spatial spring equilibrator theory,” *Mechanism and Machine Theory*, vol. 26, no. 2, pp. 155–170, Jan. 1991.

[89] R. Barents, M. Schenk, W. D. van Dorsser, B. M. Wisse, and J. L. Herder, “Spring-to-Spring Balancing as Energy-Free Adjustment Method in Gravity Equilibrators,” *J. Mech. Des*, vol. 133, no. 6, pp. 061010-061010-10, Jun. 2011.

[90] G. Haupt and J. Grewolls, “Maschinenbautechnik,” 1963, pp. 8, 423.

[91] T. Morita, F. Kuribara, Y. Shiozawa, and S. Sugano, “A novel mechanism design for gravity compensation in three dimensional space,” in *Proceedings 2003 IEEE/ASME International Conference on Advanced Intelligent Mechatronics (AIM 2003)*, 2003, vol. 1, pp. 163–168 vol.1.

[92] R. H. Nathan, “A constant force generation mechanism,” *ASME J. Mech., Transm., Autom. Des*, vol. 107, no. 4, pp. 508–512, 1985.

[93] P. Pracht, P. Minotti, and M. Dahan, “Synthesis and balancing of cam-modulated linkages,” presented at the ASME Design and Automation Conference, 1987, p. 10(2)221/6.

[94] D. A. Streit, “An energy efficient quadruped with two-stage equilibrator,” 1993.

[95] G. J. M. Tuijthof and J. L. Herder, “Design, actuation and control of an anthropomorphic robot arm,” *Mechanism and Machine Theory*, vol. 35, no. 7, pp. 945–962, Jul. 2000.

[96] J. L. Herder, “Development of a statically balanced arm support: ARMON,” in *9th International Conference on Rehabilitation Robotics, 2005. ICORR 2005.*, 2005, pp. 281–286.

[97] Herder JL, Vrijlandt N, Antonides T, Cloosterman M, and Mastenbroek PL, “Principle and design of a mobile arm support for people with muscular weakness,” *Journal of Rehabilitation Research & Development*, vol. 43, no. 5, pp. 591–604, Sep. 2006.

[98] “SpringActive.” [Online]. Available: http://www.springactive.com/odyssey.php. [Accessed: 25-Mar-2017].

[99] P. L. Weiss, R. E. Kearney, and I. W. Hunter, “Position dependence of ankle joint dynamics—I. Passive mechanics - ScienceDirect,” *Journal of Biomechanics*, vol. 19, no. 9, pp. 727–735, 1986.

[100] S. Lipfert and A. Seyfarth, “Elastic legs in human walking,” *Journal of Biomechanics*, vol. 40, p. S385, 2007.

[101] P. L. Weiss, I. W. Hunter, and R. E. Kearney, “Human ankle joint stiffness over the full range of muscle activation levels,” *Journal of Biomechanics*, vol. 21, no. 7, pp. 539–544, Jan. 1988.

[102] S. Ounpuu, J. R. Gage, and R. B. Davis, “Three-Dimensional Lower Extremity Joint Kinetics in Normal Pediatric Gait,” *Journal of Pediatric Orthopaedics*, Jun. 1991.

[103] C. Frigo, P. Crenna, and L. M. Jensen, “Moment-angle relationship at lower limb joints during human walking at different velocities,” *Journal of Electromyography and Kinesiology*, vol. 6, no. 3, pp. 177–190, Sep. 1996.

[104] H. M. Herr and A. M. Grabowski, “Bionic ankle-foot prosthesis normalizes walking gait for persons with leg amputation,” *Proceedings of the Royal Society B: Biological Sciences*, vol. 279, no. 1728, pp. 457–464, Jul. 2011.

[105] M. Grimmer, M. Eslamy, and A. Seyfarth, “Energetic and Peak Power Advantages of Series Elastic Actuators in an Actuated Prosthetic Leg for Walking and Running,” *Actuators*, vol. 3, no. 1, pp. 1–19, Feb. 2014.

[106] M. A. Holgate, T. G. Sugar, and A. W. Bohler, “A novel control algorithm for wearable robotics using phase plane invariants,” in *Robotics and Automation, 2009. ICRA’09. IEEE International Conference on*, 2009, pp. 3845–3850.

[107] M. A. Holgate, “Control of a robotic transtibial prosthesis,” Dissertation, ARIZONA STATE UNIVERSITY, 2009.

[108] J. Hitt, T. Sugar, M. Holgate, R. Bellman, and K. Hollander, “Robotic transtibial prosthesis with biomechanical energy regeneration,” *Industrial Robot: An International Journal*, vol. 36, no. 5, pp. 441–447, 2009.

[109] J. Hitt, A. M. Oymagil, T. Sugar, K. Hollander, A. Boehler, and J. Fleeger, “Dynamically controlled ankle-foot orthosis (DCO) with regenerative kinetics: incrementally attaining user portability,” in *Robotics and Automation, 2007 IEEE International Conference on*, 2007, pp. 1541–1546.

[110] J. Hitt *et al.*, “Bionic running for unilateral transtibial military amputees,” DTIC Document, 2010.

[111] M. A. Holgate, A. W. Bohler, and T. G. Sugar, “Control algorithms for ankle robots: A reflection on the state-of-the-art and presentation of two novel algorithms,” in *2nd IEEE RAS EMBS International Conference on Biomedical Robotics and Biomechatronics, 2008. BioRob 2008*, 2008, pp. 97–102.

[112] K. W. Hollander, T. G. Sugar, and D. E. Herring, “Adjustable robotic tendon using a’Jack Spring’™,” in *Rehabilitation Robotics, 2005. ICORR 2005. 9th International Conference on*, 2005, pp. 113–118.

[113] K. W. Hollander, R. Ilg, T. G. Sugar, and D. Herring, “An efficient robotic tendon for gait assistance,” *Journal of biomechanical engineering*, vol. 128, no. 5, pp. 788–791, 2006.

[114] A. M. Grabowski and S. D’Andrea, “Effects of a powered ankle-foot prosthesis on kinetic loading of the unaffected leg during level-ground walking,” *Journal of neuroengineering and rehabilitation*, vol. 10, no. 1, p. 49, 2013.

[115] A. E. Ferris, J. M. Aldridge, C. A. Rábago, and J. M. Wilken, “Evaluation of a Powered Ankle-Foot Prosthetic System During Walking,” *Archives of Physical Medicine and Rehabilitation*, vol. 93, no. 11, pp. 1911–1918, Nov. 2012.

[116] G. K. Klute, J. Czerniecki, and B. Hannaford, “Development of powered prosthetic lower limb,” *Proceedings of the 1st National Meeting, Veterans Affairs Rehabilitation Research and Development Service*, 1998.

[117] S. K. Au, J. Weber, and H. Herr, “Biomechanical Design of a Powered Ankle-Foot Prosthesis,” in *2007 IEEE 10th International Conference on Rehabilitation Robotics*, 2007, pp. 298–303.

[118] B. E. Lawson, B. Ruhe, A. Shultz, and M. Goldfarb, “A Powered Prosthetic Intervention for Bilateral Transfemoral Amputees,” *IEEE Transactions on Biomedical Engineering*, vol. 62, no. 4, pp. 1042–1050, Apr. 2015.

[119] W. Koniuk, “Self-adjusting prosthetic ankle apparatus,” US6443993 B1, 03-Sep-2002.

[120] V. Pratt, “Direct Least-squares Fitting of Algebraic Surfaces,” in *Proceedings of the 14th Annual Conference on Computer Graphics and Interactive Techniques*, New York, NY, USA, 1987, pp. 145–152.

[121] J. L. Herder, “Design of spring force compensation systems,” *Mechanism and Machine Theory*, vol. 33, no. 1, pp. 151–161, Jan. 1998.

[122] M. Schenk, S. D. Guest, and J. L. Herder, “Zero stiffness tensegrity structures,” *International Journal of Solids and Structures*, vol. 44, no. 20, pp. 6569–6583, Oct. 2007.